Development of a self-healing compliant actuator

Seppe Terryn

Dankwoord

Bij deze zou ik graag professor Bram Vanderborght, professor Guy Van Assche en professor Dirk Lefeber bedanken. Dankzij jullie steun en bijzondere interesse kreeg ik de mogelijkheden om dit interessant en volledig nieuw onderwerp uit te diepen. Wat startte als een spontaan idee om de robotica te combineren met zelfhelende materialen groeide uit tot een volwaardig project, waaruit blijkt dat dit gloednieuw domein, de "Self-Healing Robotics", nog meer te bieden heeft. In het bijzonder zou ik graag Glenn Mathijssen en Joost Brancart willen bedanken. Bij jullie kon ik steeds terecht met allerhande vragen, maar ook gewoon voor een gezellige babbel. Op beide diensten, zowel MECH als MACH, wordt er een aangename sfeer gecreëerd door een toffe bende, waarvan vele je steeds onmiddellijk een helpende hand aanreiken. Bij deze ook dank aan Gill, Perry, Maria, Marnix, Jean-Paul en Mark.

Met dit eindwerk eindig ik vijf schitterende studentenjaren. Dankzij de enorme steun die ik thuis kreeg, heb ik, samen met hechte kameraden, enorm kunnen genieten van deze jaren. Daarom zou ik graag mijn papa, mama, broerke en Yana willen bedankten. Bedankt jullie vier, om er steeds voor mij te zijn!

Seppe Terryn

Confidential: Patent application

Abstract

The powerful biological healing function has inspired chemists to impart similar properties to synthetic materials to create "self-healing materials". These materials have the ability to recover after damaged using a self-healing (SH) mechanism. So far this material technology is not yet explored in robotics. In this thesis the remarkable SH property will be introduced for the first time in robotics. Up till now robots are over-dimensioned to withstand unexpected extreme circumstances and avoid any damage. The idea is that by incorporating a self-healing ability, robots can be dimensioned based on their performance tasks, instead of on extreme unexpected loads. If such an over-load takes place, a robotic part will fail. Using the SH ability the robotic part can be healed back to its initial state, and this preferentially autonomously. It is in this way that "self-healing robotics" may lead to lighter systems and eventually to more efficient designs.

The feasibility of integrating such a SH material in robotic compliant actuators was investigated based on the available SH polymer technologies. Considering different SH mechanisms, the Diels-Alder polymer, was found to be the most suitable for a first implementation in what will be called a "SH compliant actuator". The non-autonomous, SH mechanism of these Diels-Alder (DA) polymers is based on a reversible covalent network and requires a relative low temperature (between 70 and 120 °C). A large part of this thesis is focused on analyzing the potential of these DA-polymers to be processed in a macroscopic shape, ready to be implemented and used in the compliant actuators.

Two separated studies were carried out on two different actuator types, the series elastic actuator (SEA) and the soft pneumatic actuator (SPA), for which it was examined if the SH mechanism of the DA-polymers could be incorporated in the actuator designs. In order to develop the conceptual designs of these two actuators, the (thermo) mechanical properties of the DA-polymers were characterized. The conceptual design of the SH-SEA, relies on a SH-mechanical fuse (SH-MF), which is placed in series with the compliant element of the actuator. The fuse acts as a sacrificial part and will break if the actuator is subjected to an over-load. If fractured the fuse can be cured using a SH-process, which required a maximum temperature of 120 °C. A first prototype of this SH-MF was developed, which could be healed after fracture multiple times, while retaining its initial mechanical properties.

Next the potential of developing a bending SPA, made entirely out of an elastic self-healing DA-polymer, was investigated. To do so, a single-cell soft pneumatic cell (SPC) was produced out of the DA-polymer. Analyzing the mechanical properties as well as the SH-behavior of the SPC, allowed to concluded that the SH DA-polymers are suitable to be used in soft robotics. Based on the SPC design, the development of a multi-cell prototype, a bending SPA, will be straight forward.

Finally it can be concluded that self-healing polymers, in particular DA-polymers, can be considered in several future robotic applications.

Samenvatting

Het krachtig biologische helingsproces heeft chemici geïnspireerd om gelijkaardige eigenschappen in te bouwen in gesynthetiseerde materialen om op deze manier "zelfhelende materialen" te creëren. Deze materialen hebben het vermogen om te herstellen wanneer ze beschadigd zijn, gebruik makend van een zelfhelend mechanisme. Tot nu toe is deze materiaal technologie nog niet onderzocht in de robotica. In dit eindwerk zal de opmerkelijke zelfhelende eigenschap voor de eerste maal geïntroduceerd worden in de robotica. Tot op vandaag worden robots overgedimensioneerd om zo onverwachte, extreme omstandigheden te kunnen doorstaan, zonder beschadigd te worden. Het idee is dat door een zelfhelend vermogen in te bouwen, robots gedimensioneerd kunnen worden op basis van hun normale werking in plaats van op extreme onvoorziene belastingen. Wanneer de robot overbelast wordt, zal een onderdeel falen. Vervolgens kan, gebruikmakende van de zelfhelende eigenschap, dit onderdeel volledig hersteld worden in zijn initiële staat en dit bij voorkeur volledig autonoom. Op deze manier kan "zelfhelende robotica" leiden tot lichtere systemen en uiteindelijk tot efficiëntere ontwerpen.

De haalbaarheid om een zelfhelend materiaal te integreren in een soepele robot actuator werd onderzocht op basis van de in literatuur beschikbare zelfhelende polymeren. Uit de analyse van deze verschillende polymeren bleek dat het Diels-Alder polymeer, het best geschikt is voor een eerste implementatie in een "zelfhelende soepele actuator". Het niet-autonome, zelfhelende mechanisme van deze Diels-Alder (DA) polymeren is gebaseerd op een reversibel covalent netwerk en vereist een relatief lage temperatuur (tussen de 70 en 120 °C). Een groot deel van dit eindwerk concentreert zich op het analyseren van de mogelijkheden om DA-polymeren processen te worden in een macroscopische vorm, die geïmplementeerd en gebruikt kan worden in soepele actuatoren.

Twee onafhankelijke studies werden uitgevoerd op twee verschillende actuator types, de "series elastic actuator (SEA)" en de "soft pneumatic actuator (SPA)". In beide studies werd onderzocht of het zelfhelend mechanisme van de DA-polymeren ingebouwd kon worden in het actuator ontwerp. Om het conceptueel ontwerp van deze twee actuatoren te ontwikkelen, werden de (thermo) mechanische eigenschappen van de DA-polymeren gekarakteriseerd. Het conceptueel ontwerp van de zelfhelende SEA, bestaat uit een zelfhelende mechanische zekering (SH-MF) die in serie geplaatst wordt met het soepele element van de actuator. De zekering fungeert als een opofferings onderdeel en zal falen/breken wanneer de actuator onderworpen wordt aan een overbelasting. Wanneer de zekering faalt, kan ze geheeld worden gebruik makend van een zelfhelend proces, dat een maximale temperatuur vereist van 120 °C. Een eerste SH-MF prototype werd ontwikkeld, dat meermaals geheeld kon worden na breuk met behoud van de initiële mechanische eigenschappen.

Vervolgens werd onderzocht of een "bending SPA", volledig bestaande uit een elastisch zelfhelend DA-polymeer, ontwikkeld kon worden. Hiervoor werd een ééncellige "soft pneumatic cell (SPC)" ontwikkeld uit het DA-polymeer. Zowel de mechanische eigenschappen als het zelfhelende gedrag van deze SPC werden geanalyseerd. Hieruit kan worden geconcludeerd dat de zelfhelende DA-polymeren geschikt zijn voor "soft robotic" toepassingen. Vanuit dit SPC ontwerp, is de ontwikkeling van een meercellig prototype, "een bending SPA", onmiddellijk haalbaar.

Tot slot kan geconcludeerd worden dat zelfhelende polymeren, in het bijzonder DA-polymeren, overwogen kunnen worden in diverse robotische applicaties in de toekomst.

Confidentiel: demande de brevet d'invention

Résumé

La force régénératrice biologique est source d'inspiration pour des chimistes qui essaient d'introduire des caractéristiques semblables dans des matériaux synthétiques, créant ainsi des matériaux capables d'autoréparation. Un mécanisme auto régénérateur (AR) permet la réparation de dégâts de manière indépendante. Jusqu'à présent cette technologie n'a pas encore trouvé d'applications en robotique. Le présent mémoire introduit cette remarquable qualité AR pour la première fois dans ce domaine de la recherche. A l'heure actuelle les robots sont surdimensionnés pour résister à des circonstances extrêmes inattendues et pour éviter tout endommagement. En introduisant une capacité AR, les robots pourront être dimensionnés en fonction des performances requises et non pas pour résister à des surcharges inattendues. En cas de surcharge, la rupture d'une partie du robot assurera l'arrêt de la machine. La capacité AR permettra de restaurer cet élément dans son état initial, de préférence de façon autonome. Ce système pourrait mener à des concepts plus légers et finalement à une mise en forme plus efficace.

La possibilité d'intégrer un matériau AR dans des actionneurs souples pour robots a été étudié en se basant sur les connaissances actuelles de la technologie de polymères AR. Après investigation de différents mécanismes d'AR, le polymère Diels-Alder se révélait être le plus performant pour une première application dans un « actionneur souple AR ». Le système AR du polymère Diels-Alder (DA), non-autonome, est basé sur un réseau covalent réversible et demande une température relativement basse (entre 70 °C et 120 °C). L'analyse des possibilités pour rendre à ces résines une forme macroscopique afin de les insérer dans des actionneurs souples, occupe la plus grande partie du mémoire.

L'incorporation de la capacité AR des résines DA a été étudiée séparément pour deux types d'actionneurs : le « series elastic actuator » (SEA) et le « soft pneumatic actuator » (SPA). Afin de développer la mise en forme de ces deux actionneurs, les propriétés (thermo) mécaniques des résines DA ont été caractérisées. L'AR-SEA est basé sur la mise en oeuvre d'un fusible mécanique, placé en série avec l'élément souple de l'actionneur. Le fusible sera l'élément sacrifié en cas de surcharge en sera alors rompu. La cassure pourra être ressoudée en utilisant les capacités AR du matériu de base, requérant une température maximale de 120 °C. Un premier prototype pouvait être régénéré à plusieurs reprises après rupture, tout en gardant ces caractéristiques mécaniques initiales.

Puis, la possibilité de construire un « bending SPA », exclusivement constitué d'un polymère DA élastique, a été pris en considération. Une « soft pneumatic cell » unicellulaire de polymère DA a été créée. L'analyse des propriétés mécaniques et AR a permis de conclure que le polymère DA AR peut être utilisé en « soft robotics ». A partir de la cellule SPA, le développement d'un prototype multicellulaire sera possible.

Finalement, les polymères AR et plus particulièrement les résines DA peuvent être considérés comme des matériaux valables pour le développement de futures applications dans le domaine de la robotique.

Contents

Table of Abbriviations

SH	:	Self-Healing
SEA	:	Series Elastic Actuator
SH-SEA	:	Self-Healing Series Elastic Actuator
SPA	:	Soft Pneumatic Actuator
SH-SPA	:	Self-Healing Soft Pneumatic Actuator
SPA	:	Soft Pneumatic Cell
SH-SPA	:	Self-Healing Soft Pneumatic Cell
DA	:	Diels-Alder
MF	:	Mechanical Fuse
SH-MF	:	Self-Healing Mechanical Fuse
DMA	:	Dynamic Mechanical Analysis
DSC	:	Differential Scanning Calorimetry
TGA	:	Thermogravimetric Analysis

List of Figures

List of Tables

Chapter 1

Introduction

This report introduces a new concept in robotics, the ability of materials to recover after being damaged using a self-healing mechanism. These materials are generally called self-healing materials. This introduction chapter is started with the section 1.1, in which it is explained why it would be interesting to use this new material technology in robotics. Next the project goals of this thesis will be defined in section 1.2.

1.1 Motivation

In robotics a big part consists of what is called bio-inspired robotics. In this field, robot systems are designed and inspired by biological systems. Performances, appearances and working principles of living organisms are imitated.

The human body has a remarkable great advantage, the ability to heal itself when certain damages and injuries occur. Almost in every body part a self-healing system is incorporated. The skin is healing continuous, muscles can recover from ruptures and bones can heal from fractures.

The human body is not over-dimensioned and fractures, ruptures and injuries will occur when a body part is overloaded in abnormal, extreme circumstances. When these extreme, damaging conditions are ended and the body is back in its normal state, the healing process will start up autonomously. This healing process will take some time but will, if the damage is limited, recover the body part to its original state. When this recovery is complete the part can fulfill its specific function again until another overload may occur.

Up till now, a robot on the other hand does not have this healing ability. In order to be able to withstand unexpected loads, the system is over-dimensioned instead, this with a certain safety factor. The different parts have to be designed in such a way that they can withstand the numerous extreme circumstances to avoid any damage. Increasing the safety factor often also means increasing the weight of the system, while in many robotic applications compactness and weight are of great importance. It is for these applications that

"self-healing robotics" can lead to lighter systems and more efficient designs.

The powerful biological healing function has inspired chemists to impart similar properties to synthetic materials to create "self-healing materials". Over the last 15 years [1] a broad range of Self-Healing (SH) materials has been studied. Self-healing concepts are currently used in a large range of materials. Commonly used in the self-healing concepts, is the fact that specific chemical reactions are used as part of the repair system. This will be explained more in detail in the section 3: Self-healing materials: an overview.

Ideally a robot is build up with a complete set of self-healing material. This means that the robot will be build up out of a skeleton, actuators, sensors and communication/ information processing system and a cover/skin, all incorporated with a self-healing mechanism. However, to the best of the authors' knowledge, in literature no robotic parts have been described that are composed of a self-healing material. In this project a part will be devoted to the analysis of the different existing self-healing mechanisms to determine if they are compatible with a certain specific component, the actuator. Since compliant actuators are in development for safe interaction with unknown and dynamic environments, including humans, this type of actuation is used as case study [11, 12, 13].

Of course not only this actuator can be designed in a self-healing way but we chose to concentrate on a self-healing system dealing with damage due to overload of robotic joints. Other damaging effects like wear effects, damage by falling and scraping appear and might be solved using self-healing technology. For example the skin or cover could be protected with already existing self-healing coatings. Despite that self-healing concepts have the potential of being introduced in most materials of the robot we have decided to focus our study on the self-repair of actuators. It is believed that with the introduction of the self-healing concept in these parts we will have maximum contribution in the overall dimensioning of the robots.

1.2 Project Goal

The goal of this thesis is to study the feasibility of integrating a self-healing mechanism in robotics, more specific in robotic compliant actuators and this by investigating the available SH polymer technologies. A proof of concept for a compliant actuator, with self-healing mechanism incorporated, has to be designed.

Two concepts for incorporating the self healing property in an actuator will be analyzed in parallel: the Self-Healing Mechanical Fuse (SH-MF) and the Self-Healing Soft Pneumatic Actuator (SH-SPA). For both of these concepts a conceptual design has to be made. To illustrate the self-healing actuator in practice, a prototype for the both concepts has to be built and validated.

In this thesis the focus is on analyzing the potential of certain self-healing materials to be processed in a macroscopic shape, which can be implemented and used in compliant actuators.

Chapter 2

Actuation

2.1 Compliant actuation

The actuator in which we would like to incorporate the self-healing mechanism is a compliant actuator. To define what a compliant actuator is, a definition of a non-compliant actuator, better known as a stiff actuator, is useful. A stiff actuator is a device that is able to move to a specific position or to track a predefined trajectory. Once a position is reached, it will remain at that position, whatever the external forces exerted on the actuator (within the force limits of the device). [14]

A compliant actuator, on the other hand, will allow deviations from its own equilibrium position, depending on the applied external force. The equilibrium position of a compliant actuator is defined as the position of the actuator where the actuator generates zero force or zero torque [14]. This concept is specifically introduced for compliant actuators, since it does not exist for stiff actuators. Based on papers of Jerry E. Pratt and Benjamin T. Krupp [2, 15] the principle of the compliant actuator is explained.

In traditional manufacturing operations, robots perform tedious and repetitious tasks with great speed and precision. In this setting, where the environment is controlled and the tasks are repetitious, position-controlled robots which trace predefine joint trajectories are optimal. However, in highly unstructured, dynamical environments, where little is known of the environment, force-controlled robots that can comply with the surroundings are desirable. This is the case for legged robots walking over rough terrain, robotic arms interacting with people, wearable performance-enhancing exoskeletons, haptic interfaces, and other robotic applications. [2]

Stiff, conventional actuators have characteristics that have severely limited their use in force-controlled applications. These limitations include high reflected-inertia, a lot of static friction, and the difficulty to back drive. By adding a compliant element to these conventional, stiff systems, a force-controllable actuator with low impedance, low friction, high quality force control, and good bandwidth will result [2]. The actuators following this new design are

called compliant actuators. With this development the actuators receive a spring-like behavior also found in biological systems, like many different muscle systems.

In the category of compliant actuators there are actuators with fixed stiffness, like the series elastic actuation (SEA) and actuators with variable stiffness (VSA) [16]. In this thesis the focus is on the simplest compliant actuator types in which the first SH implementation is the easiest. This however does not exclude that the methods used cannot easily be expanded to more complex actuator types like the VSAs.

2.2 Implementation of SH-mechanism

To make a first implementation of the self-healing principle in robotics, two separate applications in two different actuators will be examined. The two actuators in which the SH-ability will be incorporated are:

- Series Elastic Actuator (SEA)
- Soft Pneumatic Actuator (SPA)

Both of these actuator types are explained respectively in the next two subsections (2.2.1, 2.2.2).

2.2.1 Series Elastic Actuation

Figure 2.1 shows the architecture of series elastic actuators. These actuators consist of a motor, a gear and a compliant element. This actuator is one of the basic types of compliant actuators, which is why it was chosen as base for designing a first SH-actuator. The compliant element, often a spring, characterized by a stiffness k, is placed between the gear train and driven load to intentionally reduce the stiffness of the actuator. A position sensor measures the deflection, and the force output is accurately calculated using Hooke's Law (F=kx). A control loop then servos the actuator to the desired output force. The resulting actuator has inherent shock tolerance, high force fidelity and extremely low impedance [2, 15].
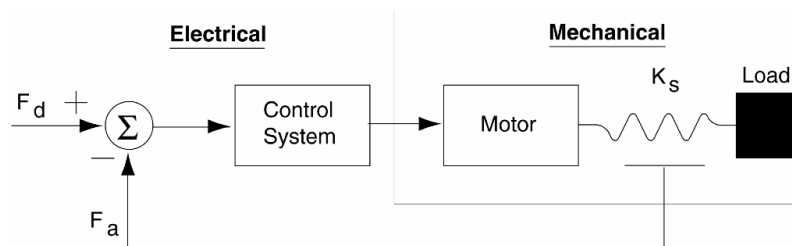
Figure 2.1: Schematic diagram of a series elastic actuator [2].

When this actuator is overloaded the system can fail in different failure modes. In many cases the motor will be overheated. When a very high torque is required, the high current will

produce a lot of heat, which will damage the motor. Another common failing mechanism of the actuator is due to the gearbox. This component will usually fail thanks to a cog fracture. Since it is currently technologically not possible to maintain a self-healing motor or gearbox, another approach will be introduced.

The idea is to design the compliant element in these SEAs as the weakest mechanical element in the construction, such that when the actuator is overloaded these compliant elements will fail first. There are two main ideas to add a self-healing mechanism to these compliant elements, which are in many applications simple springs.

- First concept: the compliant element can be replaced by a self-healing compliant element constructed out of a self-healing material.

- Second concept: a sacrificial part ,capable to heal itself, is added in series with the compliant element.

Using the first concept, the replacement element has to have the same mechanical properties as the original element to ensure that the actuator will work properly. This introduces severe restrictions to the applied self-healing material, concerning the stiffness and thermo-mechanical properties. When an overload is applied to the actuator, the self-healing spring element will fail. A detection system will have to be incorporated to detect this failure so that the actuator is brought in an unstressed, predefined position where the self-healing process is carried out. For this first concept, each type of actuator has a specific compliant design, which means that we have to find for each type of compliant actuator a different self-healing material with specific mechanical properties. For each type of actuator a new self-healing system has to be designed.

The second concept has the same working principle as the first but now a self-healing material is used in series with the original compliant element. The sacrificial part will have no (or minimal) mechanical contribution to the overall system but will fail when the actuator is overloaded. This means that there are less specific mechanical properties required. The element is chosen as weakest element and therefor will protect the compliant element and other components of the system. Another benefit of this design is that it is more compatible with the other different types of compliant actuators and can even be used for stiff actuators.

This principle of a sacrificial component already exists. Several types, working with different mechanisms, are already commercialized and go under the name of mechanical fuses [17, 18]. Most of these fuses have a limited lifetime of only one fail cycle, although there are fuses that can be easily reassembled after an overload [18].

2.2.2   Soft Pneumatic Actuation

Nowadays there is an increase in interest for a new type of compliant actuators, made out of highly compliant elastomers (f.e. Ecoflex or Ecoflex/polydimethylsiloxane: PDMS [19]), called Soft Pneumatic Actuators (SPA) [3, 4, 19, 20, 21, 22]. The SPAs, as the name tells, are actuated by compressed air but, unlike other pneumatic actuators which were already

presented in literature [23, 24], they are made almost entirely out of soft material. There have been constructed a variety of different SPAs [19] but they all work according the same principle. The SPAs consist of air chambers made out of the very organic flexible polymers. When pressurized these air chambers are inflated. The organic polymers used are usually approximately isotropic in their response to stress and therefor constrained in the range of motion they can generate on actuation. Therefor the soft actuators have to be designed in such a way that a controlled anisotropy is introduced in the response of the elastomers to stress, caused by pressurizing the air chambers. To introduce this anisotropy, non (or less) -stretchable but flexible materials are used in the designs, which restrict the elongation of parts of the soft actuator. The working principle will be clarified by an example of a SPA, explained in the next paragraph. This same principle of design has led to actuators that respond to pressurization with a wide range of motions: bending, extension, contraction, twisting and others [19].

To clarify the working principle of SPA better, the working mechanism of a particular simple SPA, the Multi-Chambered Bending [3] SPA (BSPA), is explained and visualized in figure 2.2.
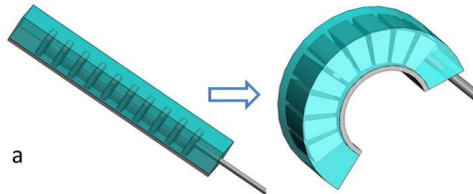
Figure 2.2: Bending SPA (BSPA)[3].

In the BSPA, air pressure deforms the actuator from straight to curved. This actuator is a block made out of highly soft and elastic polymer in which air chambers that inflate at a certain pressure, are embedded. A layer of non-stretchable polymer is attached to one of the sides of the actuator, allowing very little planar strain. Consequently, the pressurization of air chambers produces inflation on the top surface while the strain on the bottom surface remains essentially zero. This produces a bending motion where the distance between the two ends of the actuator decreases as the curvature increases. Other types of SPAs work with the same principle of inflatable air chambers and limiting the strain in one direction.

The SPAs are inherently soft, light, easy to fabricate and highly customizable [3]. However the torque and force output of these actuators is rather low, making them interesting as an alternative for conventional actuators in a limited amount of applications (f.e. small robotic joints), this in contrast to other (non-soft) Pneumatic Actuators used in robotics [23, 24, 25, 26]. One of the major drawbacks of these SPAs is the control of the actuation. Certainly position control is quite hard with these actuators. The actuation is a function of the pressure difference (ΔP) between the interior of the air chambers and the surroundings. Lately new research has been done in finding a way to characterize SPAs [3], which will assist in advancing the control of these actuators.

The actuation- and deactivation speed is dependent on the mass flow rate of the air (or other fluidum) entering or leaving the air chamber and is therefore limited. While the mass flow rate for entering air is dependent on the pressure system used, the mass flow rate during exhaust dependents on the air chamber pressure (ΔP). Another disadvantage is the required pressure system. These soft actuators may be small and light, they require however a system to pressurize the chambers.

Despite the drawbacks the SPAs can be very useful in certain applications, for example in hand rehabilitation [4] (figure 2.3). Often rehabilitation for improving hand function requires the patient to perform repetitive task practice (RTP), which involves breaking a task down into individual movements and practicing these exercises to improve hand strength, accuracy, and range of motion. These methods, however, are labor intensive and costly due to the required long hours of training with a physical therapist. In this application the required torque and force are limited, which is why the SPAs, with their inherent softness, can provide as an excellent alternative.
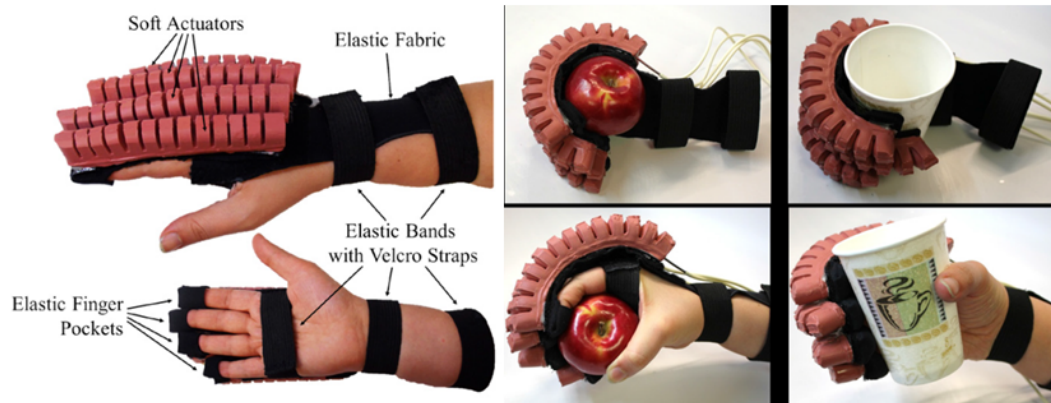
Figure 2.3: Application of the Bending SPA (BSPA): a glove containing 4 BSPA for hand rehabilitation, where repetitive movements are required [4].

In this thesis a design will be made for an SPA constructed entirely out of elastic self-healing material.

2.3 Conclusion

In highly unstructured, dynamical environments or in places where interaction with people is required, compliant actuators, that can comply with the surroundings, are desirable. Usually these actuators are over-dimensioned to withstand unexpected extreme circumstances and avoid any damage. However, in many robotic applications compactness and weight are of great importance. A self-healing compliant actuator might be a solution to this over-dimensioning.

The feasibility of developing a compliant actuator, in which a self-healing mechanism is incorporated, will be investigated in this thesis. Two compliant actuators will be analyzed in particular, with the focus on implementing a SH-property: the series elastic actuator (SEA) and the soft pneumatic actuator (SPA).

In the SEA a self-healing polymer part will be placed. The idea is to design this part as the weakest mechanical element in the construction, such that when the actuator is overloaded this elements will fail first, protecting the other components of the actuator. To realize this, two main concepts were introduced: the self-healing compliant element concept and the self-healing mechanical fuse concept. Further in the thesis, in chapter 5, a choice will be made between these two.

Parallel with the study on a self-healing SEA (SH-SEA), the feasibility of designing a SH-SPA, constructed entirely out of elastic self-healing polymers, will be analyzed.

In the next chapter the available SH polymer technologies will be analyzed with the focus on their implementation in a self-healing compliant actuator.

Chapter 3

Self-healing materials: an overview

As already mentioned a broad range of self-healing materials has been developed over the last 15 years [1], based on a variety of chemical principles [1, 5]. These materials can detect when they have been damaged and heal themselves either spontaneously or with aid of a stimulus. Following the paper of [1] Williams the different self-healing materials can be classified based on their chemistry. The different classes and the chemistries required for these various classes and subclasses are visualized in figure 3.1.
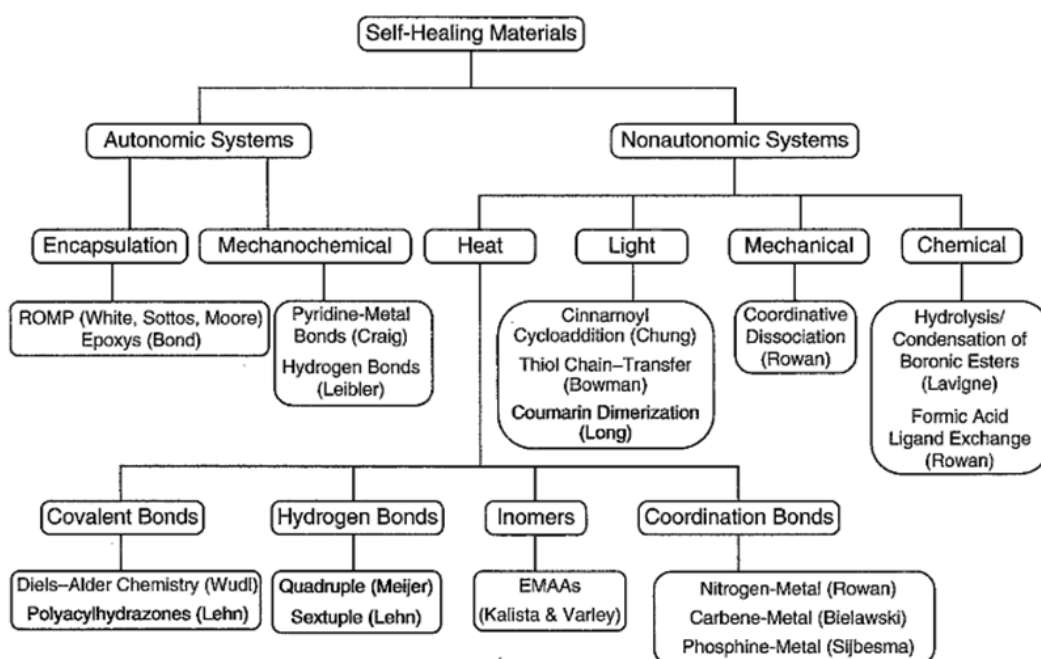
Figure 3.1: Overview of self-healing materials [1].

In the next sections 3.1 and 3.2 the classes will be briefly explained and analyzed if they are suitable for practical use in the SEA and SPA. In section 3.3 one of the self-healing materials will be chosen, to be used for a first incorporation in a self-healing compliant actuator design.

First two distinct classes can be defined: autonomic self-healing materials and non-autonomic systems. Autonomic systems require no stimulus (other than the formation of damage) for operation. These mechanisms do not require human intervention and are entirely self-contained. They most closely resemble biological systems, which deliver healing agents to compromised regions as soon as damage is inflicted. Non-autonomic systems on the other hand require some type of externally applied stimulus (such as heat or light) to enable a healing function. Yet this allows the healing process to be performed in a controlled way [1].

3.1 Autonomic self-healing materials

3.1.1 Encapsulation [1]

A subcategory of autonomic systems are the self-healing mechanisms using encapsulation. In this case, reactive chemical reagents are stored through compartmentalization, usually in the form of microcapsules, inside the material. When damage is incurred, the capsules will break and the chemicals are released and interact in such a manner that void spaces become filled, and through a chemical reaction the surfaces bond together. The principle is visualized in figure 3.2.

A disadvantage of systems working with a form of encapsulated reagents is that after the
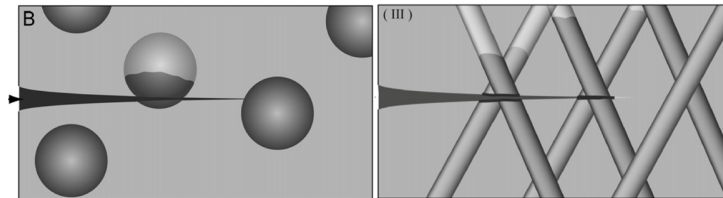
Figure 3.2: left: Self-healing material which uses network encapsulation[5]. right: SH-material which relies on a vascular network instead of a discrete encapsulation [5].

healing process the material properties will change locally. An even greater disadvantage is that the healing process can only operate once (or a limited number of times) at the same location because once the capsules are broken the healing mechanism is no longer present at that specific location. This means that the number of damage-healing cycles is strongly limited.

Due to these two drawbacks this encapsulation self-healing system is not suitable for application in SEAs. However encapsulation can be interesting for surface applications in robotics to protect, for example, the cover/skin against appearing scratch damages, which usually do not take place at the exact same location. A solution to these drawbacks has been developed,

which uses a vascular network instead of a discrete capsulation, but is too complex to use in SEAs (figure 3.2).

3.1.2 Mechanochemical

Other autonomic systems are joined under the name: mechanochemical systems. These mechanisms rely on weak reversible interactions (weak metal-amine bonds or weak hydrogen bonds), in conjunction with a polymeric structure designed to bear and later release stress.

These weak reversible interactions will break under a sufficient mechanical stress. But in unstressed condition at ambient temperature, the bonds will be reconstructed again due to the reversible behavior of the reaction, regenerating the chemical bond. As no external stimulus is used this mechanism is classified as autonomic.

The strength, fracture stress, of the polymers using this mechanism can be increased by the composition and the concentration of the weak bonds in the polymer structure. However high strength, mechanochemical polymers cannot be constructed due to the weak bonds. These materials are not very suitable for the application of the SH-actuator due to their mechanical properties (strength, fracture tension, elasticity). However the ability to perform self-healing at ambient temperature, without an external stimulus or encapsulation, is a huge advantage in comparison with the other non-autonomous self-healing mechanisms, which will be discussed in the following section 3.2.

3.2 Non-autonomic self-healing materials

As already mentioned non-autonomic self-healing materials always require some type of external stimulus. This stimulus can be in the form of heat, light, a mechanical or chemical stimulus [1].

3.2.1 Light

Light can be used to induce chemical based healing processes. An advantage of this mechanism is that photoreactions are usually very fast and can be selectively initiated by applying light of an appropriate wavelength. Light also enables greater control over the healing process since it can be localized to specific sites [1]. A big drawback is that the healing process is usually only limited to the surface areas only, because of the limited penetration depth of the light, due to its absorption. Hence bulk or macroscopic healing is not possible and therefore this principle is not applicable for implementation in SEAs.

3.2.2 Heat

Heat is used in most of the self-healing mechanisms already developed. Compared with the other non-autonomic self-healing systems, these mechanisms are most applicable in the SEA design, because of their relatively easy thermal control. Based on their chemistry they can be classified as follows.

Reversible Covalent Bonds

To explain the principle of these materials consisting of reversible covalent bonds we concentrate on a self-healing polymer network developped at the departement of Physical Chemistry and Polymer Science of the Vrije Universiteit Brussel by J. Brancart [6], based on the concept of the reversible Diels-Alder (DA) reaction between a furan functionalized compound and a bismaleimide (figure 3.3). Healing of macroscopic and microscopic defects takes place in a relative low temperature window ranging from 70 to 130 °C [6].
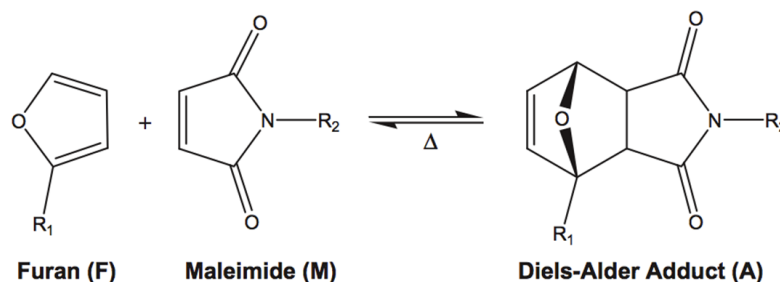
Figure 3.3: Diels-Alder reaction [6].

This DA reaction is a reversible cyclo addition reaction. It forms cyclic or bicyclic compounds at low temperature but reverts back to its starting materials upon heating. This is because at elevated temperature of 80 to 130 °C, where the reverse or retro-Diels-Alder reaction becomes favorable, the bicyclic structures disassemble, enabling the material to depolymerize to its original building blocks or monomers. At these temperatures, the monomers are liquid and can rapidly flow, which enables the material to be shaped into its original form.

Because of the almost complete reversibility of the Diels-Alder reaction the number of self-healing cycles is unlimited, which makes this self-healing mechanism favorable for implementation in the SEAs. The healing process requires heat but the temperature needed is acceptable and can be provided locally, for example by a Joule heating device.

Coordination Bonds

Coordination bond polymers are composed of monomers that interact non-covalently. Common interactions include hydrogen bonds, metal-ligand coordination, and van der Waals forces. Mechanical stress in these polymers causes the disruption of these specific non-covalent interactions, leading to monomer separation and polymer breakdown. These weak interactions are of particular interest for self-healing materials because of their reversible nature.

Different healing principles have been developed based on metal-ligand-mediated reactions in a lightly cross-linked polymer, usually in the form of gelatinous material. One disadvantage of this self-healing principle is that often the 'healed' material has an entirely different structure and a set of physical properties different from the 'unhealed' material [5]. The original mechanical properties can only be retained if high heating is used to make the polymer flow

ultimately [1]. The gelatinous form together with the disadvantages of this mechanism, make metal-ligand polymers less useful for self-healing actuator application.

A promising new metal-ligand system, which is probably also useful in robotics, has been developed which uses thermally reversible interactions between N-heterocycli carbenes and transition metals [1] to generate organometallic polymers. These materials are unusual in the sense that they show an extensive amount of bond unsaturation, a key requirement for conductive properties and a feature that could ultimately lead to self-healing functions that are triggered by electrical stimuli. Such systems could allow current to be used as a source of heat and feedback, providing potential for use in self-healing and reconfigurable electronics.

Ionomers

Ionomers are a class of polymers that contain as much as 20% of charged or ionic species as a part of their structures. These ions are able to interact with one another in a manner very similar to salt bridges seen in proteins, providing secondary structures to materials through the formation of physical crosslinks (figure 3.4). When stressed, these attractive electrostatic forces can be broken. Operating in tandem, these processes provide mechanisms by which the materials can cycle between stressed and relaxed state [1].
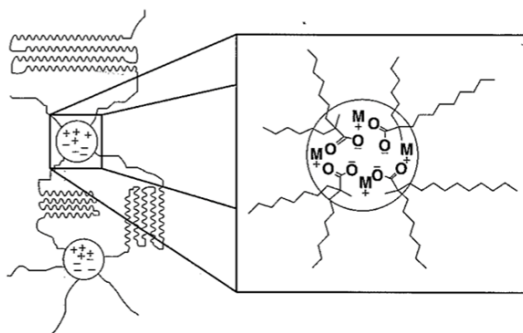
Figure 3.4: Structure of a model ionomeric system [1].

These polymers existed since the 1960s but the exploration of their self-healing behavior has only been initiated in recent years [5]. Ionomers used for self-healing purpose are generally copolymers of ethylene and methacrylic acid. The combination of neutral organic and ionic regions in the polymer chains results in biphasic materials containing relatively strong organic crystallites and weaker ionic aggregates, called multiplets. As heating occurs, whether through direct application or as a result of the friction resulting from damage, the multiplets dissociate, whereas the crystallites retain their structure. Further heating melts the crystallites, so that the polymer eventually reaches a fully molten state at high temperatures, >350 °C. Cooling reverses these processes, but the material does not regain its native structure until the multiplets re-form, which can take days [1].

This self-healing polymer has the advantage of repeated healing. But for a macroscopic

healing process, as needed in the SEA-application, a local high temperature is needed because there has to be a local melt state in the polymer. This high temperature makes this self-healing system less favorable than the mechanisms based on covalent bonds. However this does not exclude it from being suitable for incorporation in SEAs.

Although classified as non-autonomous, the damage event can provide enough energy, generally in the form of heat as a result of friction, so that the material effectively behaves as an autonomic self-healing material [1]. This is what happens if the self-healing material is used for healing of ballistic impacts, the application where these polymers are used mainly. For example there exist already ionomer plates, which remain fully intact after a bullet impact. The bullet will penetrate the polymer and due to the heat induced by friction the hole, left behind by the bullet, will be closed immediately. These "Impact Seal Self-Healing Targets" are being commercialized and used as long lifetime targets on shooting ranges.

3.3 Selection of a self-healing concept for the SEA application

The table 3.1 summarizes the advantages and disadvantages of the different self-healing concepts, explained in the previous paragraphs, in function of the application of a self-healing actuator.

From the table 3.1 it can be conclude that two self-healing mechanisms are suitable for the application of SH-actuators: Diels-Alder polymers and ionomers. However higher heating is required for the SH-healing process of Ionomers. We will use the Diels-Alder self-healing mechanism in the further design phases.

3.4 Conclusion

A large overview was given on the different self-healing mechanisms in polymers which exist in literature. These mechanisms were analyzed one by one, in order to see whether they were suitable to be used in a compliant actuator design. After this analysis, the Diels-Alder (DA) self-healing polymers were chosen to be the most suitable. The Diels-Alder polymers will be used in the design of a first self-healing compliant actuator. Before a conceptual design was made on a first self-healing actuator, the main (thermal) mechanical properties of these DA polymers were measured and analyzed. The next chapter 4 is devoted to the (thermo) mechanical properties of the DA-polymers.

Table 3.1: Analysis of the different SH-mechanisms for SEA application.

Classification	SH-mechanism	Advantages	Disadvantages	Suitable for SH-actuator
Autonomous	Encapsulation	Fully autonomous principle	Very limited self-healing cycles Complex structure	Not very suitable due to the limited cycles
	Mechanochemical	Fully autonomous principle Healing at ambient temperature Large self-healing cycle	Weak bonds which limit the mechanical properties	Not suitable due to the insufficient mechanical properties But potential in robotics
Non-Autonomous	Light	Photoreactions are usually very fast Good control of the SH-process due to the localization of light	SH is limited to the surface	Not suitable since a bulk SH is required in the application
	Reversible covalent bound: Diels Alder	Recovery of initiated mechanical properties SH-cycles are not limited Strong reversible covalent bonds Relatively low temperature of 80°-130°	Heating device is required	Suitable for the SH-actuator
	Coordination Bond		Non-recovery of initiated mechanical properties Weak bonds which limit the mechanical properties Gelatinous form	Not suitable for SH-actuator due to the insufficient mechanical properties (gelatinous form) and the limited SH-cycles
	Ionomers	Recovery of initiated mechanical properties SH-cycles are not limited	Heating device is required Relatively high temperature The complete SH-mechanism takes long time	Suitable for SH-actuator but higher temperature is required

Chapter 4

Diels-Alder self-healing material

In chapter 3 an analysis was made of the different self-healing mechanisms in polymers which are available in literature. In order to create a self-healing compliant actuator a Diels-Alder polymer system with reversible covalent bonds was chosen. This section starts with a brief introduction on the Diels-Alder polymers. This is followed by a section, describing the synthesis of these polymers and a section, explaining how the self-healing process of these polymers works. Next the thermal and mechanical properties of the DA-polymers will be illustrated, which were derived by carrying out different thermo-mechanical experiments. The chapter is terminated with a conclusion.

4.1 Introduction on the Diels-Alder polymers

The DA-polymer used, is a reversible polymer network, formed by the DA cross-linking reaction between a synthesized furan functional compound (A) and a bismaleimide (B) (figure 4.1). The DA-reaction is an equilibrium reaction for which the extent of the reaction is a function of temperature. The reaction equilibrium is shifted from Furan (diene) and Maleimide (dienophile) towards the cyclo-DA-adduct (and backward) by decreasing (increasing) the temperature. Four furan rings, present on the furan functional compound (A), form DA-bonds with the two maleimide rings, presented on the maleimide functional compound (B). This results in a thermo-reversible network structure.

At the Materials and Chemistry department (Research group Physical Chemistry and Polymer Science, FYSC) of the Vrije Universiteit Brussel (VUB) [6] four series of the DA-polymer were developed, using four different functional furan compounds (component A in figure 4.1) in the synthesis. These four furan compounds differ in degree of polymerization DP_n. The DP_n is defined as the number of monomeric units in a polymer (4.1).

$$DP_n = X_n = \frac{M_n}{M_0} \tag{4.1}$$

In which M_n is number-average molecular weight of the polymer and M_0 is the molecular weight of the monomer unit. Since the furan compound consists of non-cross linked polymer chains, the 4 furan compounds differ in furan spacer length, the polymer chain length of the
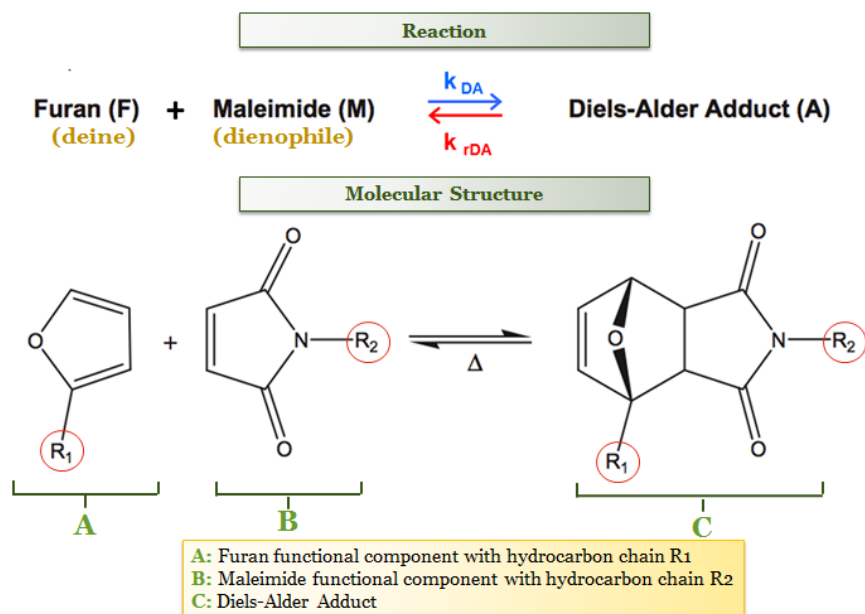
Figure 4.1: Diels-Alder reaction [6].

hydrocarbon chain (R1 in figure 4.1) in this furan functional compound (A). By varying this polymer chain length polymer series are synthesized, with different mechanical properties but with the same self-healing mechanism incorporated, the reversible DA-bonds. The differences in mechanical properties between the 4 series will be explained in section 4.4.1.

4.2   Synthesis

The synthesis of the Diels-ALder polymer series, will be discussed in this part of the report. The section is divided into two subsections, one part in which the reactants used in the synthesis are specified, followed by a second part in which the actual synthesis of the polymers is explained

4.2.1   Materials

The reactants, the monomers, used in the synthesis of the reversible DA-polymer network system are visualized in figure 4.2 and were purchased from Sigma-Aldrich:

- (A): 4 Jeffamine D-series: Poly(propylene glycol) bis(2-aminopropyl ether) with average degree of polymerization n (determined by nuclear magnetic resonance spectroscopy)

  - n = 3.1: J230, M_n = 256 g/mol
  - n = 6.9: J400, M_n = 477 g/mol
  - n = 44.2: J2000, M_n = 2640 g/mol
  - n = 71.1: J4000, M_n = 4200 g/mol

- (B): furfuryl glycidyl ether (FGE, 96 %)

- (C): 1,1'-(methylenedi-1,4-phenylene)bismaleimide (DPBM, 95%)
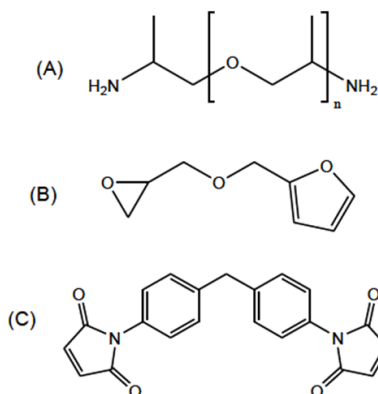
Figure 4.2: Monomers used for the synthesis of the reversible network system: (A) Jeffamine D-series Jx (x = 230, 400, 2000, 4000), (B) FGE, and (C) DPBM [6].

4.2.2 DA-network polymer Synthesis

The synthesis of the DA-polymer network was performed in two steps and based on a paper by Scheltjens et al. [6]. In a first step, FGE was irreversibly bonded to Jx (x = 230, 400, 2000, and 4000) through an epoxy-amine reaction, yielding a furan functionalized compound. This reaction was performed at 60 °C for minimum 7 days after which the reaction was completed at 90 °C (to speed up the reaction) for 2 days. The epoxy-amine which was formed in this first step is presented in figure 4.3. From now on the two molecules visible in figure 4.3 will be represented by a schematic representation, also visible in the figure.

In a second step, the furan functionalized compound (FGE-Jx) was mixed with DPBM in a stoichiometric ratio of one (r= $n_{Maleimide}$ / n_{Furan} = 1) to obtain the reversible polymer network through DA reaction. Prior to the DA reaction, the DPBM was dissolved in chloroform (a 20 w% solution) to obtain a homogeneous reversible network. The reaction is presented in figure 4.4, as well as a schematic representation of the reversible polymer network which is formed. The polymer network presented in figure 4.4 is a schematic representation. In reality the network is 3 dimensional, less structured and the jeffamines in the furan functionalized compounds will have small variations in polymer chain length.

Dependent on the DPBM-FGE-Jx series, different methods are used to produce bulk samples. The elastomer polymer series (section 4.4.1), based on J2000 and J4000, are processed to sheets (≤ 1mm). In order to form these sheets (4.2.2 a and b) solvent casting was carried out at room temperature, on a Teflon surface. The casted polymer was placed in a vacuum oven at a temperature of 60 °C for 24 hours to remove as much chloroform as possible. After this the oven was gradually cooled down to 50 °C during 2 hours, after which the polymer
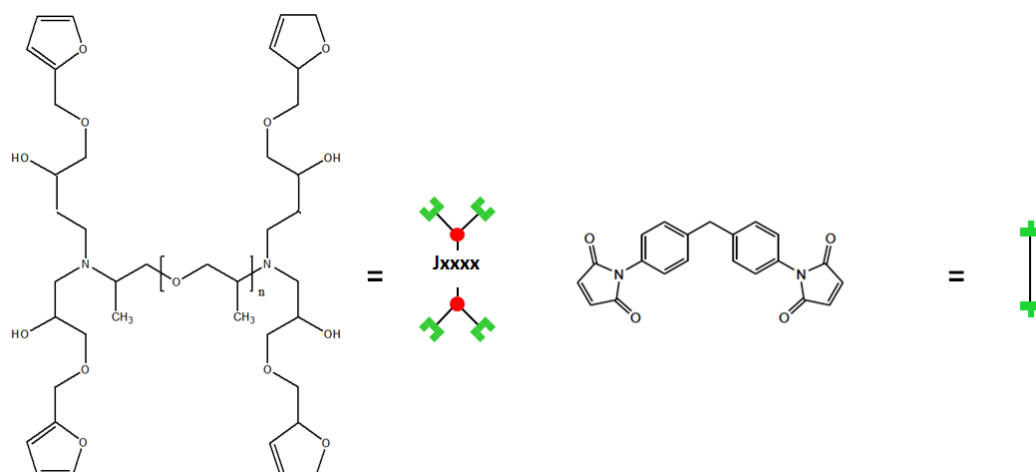
Figure 4.3: Left: The molecular structure of the epoxy-amine (furan functionalized compound: A in figure 4.1) formed by a irreversible reaction between FGE and Jx (x=230, 400, 2000 and 4000). Right: The molecular structure of 1,1'-(methylenedi-1,4-phenylene)bismaleimide (DPBM, 95 %) (maleimide functionalize compound: B in figure 4.1). From now on these two molecules will be represented by a schematic representation.
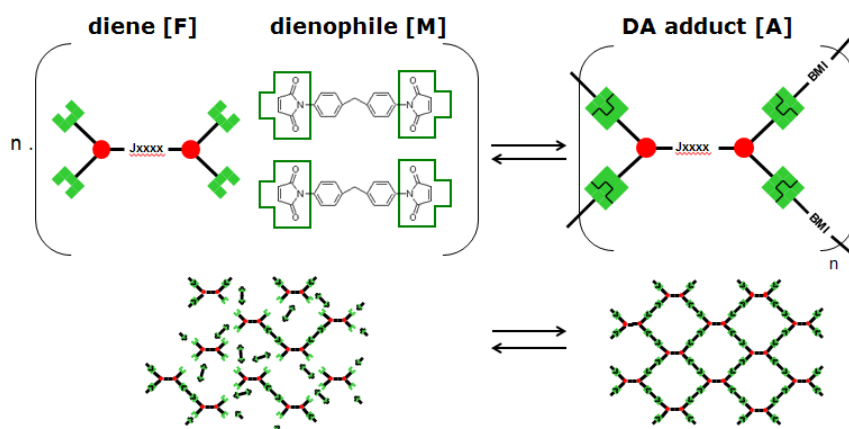
Figure 4.4: Reaction between the furan functionalized compound (diene: FGE-Jx) and the DPBM, which are mixed with a stoichiometric ratio of one (r=1) to form a 3D reversible, amorphous, polymer network.

was cooled down naturally to room temperature.

The thermoset polymers (section 4.4.1), based on J400 and J230, are processed to porous powder. In this master thesis the J230 series is not used due to its high brittleness. In previous work [6], in FYSC-VUB, the DPBM-FGE-J400 series was, like the J2000 and J4000 series, synthesized into a sheet. In this thesis the synthesis process was adapted to form a

porous powder at the end of the polymer synthesis. First the DPBM-FGE-J400, dissolved in chloroform, was casted into a petri dish at 21 °C. This was placed into a vacuum oven at 60 °C. After only 8 hours, the polymer was taken out the of oven, containing still 30 w% of chloroform. Because of the chloroform, the polymer had a gel like texture (figure 4.2.2 a), in contrast to a hard glassy characteristic when almost all the chloroform is removed (30 w%), and it could easily been grinded (figure 4.2.2 b). After this the remaining chloroform was removed using vacuum at 25 °C for 4 hours and a polymer network structure was produced as a porous powder.
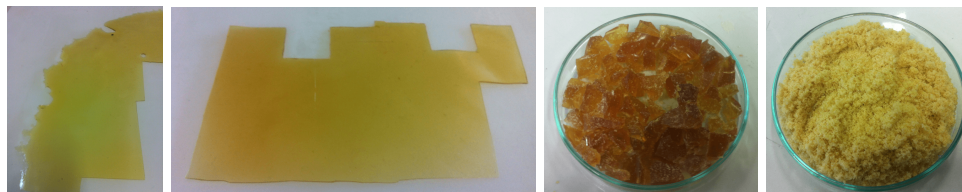
Figure 4.5: a) DPBM-FGE-J2000 sheet. b) DPBM-FGE-J4000 sheet c)Petri dish with gel like DPBM-FGE-J400 dissolved in 30 w% Chloroform (CH_3Cl) after been placed in vacuum oven at 60°C for 8 hours. d) Petri disk with grinded DPBM-FGE-J400 dissolved in 30 w% Chloroform (CH_3Cl).

4.3 Self-Healing mechanism

4.3.1 Simulation of temperature dependence of the Diels-Alder network

Like mentioned in the introduction of this chapter, the Diels-Alder reaction between furan and maleimide functional groups is a reversible reaction. At low temperatures the Diels-Alder adduct is formed. As the temperature is increased the reaction equilibrium is shifted towards the breaking of the reversible bonds. A Kinetics/Equilibrium simulation is provided by Scheltjens [6], which in the first place models the temperature dependence of the equilibrium conversion for the Diels-Alder reaction between DPBM, the maleimide carrying molecule and FGE-Jeffamine, the furan carrying molecule. The equations used in this simulation are explained in Appendix: Kinetics/Equilibrium simulation.

With the simulation, the equilibrium conversion (x) to Diels-Alder Adduct can be modeled as a function of temperature. In figure 4.6 the equilibrium conversion (x) to Diels-Alder Adduct is plotted as a function of temperature for the DPBM-FGE-J400 series over a temperature interval from 20 °C to 140 °C. The equilibrium conversion-versus-temperature graphs for the other DPBM-FGE-J2000 and J4000 can be found in Appendix A.1.

To explain the different zones which are present on the graphs (figure 4.6), two transition temperatures have to be introduced: the Glass Transition Temperature (T_g) and the Gel Transition Temperature (T_{gel}). The T_g is the temperature at which a polymer undergoes a reversible transition from a hard and relatively brittle state into a molten or rubbery state.
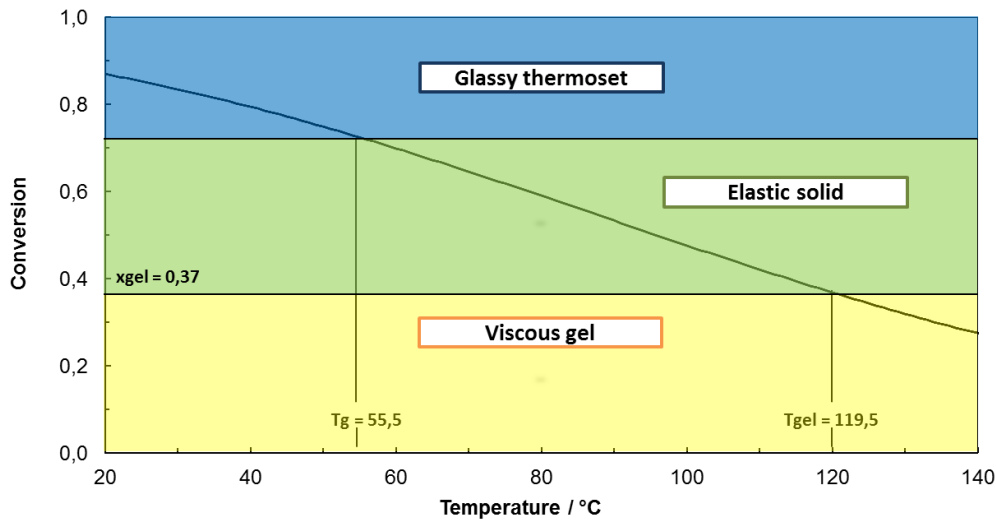
Figure 4.6: Equilibrium simulation of the Diels-Alder reaction equilibrium for DPBM-FGE-J400 starting at equilibrium.

Figure 4.7: Equilibrium Diels-Alder reaction, function of temperature. At low temperatures the network is formed due to a high conversion to Diels-Alder bonds. At elavated temperatures a lot of Diels-Alder bonds will break, the conversion will drop and the mobility of the polymer chains will increase. At relative high temperature the polymer will receive a gel-like structure.

A thermoset has a glassy behavior below its T_g and a rubbery behavior above its T_g. The T_{gel} and corresponding conversion (x_{gel}) are the temperature and conversion, respectively, at which an incipient network is formed in a crosslinking system. Above the x_{gel} the polymer will have a network structure and therefor will be a solid. However below x_{gel}, due to the low cross-link density, the network falls apart, which result in a viscous behavior. In other words, as the temperature increases, DA-bonds in the polymer network are gradually broken, as the conversion decreases, changing the structure of the polymer from a solid network structure to a viscous liquid-like structure (figure 4.7). To summarize the three zones defined by these two transition temperatures are:

- Yellow zone: Viscous Gel ($x_{gel} > x$)
    - Relatively high Temperature→ low cross link density→ no network → Viscous Gel-like behavior
- Green zone: Elastic Solid ($x_g > x > x_{gel}$)

  - Relatively mean to high temperature → medium to high cross link density→ network structure
    → Elastic solid behavior
- Blue zone: Glassy Thermoset ($x > x_g$)
  - Relatively low temperature → high cross link density→ network structure → very limited chain
    mobility → glassy, brittle behavior

Besides plotting the equilibrium conversion/temperature plot, the simulation can take into account the kinetics, because of this, the conversion variation resulting from a cooling or heating temperature profile can be modeled (Appendix A.1). This part of the simulation will be used further in the report (section 5.3) to design a cooling temperature profile for the self-healing polymers build in the applications.

4.3.2 Actual SH-process

In this subsection the SH-process for the healing of a macroscopic fracture in a Diels-Alder polymer is discussed. The SH-process can be divided into three stages (figure 4.8):

- **Heating process** up to a few degrees below T_{gel}, defined as "Near Gel Temperature (T_{Ngel})"
- **Isothermal process** at T_{Ngel} such that macroscopic gaps are filled
- **Controlled cooling** process from T_{Ngel} to $T_{ambient}$ or to T_g (if $T_{ambient} < T_g$) to retrieve high conversion at the end of the SH-process

The SH-process starts with a heating process up to T_{Ngel}, and this preferably locally, near the fracture. The higher the temperature, the more the reverse or retro-Diels-Alder reaction becomes favorable and the more Diels-Alder bonds will break. At T_{Ngel} the DA-polymer still has a network structure, however, enough Diels-Alder bounds are broken to give the polymer chains the necessary mobility. The reaction rate of the retro-Diels-Alder reaction (Appendix equation 1: $\frac{d[F]}{dt}$) increases with temperature, and therefor the kinetics of this reaction become faster with an increase of temperature. Because of this, the heating process until T_{Ngel} can be done as fast as possible and the duration (figure 4.8: t1) will be limited by the maximum heating temperature ramp of the heating devices used for the SH-process.

At the elevated temperature T_{Ngel} a lot of DA-bonds will be broken, giving the polymer the required mobility to seal/close the macroscopic gap (figure 4.7). The polymer has to remain at this temperature until the macroscopic gap is filled entirely. The duration of this isothermal process (figure 4.8: t2 - t1) depends on the DA-polymer series (section 4.4.1) used and the dimensions of the macroscopic gap, but is relatively fast. A self-healing process was carried out on a DPBM-FGE-J2000 sample, with thickness of 0.75 mm, in which a macroscopic fracture of 57.50 μm was made with a scalpel (figure 4.9). The isothermal process to close this gap took only 20 minutes. The temperature of this stage of the SH-process is limited by the T_{gel} because heating of the the polymer above T_{gel} will lead to unwanted macroscopic deformations/flows of the polymer piece. Therefor this isothermal process is done at a few degrees below T_{gel} at T_{Ngel}. At lower temperature, 10 to 15 °C below T_{gel}, filling of the macroscopic gap will also take place, but over a much longer period.

After the gap is closed, the polymer can be brought back to room temperature. This however has to be done with a slow, controlled cooling process (figure 4.8). This slow cooling
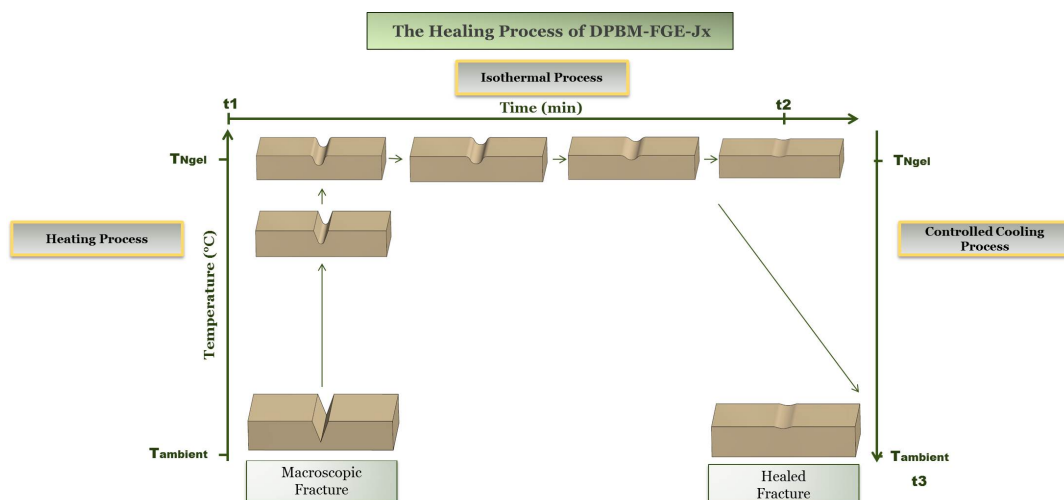
Figure 4.8: Schematic illustration of the Self-Healing process of DPBM-FGE-Jx series: Illustration the required time and temperature for the 3 parts of the SH-process: the heating part and controlled cooling part.
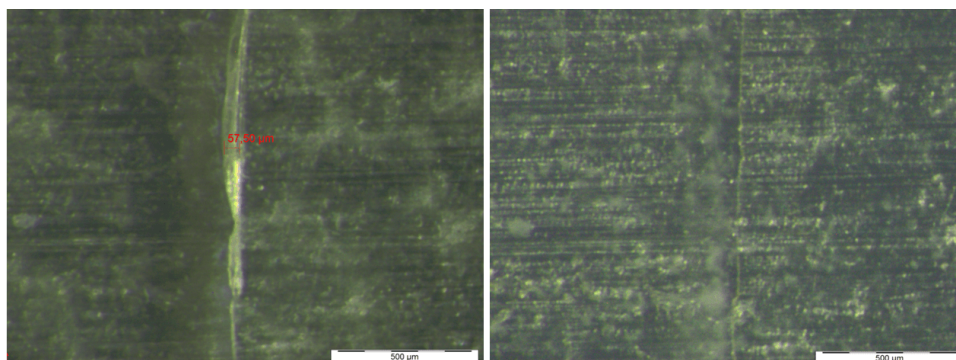
Figure 4.9: Photos taken with an optical microscope for the SH-healing process of a DPBM-FGE-J2000 sample with 0.75 mm thickness havind a macroscopic gap of 57.50 μm. Left: Before the SH-process Right: after SH-healing process: heated up from $60°$C to $90°$C with steps of $5°$C every 10 min, then stayed 20 min at $90°$C after which continued with steps of $5°$C every 10 min until 100 $°$C (the photo was taken after naturally cooled down to room temperature). The video can be seen at: https://www.youtube.com/watch?v=ERI-25qhNyk.

is important since the polymer requires time to form the polymer network by forming the DA-cross-link bonds. The reaction rate of the Diels-Alder reaction decreases with increasing temperature and therefor the kinetics of the reaction become slower with increasing temperature. The polymer has to remain long enough at relatively high and medium temperatures, where the kinetics of the DA-reaction are favored such that the network can be formed in a reasonable time period. When cooled down too fast, Maleimide- and Furan polymer groups will get trapped in the polymer network without forming DA-bonds, making the conversion

rate drop significantly. The cooling temperature profile from elevated temperature to ambient temperature is extremely important and will affect the recovery of the initial material properties.

Finally it should be noted that for the DA-series that have a glassy thermoset behavior (section 4.4.1: DPBM-FGE-400) at ambient temperature, the controlled cooling process will be carried out until the T_g, instead of until $T_{ambient}$. Like mentioned before, glassy thermosets have a T_g which exceeds $T_{ambient}$. When in the third stage of the SH-process the temperature reaches the T_g, the thermoset forms a highly cross-linked, glassy network in which the polymer chains have very little mobility. For lower temperatures than this temperature the conversion will increase very slow towards the equilibrium conversion, about a factor 1000 slower than above T_g. Therefor the controlled cooling process will always be carried out until T_g is reached for this series.

To recapitulate, the SH-process can be spit in three stages, which all have a specific purpose:

- **Heating process**: To give the polymer the required mobility to fill the macroscopic gap.
- **Isothermal process**: To give the polymer the required time to fill the macroscopic gap
- **Controlled cooling**: To recover the initial (or similar to the initial) conversion and therefor the initial material properties.

4.4 DA-polymer properties

4.4.1 DA-polymer series

As mentioned in the introduction of this chapter, four different series of the DA-polymer are developed at the FYSC research group of the Vrije Universiteit Brussel (VUB) [6].

The four series can be classified in two big groups, based on their thermo-mechanical behavior (figure 4.10):

- The series J230 and J400 contain furan compounds with short polymer chain length. Due to these short chains, the network has a high cross-link density, which affects the glass transition temperature (T_g) of the polymer. The series are Glassy Thermosets (brittle) due to a glass transition temperature which exceeds the ambient temperature ($T_{ambient}$)
- The series J2000 and J4000 on the other hand are built up out of furan compounds with long polymer chain length, limiting the cross link density. These series are Elastomers, with ductile characteristics, because of having a T_g lower then $T_{ambient}$.

4.4.2 Glass Transition temperature and Gel transition temperature

As mentioned in section 4.3.1, the glass transition temperature (T_g) is the temperature at which, while heating, a polymer undergoes a reversible transition from a hard and relatively
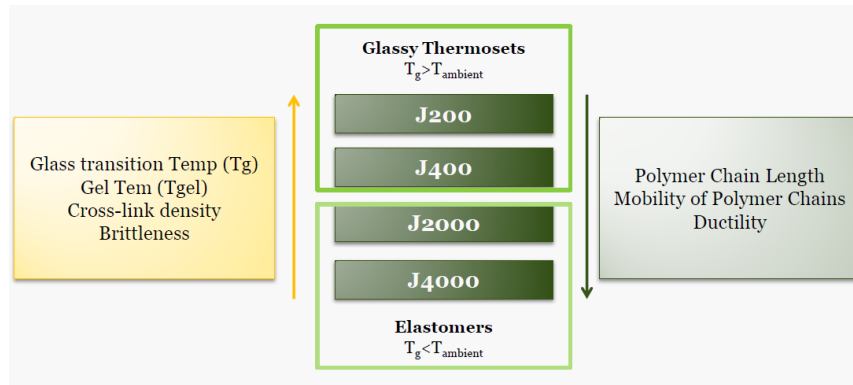
Figure 4.10: Classification of the DPBM-FGE-Jx series into 2 big groups: Glassy Thermosets and Elastomers.

brittle state into a molten or rubbery state. The T_g of the polymer series was measured by a Differential Scanning Calorimetry (DSC), by Scheltjens et al. [6] and listed in the table 4.1. The T_{gel} and corresponding conversion (x_{gel}) is the temperature (conversion) at which an incipient network is formed in a crosslinking system. It can be determined by dynamic rheometry, by locating the cross-over between G' (storage modulus) and G" (loss modulus), this is at a loss angle of 45 °. T_{gel} is independent of the oscillatory frequency. The values of T_{gel} can also be found in table 4.1.

Table 4.1: T_g: Glass Transition Temperatures of the DPBM-FGE-Jx series: Measured using Differential Scanning Calorimetry (DSC) [6]. T_{gel}: Measured by determining the location of cross over between G' (storage modulus) and G" (loss modulus), using Dynamic rheometry measurement at 0.01 Hz, 0.3174 Hz, and 1 Hz, performed at a scanning rate of 2 °C/min[6]. The results of the density measurements for the different DPBM-FGE-Jx series are also presented, as well as the absolute error.

Transition temperatures of DPBM-FGE-Jx				
Classification	Glassy Thermosets		Elastomers	
Series	J230	J400	J2000	J4000
DSC: Tg (°C)	63.9	55.5	-55.3	-64.6
Tgel (°C)	(>120)	119,5	98,5	81,0
Density (g/ml)		/	1,19 ± 0,01	1,13 ± 0,02	1,05 ± 0,02

Experiments of Scheltjens and Brancart [6] have proven that self-healing can be carried out 10 °C to 20 °C below the gel-point temperature in the order of minutes. The T_{gel} is however very important since it defines the temperature limit for the self-healing process. If heated above this temperature, during the SH-process, the network will fall apart, resulting in unwanted macroscopic deformations of the SH-piece.

The densities of the different DA-polymer series: DPBM-FGE-J400, J2000 and J4000, were

measured. The results were also presented in the table 4.1 and the measurements and calculations can be found in Appendix A.2.

4.4.3 Mechanical properties

In this section the experiments done to derive the basic mechanical characteristics: Complex Modulus: Storage Modulus, Loss Modulus, Tan(δ) and Fracture tensile, of the 3 polymer series, DPBM-FGE-J400, -J2000 and -J4000, will be described and the data received from the preformed tests will be analyzed. However to do this some background on the thermo-mechanical behavior of polymers, and in specific of the DA-polymer series, is required. Therefor this section starts with some theory on the visco-elastic behavior of polymers is described and the method used for viscoelastic property characterization, the dynamical mechanical analysis.

Characterization of the viscoelastic behavior of the DA polymers

Theoretical: Viscoelastic behavior of polymers
In contrast to metals, polymers have a viscoelastic behavior, that is intermediate between that of an ideal elastic solid and that of an ideal viscous liquid, showing characteristics of both [7]. The timescale and temperature of observation are critical to the relative degree of solid- and liquid like behavior exhibited by viscoelastic materials. Generally, they will behave more solid like at lower temperature or short timescale, but more liquid like at higher temperatures or longer timescales. There are three fundamental test methods for characterization of the visoelastic behavior of polymers: creep, stress relaxation and dynamic mechanical analysis (DMA). Of the different methods for viscoelastic property characterization, dynamical techniques are most popular, since they are readily adapted for studies of both polymeric solids and liquids [7]. They are collectively referred to as Dynamic Mechanical Analysis or DMA.

In this thesis the viscoelastic property of the DA-polymer series will be characterized using dynamic mechanical analysis. However the three fundamental tests, creep, relaxation and DMA, are related, and numerical techniques are available for calculating creep and stress relaxation data from dynamic mechanical data [7]. In the following subsection the characterization parameters used to describe the viscoelastic behavior with the DMA method are presented. In Appendix A.3 these parameters are explained in detail as well as the DMA, which is used to measure these parameters. For readers, who do not have a theoretical background on polymers, it is advised to take a look at this Appendix A.3.

Theoretical: Dynamic Mechanical Analysis: parameters
In a DMA, a sinusoidal stress is applied and the strain in the material is measured, allowing one to determine the Complex modulus. This Complex modulus is a parameter which fully characterizes the viscoelastic behavior and consists out of the Storage modulus (E') and the Loss modulus (E"): $E = E' + iE''$. E' is known as the storage modulus and is a measure of the elastic character or solidlike nature of the material. E" is known as the loss modulus and is a measure of the viscous character or liquidlike nature of the material. The larger E' is relative to E", the more of the energy required to deform sample is elastically recoverable.

The larger E" is relative to E', the more of the deformation energy is viscously dissipated in heat. For an ideal elastic solid E' is simply the Young's modulus of the material and E" is zero. For an ideal viscous liquid the storage modulus is zero and the loss modulus is related to the viscosity of the material. In a physical sense, the storage modulus is related to the stiffness of the material, while the loss modulus is reflected in the damping capacity of the material. The ratio between the loss modulus and storage modulus is defined as the material loss factor or loss tangent, more commonly: $\tan(\delta) = \frac{E''}{E'}$. $\tan(\delta)$ ranges from zero for an ideal elastic solid to infinity for an ideal liquid. It represents the ratio of energy dissipated to energy stored per cycle of deformation. These three parameters, E', E" and $\tan(\delta)$ are explained more in detail in Appendix A.3, in which the formulas for obtaining these parameters using a dynamic mechanical test are also given.

Theoretical: viscoelastic behavior of the DA-polymers
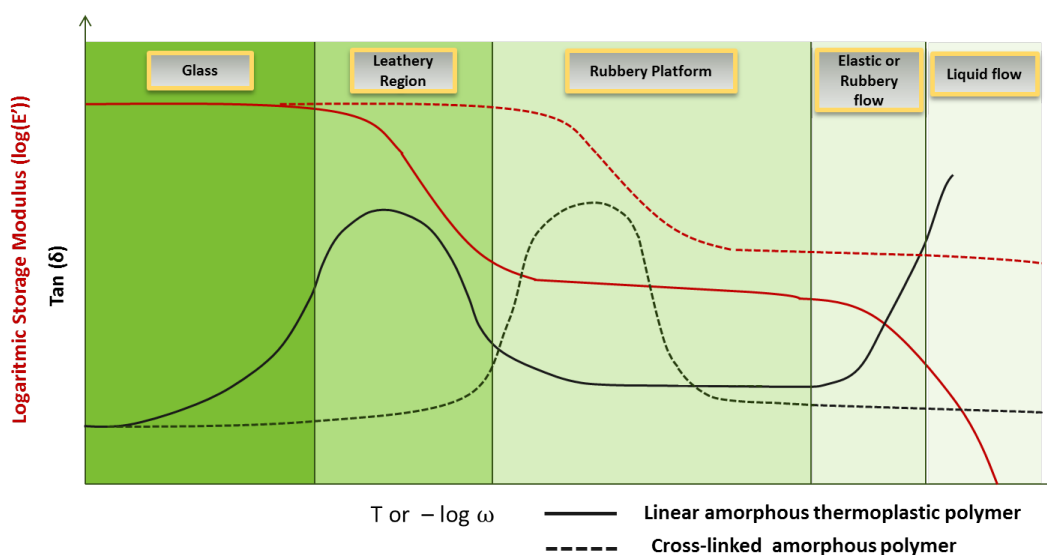
Figure 4.11: Illustration of the $\tan(\delta)$ and the Storage Modulus (E') characteristics for a linear amorphous polymer and a cross-linked amorphous polymer, illustrating various distinct physical states that the polymer assumes with varying temperature or frequency [7].

With the parameters explained in the previous paragraph, the viscoelastic behavior of the DA-polymer series, which is a function of temperature and frequency of the applied stress, can be illustrated. However before discussing the behavior of the DA-polymers, the behavior of less complex polymers will be explained (polymers without a reversible bonds in their network). In figure 4.11 an illustration is given on the theoretical viscoelastic behavior of a linear amorphous polymer and a cross-linked amorphous polymer. The parameters characterizing the viscoelastic behavior, Storage modulus and $\tan(\delta)$ are plotted in function of temperature (T) and frequency of the applied stress, in logaritmic scale ($\log \omega$).

Let us first explain the behavior of a linear amorphous polymer. All linear amorphous polymers exhibit five physical states, presented in figure 4.11: the glassy, leathery, rubbery, rubbery flow and viscous state. We will go through this graph from left to right. In the figure 4.11 the left region corresponds to the glassy state. The Storage modulus is in this region fairly constant (10^9 Pa). This is followed by a glass transition, where the polymer changes from a glassy to a rubbery consistency. In this transition region, the leathery region, the modulus decreases by three orders of magnitude to 10^6 Pa. Starting out as a rigid glass, the polymer then softens, varying from a stiff leathery consistency to a soft, pliable consistency. Above the glass transition in the rubbery plateau, the polymer has the truly elastic characteristics with modulus values in the order of 10^6 Pa. At higher temperatures the polymer exhibits elastic behavior but a noticeable tendency to flow, termed "rubbery flow". In this region the modulus values are of the order of only 10^5 Pa. At very high temperatures, the storage modulus drops very fast and the polymer starts to fully flow.

Cross-linked amorphous polymers do not exhibit the rubbery flow and the viscous liquid responses. If we consider a similar polymer as the amorphous polymer described in the previous paragraph, but with now cross-links (irreversible bonds) between the polymer chains the graph will change as follows: The cross-linking will influence the glass transition, shifting it to higher temperatures. Due to the cross-links the modulus will also be higher in the rubbery plateau. The cross-links, which are irreversible, will prevent the polymer to flow.
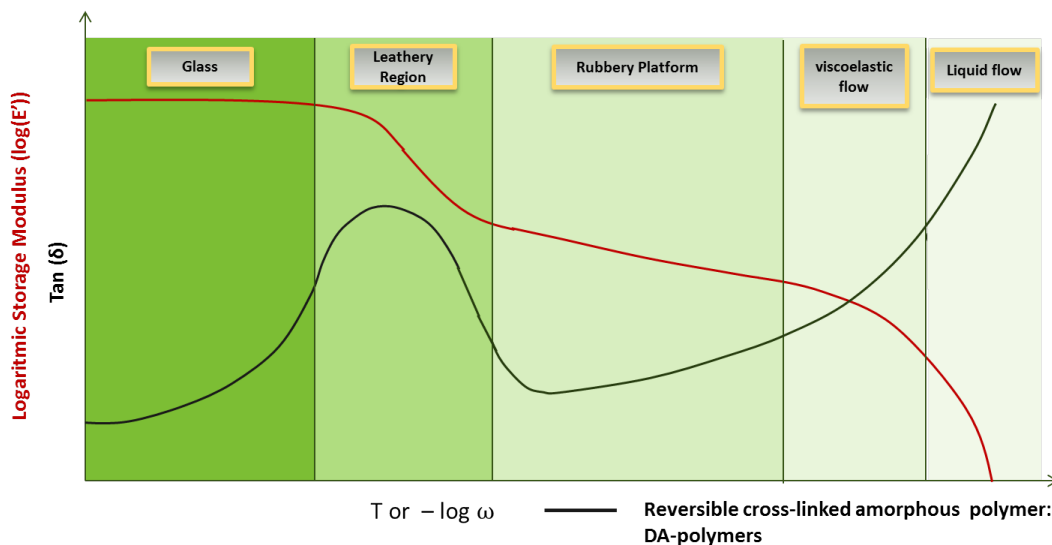
Figure 4.12: Illustration of the tan(δ) and the Storage Modulus (E') characteristics for a reversible cross-linked amorphous DA-polymer illustrating various distinct physical states that polymer assumes with varying temperature or frequency [7].

The DA-polymers consist of a network that is formed by cross-links of DA-bonds. Therefor at

relative low temperatures the DA-polymers have a visco-elastic behavior in function of temperature (and frequency) similar to the one of a cross-linked amorphous polymer. However, as explained in section 4.3.1, the concentration of DA-bonds, which form the network of the DA-polymer, decreases for an increase of temperature. At relatively high temperature almost all DA-bonds will be broken and the DA-polymers will have a viscoelastic behavior similar to the one of the linear amorphous polymer. In other words, if the DA-polymers are gradually heated up, the DA-bonds are broken and therefor the polymer exhibits a gradual transition from a viscoelastic behavior similar to the cross-linked polymer to a behavior similar to a linear polymer having fairly short polymer chains (figure 4.12).

On figure 4.12 the theoretical viscoealstic behavior as a function of temperature and $\log(\omega)$ is given for the DA-polymers. Due to the reversible DA-bonds, the Storage modulus will drop in the rubbery plateau. In contrast to the cross-linked amorphous polymer, the cross-link density reduces for an increase in temperature, such that the DA-polymers will exhibit a lightly viscous flow at high temperatures. In section 4.4.1 it was explained that the DPBM-FGE-Jx series differ in cross-link density. For an increasing cross-link density, the graph in figure 4.12 will change as followed:

- The glass transition will be shifted to the right.
- Due to this shifting the rubbery plateau will become shorter, since the rubbery flow and liquid flow region remain the same or shift to lower temperatures.
- The Storage modulus will be higher during the rubbery platform

Theoretical: Determining T_g by DMA Temperature Ramp Method [7]
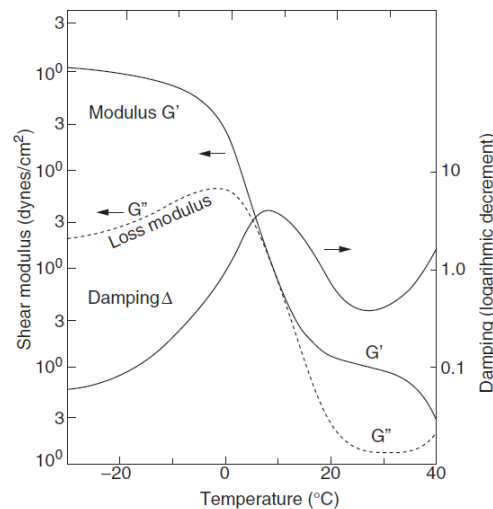
Figure 4.13: Theoretical DMA based on a Butadiene-Styrene Copolymer: Storage Modulus (E'), Loss Modulus (E") and Tan(δ) in function of temperature. The data illustrates that E" and Tan(δ) have different maxima [7].

The glass transition temperature (T_g) can be identified using a thermal DMA measurement, the Temperature Ramp Method. subjected to a sinusoidal strain (ϵ: eq. 5 Appendix A.3)

with a constant amplitude and frequency. The sinusoidal stress (σ: eq. 6 Appendix A.3) is measured for an increase in temperature with a constant temperature ramp. The storage modulus (E'), loss modulus (E") and tan(δ) can be calculated over the temperature interval. The T_g is generally easily to obtained from the DMA data because of the sharp decrease in storage modulus, E' and and the corresponding loss dispersion in E" or tan(δ) that occur at T_g, which can be seen in the theoretical graphs in figure 4.13. The criterion for selecting T_g from DMA data is either the peak in the loss modulus or the peak in tan(δ). Either one is valid, but the values are different. The $T(_g)$ obtained from the peak tan(δ) is usually several degrees higher than that from the E" peak. The tan(δ) peak corresponds more closely to the transition midpoint or inflection pont of the decreasing log(E") curve, while the loss modulus peak more closely denotes the initial drop of E' from glassy state into the transition. For polymers that have unusually broad glass transitions, e.g. in high crosslinked polymers, the peak tan(δ) will occur at a much greater ΔT. In general, the temperature at the maximum loss modulus is the more appropriate value. It is a reasonable criterion from molecular and practical or engineering perspective because the upper use temperature of many polymers is the "softening" point. The onset point is related to the initiation of segmental molecular motions of the polymer structure associated with T_g. At the tan(δ) peak this softening point has already been exceeded, which is why in this thesis we will use the maximum loss modulus value.

Experiments: Dynamic Mechanical Analysis
To analyze the (thermo) mechanical properties of the three DPBM-FGE-Jx series, three different experiments where carried out:

- Dynamical Mechanical Analysis (DMA)
  - Temperature Ramp method at a fixed frequency: To visualize the visco-elastic behavior and determine the T_g.
  - Multi-frequency test at fixed temperature: To show the influence of frequency on the complex modulus.
- Stress-Strain measurement until fracture: To measure the fracture tensile strength.

The three test will be discussed sequentially in the next subsections:

DMA: Temperature Ramp Method
In order to visualize the viscoelastic behavior of the self-healing polymer series, a DMA test, using the temperature ramp method was done on all three different series.

This Temperature Ramp Method was used on the three polymer series: DPBM-FGE-J400, J2000 and J4000. Since the mechanical properties are function of frequency, a DMA thermal analysis such as the temperature ramp method is typically carried out at a frequency of 1 Hz. For the DBPM-FGE-J400 and J2000 a fixed strain amplitude of 0.1 % was used, the test with the DBPM-FGE-J4000 was done with an amplitude of 1.0 %. All three tests were carried out over a temperature interval from -90 °C to 100 °C with a temperature ramp of 2 °C/min. The temperature was limited to 100 °C, because if the polymer would flow too easily it would damage the equipment. In figures 4.14, 4.15 and 4.16 the storage modulus, loss modulus and tan(δ) are plotted on a log scale in function of temperature on a linear scale. In the table 4.2 the Storage modulus, Loss modulus and the ratio between these two,

the tan(δ) at room temperature (25 °C) are presented for
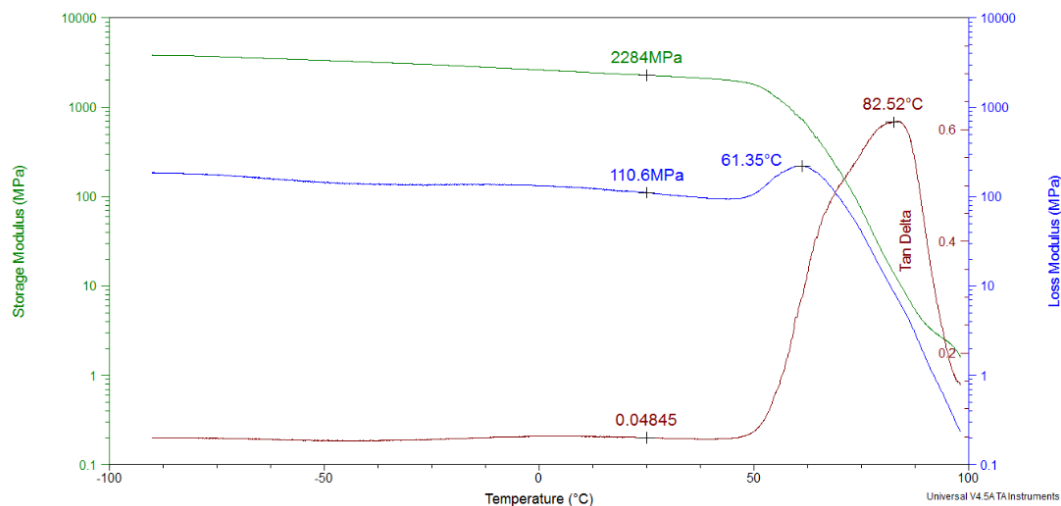
Figure 4.14: DMA Temperature Ramp method of a DPBM-FGE-J400 sample (solvent casting out of 10 w% CH$_3$Cl: sample size: length = 13.74, width = 4.08 and thickness = 0.36 mm, poisson ratio = 0.44, frequency = 1 Hz, strain amplitude = 0.10 and temperature interval from -90°C to 100°C with a temperature ramp of 2°C/min.
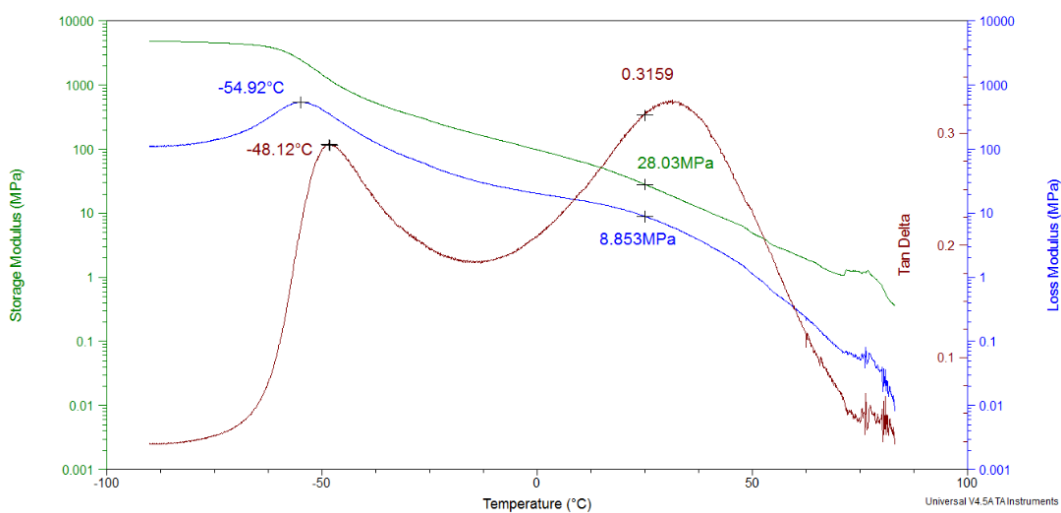
Figure 4.15: DMA Temperature Ramp method of a DPBM-FGE-J2000 sample (solvent casting out of 20 w% CH$_3$Cl: sample size: length = 19.93, width = 4.80 and thickness = 0.55 mm, poisson ratio = 0.44, frequency = 1 Hz, strain amplitude = 0.10, temperature interval from -90°C to 100°C with a temperature ramp of 2°C/min.

The DPBM-FGE-J400 series has a high cross-link density. The same trend, shown in the
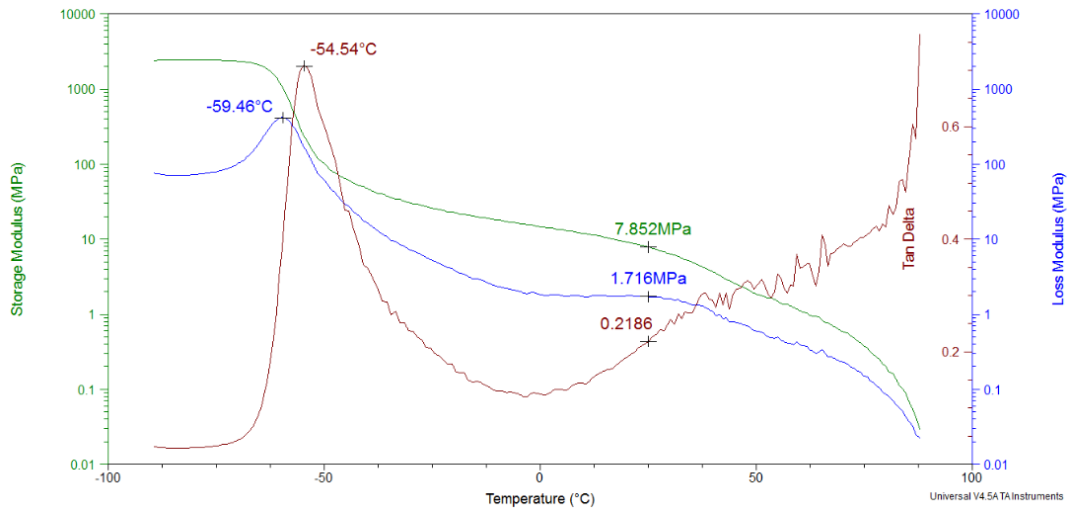
Figure 4.16: DMA Temperature Ramp method of a DPBM-FGE-J4000 sample (solvent casting out of 20 w% CH$_3$Cl: sample size: length = 6.93, width = 5.30 and thickness = 0.51 mm, poisson ratio = 0.44, frequency = 1 Hz, strain amplitude = 1.00 and , temperature interval from -90°C to 100°C with a temperature ramp of 2°C/min.

Table 4.2: Storage modulus, Loss modulus and tan(δ) of the three DPBM-FGE-Jx series at room temperature. Measurements were done using the DMA temperature ramp method (figure 4.14, 4.15 and 4.16).

Mechanical Properties DPBM-FGE-J series at 25°C			
Series	Storage Modulus (MPa)	Loss Modulus (MPa)	Tan(δ)
J400	2284	111	0,049
J2000	28,03	8,85	0,316
J4000	7,85	1,72	0,219

theoretical figure 4.12 is visible in the figure 4.14, but because of the high cross-link density, the glass transition region is shifted to the right. The glassy thermoset behavior of the J400 series is visible: the glass transition temperature (T$_g$) at 61.35 °C is above ambient temperature (25 °C). At ambient temperature the polymer finds itself in the glassy region (figure 4.12), where the storage modulus (2284 MPa) is high relatively compared to the loss modulus (111 MPa), which results in a low tan(δ), and indicates that at 25 °C there is almost no viscous contribution. At this temperature almost all the energy required to deform sample is elastically recoverable and the J400 series behaves like an elastic solid. Therefor we will consider the J400 series as elastic instead of viscoelastic at ambient temperature, with a Young's modulus equal to the storage modulus.

The DPBM-FGE-J2000 and J4000 series have a smaller cross-link density. Therefor it can be noticed in figure 4.15 and 4.16 that the glass transition region is shifted to the left. In contrast with the J400, the glass transition temperatures (T$_g$), T$_g$(J2000) = -54.92 °C and T$_g$(J4000) = -59.46 °C, are below the ambient temperature (25 °C). Therefor the polymers

find themselves in the rubbery region in figure 4.12, exhibiting an elastomeric behavior. At ambient temperature the loss modulus E" is significant relative to the storage modulus E' (E"(J2000) = 28.03 MPa and E'(J2000) = 8.85 MPa, E"(J4000) = 1.716 MPa and E'(J4000) = 7.852 MPa). The viscoelastic behavior of the two series makes it impossible to neglect the viscous contribution and attention should be given to this in the further applications.

The glass transition temperature T_g of the three polymer series is derived from the graphs, using the method explained in the theoretical part. The T_g of the three polymer series found are joined together with the T_g results obtained from DSC measurements [6] (section 4.4.2) in table 4.3. It should be noticed that the values obtained using both methods differ a few degrees, this can be due to measurement errors but of course also due to the frequency dependency of the T_g.

Table 4.3: Glass Transition temperatures (T_g) of the three DPBM-FGE-Jx series, measured with both Differential Scanning Calorimetry (DSC) [6] and Dynamical Mechanical Analysis: Temperature Ramp Method (figure 4.14, 4.15 and 4.16).

Glass Transition temperatures of DPBM-FGE-Jx				
Classification	Glassy Thermosets		Elastomers	
Series	J230	J400	J2000	J4000
DSC: Tg (°C)	63.9	55.5	-55.3	-64.6
DMA: Tg (°C)	/	61,4	-54,5	-59,6

DMA: Frequency Sweep Method

As mentioned in the theoretical parts above, the viscoelastic behavior of polymers depends on the frequency of the stress applied to the polymer. To analyze the influence of the frequency on the Storage modulus, Loss modulus and $\tan(\delta)$, a DMA using the Frequency Sweep Method was carried out. In this method the temperature is held constant, while the sample is subjected to a sinusoidal strain (ϵ: eq. 5 in Appenix A.3) with a constant amplitude and varying frequency. This DMA Frequency Sweep Method was performed for the three DPBM-FGE-Jx series, using discrete frequencies: 0.1; 0.3; 0.6; 1.0; 3.0; 6.0 and 10,0 Hz. Based on the frequency range used in robotic actuation, the testing frequencies were chosen in the frequency interval [0.1 - 10] Hz. The results are presented in Appendix A.4. For the DPBM-FGE-J400, the moduli does not change a lot in this frequency interval, the $\tan(\delta)$ varies between 0.031 and 0.033. Therefor the influence of frequency will be considered to be negligible for this series. For the DPBM-FGE-J2000 and J4000 series the moduli are influenced more by the frequency: $\tan(\delta)$ varies between 0.31 and 0.37 for the J2000 series and between 0.23 and 0.29 for the J4000 series. Because of this frequency dependency these two series will not be suitable for applications in which large frequency variations are required.

Fracture parameters: Static Stress-Strain Test

To derive the fracture stress and strain a Static Stress-Strain Test until fracture was carried out for the three series. This test was done with minimum four samples for each series. For each series a mean value of the fracture strain and fracture tension was calculated and the maximum deviation. The stress-strain curves and the fracture measurements are represented

in figures 9, 10 and 11 in Appendix A.5 and the table 4.4. It can be noticed that the variation of the fracture measurements, fracture tension and fracture strain, vary over a broad range, especially for the DPBM-FGE-J400 series (due to practical reasons). These variation are due to small defects, cracks or remaining CH_3Cl bubbles, in the rectangular samples, but also due to measurement errors. The samples used are relatively small (standard samples for the DMA: length = 40 mm, width = 5.5 mm, thickness depends on the sample sheet), in particular the DPBM-FGE-J400 samples which have the f.e. following dimension: length = 20 mm, width = 1.5 mm, thickness = 0.3 mm. The length of the sample is automatically measured by the setup, however the width and thickness are manually measured using calipers. Due to measurement errors and the limited precision of the measurement of width and thickness, a relatively large error is induced on the measurements, especially for the smallest samples used for the J400 series measurements.

Table 4.4: Results of the stress-strain tests on the DA-polymer series: DPBM-FGE-J400, J2000 and J4000. For each series four samples were tested, the results presented are the mean of these four measurements. For both the mean fracture stress and strain the maximum total deviation is given.

Fracture measurements			
DA-Series	Fracture Strain	Fracture Strain Variation	Fracture tension	Fracture tension Variation
	(%)	(%)	(MPa)	(MPa)
DPBM-FGE-J400	1,24	± 0,69	17,67	±9,65
DPBM-FGE-J2000	130,9	±39,0	3,10	±0,41
DPBM-FGE-J4000	445,9	±128,7	2,41	±0,79

4.4.4 Mixing Ability

The studied polymer series differ only in spacer length, which makes it possible to mix different furan compounds with different degree of polymerization during the synthesis of the SH-material. Using this mixing method a DA-polymer is obtained with a mixture of spacer lengths. In this way a polymer with desirable material properties lying in the broad interval between the two extreme (J230 and J4000) series can be obtained. This mixing ability is a great advantage since it provides a certain degree of freedom in the self-healing actuator design.

4.5 Conclusion

The syntheses of the three polymer series, which will be used in the applications explained in the following chapters 5 and 6, were discussed. This was followed by a general explanation of the SH-process of the DA-polymers. The Kinetics/Equilibrium simulation was introduced. This simulation will be used to design the temperature profile for the SH-process of the DA-polymer series used in the applications. Next a theoretical part was given on the viscoelastic behavior of polymers and in specific of the DA-polymer series. The thermo-mechanical properties of the three polymer series: DPBM-FGE-J400, J2000 and J4000 were measured using

different tests in the DMA setup.

Comparing results of these experiment between the different series, it can be concluded that the mechanical properties: storage modulus, loss modulus, fracture strain and stress, vary over a broad range. By varying the spacer length of the furan functionalized compound, series are synthesized with different mechanical properties but with the same self-healing mechanism incorporated, the reversible DA-bonds. The DPBM-FGE-J400 series has a glassy thermoset behavior, while the J2000 and J4000 have an elastomeric behavior. In addition, due to the mixing ability, the mechanical properties of the DA-polymers, can be designed to be anywhere between the properties of the most brittle, glassy thermoset, the J230 series and the most ductile elastomer, the J4000 series. In this thesis we will not synthesize or use a mixed series, however in the future this mixing ability might be very useful since it introduces a certain degree of freedom in the self-healing actuator design.

The (thermo) mechanical properties derived in this chapter will be used in the designs of the two different actuator applications in which the DA-polymers will be incorporated. The design, production and evaluation of these two actuator applications will be discussed in the two following chapters 5 and 6.

Chapter 5

Self-Healing Series Elastic Actuator (SH-SEA)

The process to obtain a first conceptual design for a self-healing series elastic actuator (SH-SEA) will be described in this section. In the first subsection 5.1 the choice will be made between the two main ideas for importing the self-healing mechanism in a series elastic actuator (SEA): the SH-mechanical fuse concept and the SH-compliant element concept, proposed in section 2.2.1. After which the conceptual design for the chosen mechanism is explained. In the second subsection 5.2 the techniques to process the self-healing mechanism into the required shape, according to the conceptual design, are described and a first prototype is presented.

5.1 Conceptual design

5.1.1 Concept choice: compliant element or mechanical fuse concept

During the design phase the practical use of the chosen self-healing materials (section 3.3), the Diels Alder Self-Healing material series, will be taken in account. As already mentioned in section 4.4.1, thermosets as well as elastomer-like DA-polymers can be produced by varying the spacer length and by using the mixing ability. Due to this big advantage, the DA-polymers can be used for the two self-healing concepts.

In the SH-mechanical fuse concept a thermoset DA-polymer, e.g. -J230 or -J400 or thermoset mixture between these two (section 4.4.4), will be used. As already mentioned in section 4.4.3, these thermoset series can be considered to be fully elastic instead of visco-elastic at ambient temperature, with a Young's modulus equal to the storage modulus. These polymer series possess a rather high Young's (Storage) modulus and therefor, exhibit small strains before fracture. Due to these negligible strains the mechanical fuse, in series with the original compliant element, will have no (or minimum) mechanical contribution. In the second concept, the SH-compliant element will be built out of an elastic DA-polymer, e.g., out of series -J2000 or -J4000 or an elastic mixture.

Three important aspects have to be taken in account in the choice between the two main concepts and are explained in the following subsections: the fracture surface, the cooling gradient and the dynamic or static behavior during normal operation.

The importance of the fracture surface

To create a self-healing actuator, which can function entirely independent, the fracture surface will be a very important design parameter. After fracture the two formed fracture surfaces need to be brought together to start the healing process by local heating. To do this in an easy way it is preferable that the two surfaces fit properly, in such a way that minimal local heating is required and that the healing process can be carried out in a static joint position. More specifically, we want that the polymer will not have a viscous deformation before fracture occurs, which may result in local necking (figure 5.1).

viscous behavior   non-viscous behavior
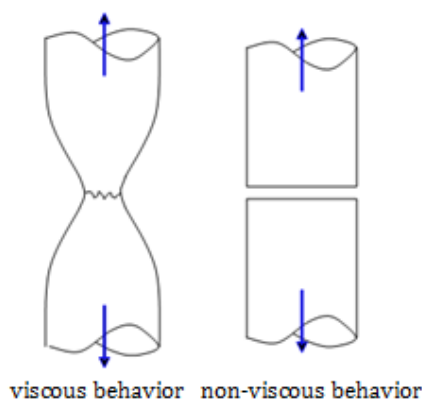
Figure 5.1: Left: Theoretical fracture of polymer with visco-elastic behavior, containing a viscous component (plastic deformation) at ambient temperature, resulting in a fracture with necking. Right: Theoretical fracture of a polymer with elastic behavior, containing no (or a very small) viscous component at ambient temperature, resulting in a brittle fracture with no necking.

Due to this necking the surfaces will not fit properly and therefor, the automatic, stand alone, healing process will become more complex. The two surfaces have to be pressed together simultaneously with local heating such that the surfaces can recombine and heal gradually. This requires more precise position control and heating over a larger area in comparison with the brittle fracture surface healing system. This is because it is important to obtain the initial shape and cross-section of the fuse after healing to maintain the same mechanical fuse properties, namely fracture tensile strength.

The Diels-Alder elastomer polymer series, -J2000 and -J4000, which will be used in the compliant element concept, are elastic solids with lower storage Modulus due to longer chain segments between cross-links and possess a non-negligible viscous component at ambient

temperatures (section 4.4.3). This viscous behavior induces necking before fraction at ambient temperature, which is observed for the samples of the elastomeric polymer series. The brittle -J400 series, used in the mechanical fuse concept, however, has a negligible viscous component and will break with a clean fracture surface, without the occurrence of necking.

The importance of the cooling gradient

As mentioned in section 4.3 the cooling temperature profile from elevated temperature to ambient temperature, at the end of the self-healing procedure, is extremely important and will affect the recovery of the initial material properties. The material has to remain long enough at elevated temperature, at which the polymer chains have certain mobility, such that the furan and maleimide groups can be organized to form the DA-connections. The mobility of the furan functionalized compound depends on the Jeffamine series used in the synthesis. The longer the polymer chain of this compound, the more mobile these chains are (section 4.4.1). However, longer chains result in a lower Diels-Alder bond concentration. At elevated temperature, where the network falls apart, there are less maleimide and furan present. Due to this lower concentration, when cooling down, it takes longer to form the network. Therefor, it should be noted that for the series with larger polymer chains (J2000 and J4000) a slower cooling rate is required.

Dynamic or static behavior during normal operation

It is important to look how the two concepts are functioning during normal operation of the self-healing actuator. In the mechanical fuse concept the mechanical contribution of the fuse is minimized. Due to this we obtain a system part which is fully static during "normal" operation and which is only dynamic when the SH-actuator is overloaded, e.g. when fracture occurs. However, in the compliant concept, the self-healing system part will be dynamic during "normal" operation. Due to the high tensions in the material (near fracture tension), the viscous component at ambient temperature of the elastic SH-polymer will cause permanent plastic deformations, which changes the mechanical properties of the compliant element. Therefor, the mechanical properties of the compliant element will change during operation of the actuator, which is unwanted.

Conclusion: concept choice

In the previous three sections, three disadvantages of using the elastic polymers in the design are mentioned: the viscous behavior leading to necking, the healing that takes more time and the dynamic behavior in "normal" operation. This is why in what follows the focus will be on the SH-mechanical fuse concept, since the realization of this concept will be more feasible. However, this does not imply that the SH-compliant concept is not feasible. For the self-healing material in the Self-Healing Mechanical Fuse (SH-MF) the DPBM-FGE-J400 series will be used, since the J230 is too brittle to work with due to its very high cross-link density.

5.1.2   Self-Healing Mechanical Fuse (SH-MF) conceptual design

SH-MF: Main idea

Before going into detail in the actual conceptual design, the main idea of the SH-MF is briefly repeated. The mechanical fuse, as the name indicates, will protect the expensive, and components, which are difficult to replace, of the compliant actuator, more specific: the motor, the gearbox and the compliant element. The mechanical fuse has to break sacrificially before a potential damaging overload occurs on one of the three previously mentioned components. When the fuse is broken, the compliant actuator will be put into an offline mode, in which the self-healing mechanism of the fuse can be started. When the healing of the fuse is completed the actuator can be put online again. Using this principle all components of the actuator are protected and there is no need for these components to be over-dimensioned to withstand the overloads. The objective is to design this self-healing cycle fully autonomous, such that no human interference is required. The SH-MF can be placed into, for example, one of the most simple compliant actuators, the Series Elastic Actuator (SEA) (figure 5.2), in series with the compliant element, which is usually a spring. However, the SH-MF principle could also be used in other, more complex compliant actuators: for example in a MACCEPA or a SPEA [14, 16].
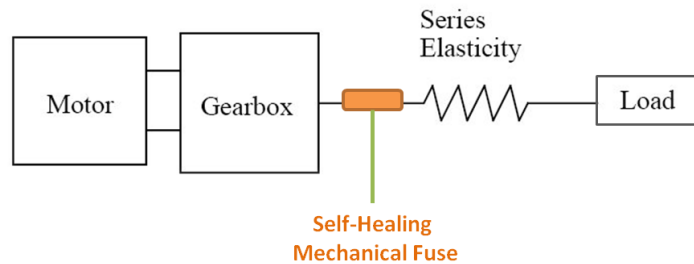
Figure 5.2: Schematic illustration of the Self-Healing Mechanical Fuse Concept imported in series with the compliant element of a Series Elastic Actuator (SEA) to for a Self-Healing Series Elastic Actuator (SH-SEA).

SH-MF: conceptual design

In this subsection the actual conceptual design of the SH-MF will be briefly illustrated. The different components will be discussed and the decision leading to the final design are rationalized. In figure 5.3 the design is visualized. The SH-MF has a length of 94 mm and a width of 12 mm. For the implementation of the SH-MF in the robotic actuator it would be more ideal if the fuse would be smaller, but for practical reasons this first type will be designed in the centimeter scale. In figure 5.4 the assembly of the different individual components and the assembled mechanical fuse are presented.

In figure 5.4 the self-healing parts can be seen in orange. These are two cylindrical parts
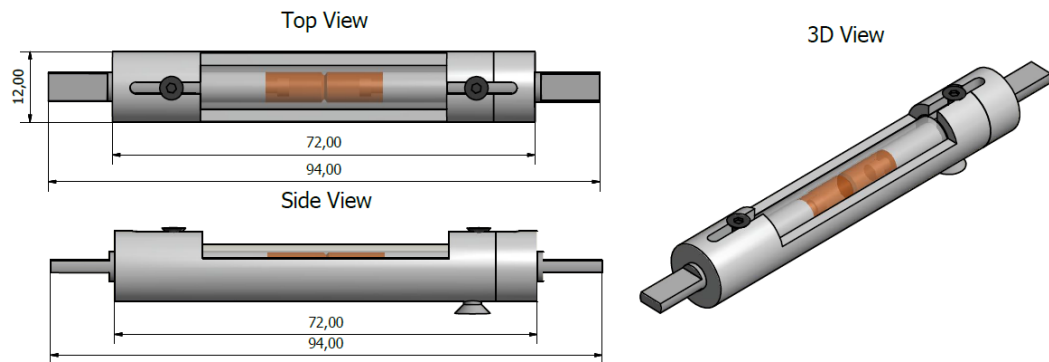
Figure 5.3: Illustration of the Self-Healing Mechanical Fuse concept design. Dimensions indicated are in mm.
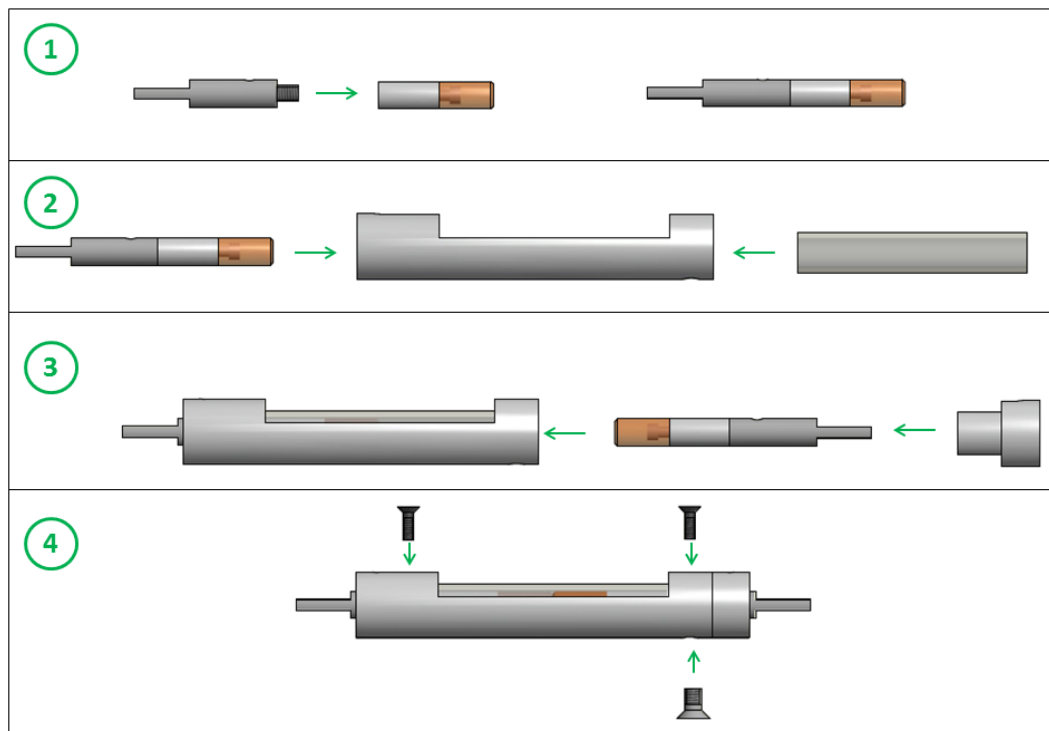
Figure 5.4: Illustration of the different parts of the Self-Healing Mechanical Fuse (SH-MF) concept design. The assembly of the SH-MF is illustrated stepwise.

which will be joined together using the self-healing property to form the center of the fuse. Before getting more in detail on the mechanical design of the fuse, the shape of these SH-parts will be explained.

The self-healing parts are designed to be cylindrical because of the construction limitations on the design of the self-healing fuse. But it has an advantage as well: during construction and healing misalignments due to small rotations of the parts relative to one another are not an issue. The diameter of the cylindrical part is 5 mm and the length is 10 mm. To induce the brittle fracture on a desired precise location and not for example at the connection of the SH-material to the other system parts, a groove will have to be made into the cylindrical self-healing part. A lot of different groove shapes exist like for example circular-, U- or V-shape grooves and a choice has to be made to obtain the largest stress concentration on the desired fracture location. Based on theoretical curves presented in literature [8] a V-groove, of 0.25 mm deep and with an angle of 90°, was chosen in the design (for calculations: Appendix: Stress-Concentration Groove), resulting in a stress concentration factor $K_t = 2,2$. Therefor the end edges of the cylindrical SH-part will be made into a chamfer with an angle of 45° (figure 5.5) and a depth of 0.25 mm.

The DPBM-FGE-J series stick very well on glass and metal when heated near their gel temperature (T_{gel}). This property is used to connect the self-healing polymer part to a steel pin. To create a solid connection, which will not break when the mechanical fuse is put under a load, the steel pin is provided with a T-shape end, over which the SH-material will be pressure molded (section 5.2). Afterward this is connected to a longer steel pin using a threaded connection (figure 5.4 (1)). From now on this assembly will be addressed as the "SH-Assembly".
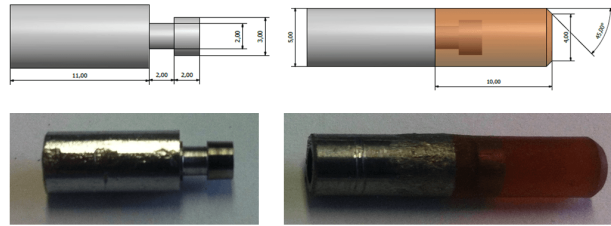
Figure 5.5: left: Sketches and pictures of the steel pin, with a T-shape end. Right: the part created by connecting the SH-part on the steel pin (this connecting process is discussed in section 5.2).

Two SH-Assemblies are inserted into a glass tube (figure 5.4 (2) and (3)), which is placed in an aluminum "cover". The two SH-Assemblies can slide in this cover part. The glass tube is used such that we can visualize the fracture. The rotation of the cylindrical SH-Assemblies around the axial axis is prevented by inserting screws in these components which slide in grooves made in the cover.

How will this fuse work in principle if we consider that it will be inserted in a SEA (section 5.1.2)? Before the fuse can be used, the two self-healing parts are joined together by a self-healing process, as mentioned above. This healing process can be done before inserting the fuse in the SEA or afterward if the SEA is containing a controlled heating device which can function fully autonomously. Once healed, the actuator can be put online. Whenever

an overload occurs, it will make the tensile stress acting on the fuse exceed the maximum tensile strength, and the joined SH-part will brake at the location of the V-groove. Due to this V-groove and the brittleness of the material, the two SH-parts, with just about the same shape as the initial two SH-parts, will be retrieved. The two screws inserted into the SH-Assemblies not only prevent rotation of the parts but will also limit the sliding of the two components in the cover. Two stages of the MF can be considered: the "working stage" in which the SH-material is not fractured and the MF has a minimum length, and the "fractured stage" in which the SH-material is fractured into two pieces and the MF has a maximum length. When implemented in a soft actuator the length of the MF will be measured continuously to check the stage of the MF. Adequate actions will be taken by the system if the MF is fractured and the actuator system will be put as fast as possible in an offline, safe mode.

The idea is that when the SH-MF is fractured the actuator system will start the SH-process fully autonomously. To do this a heating device with a pre-programmed controller should be implemented in the SH-actuator system. With the controller the heating device can produce a specific temperature profile (section 5.3) required for the SH-process. In this thesis, however, the SH-MF will not yet be implemented in an actuator design. The SH-process will be done in an oven, of which the temperature will be controlled manually.

SH-MF: first prototype

A first prototype of the Self-Healing Mechanical Fuse (SH-MF) was 3D printed in ABS-plastic (pictures are presented in Appendix A.10). This was done because 3D printing is relatively cheap and fast. Using this first prototype, the design could be checked for possible mistakes. After the analysis of this prototype, some small adaptations were made in the design (e.g., adaptations on dimension to improve assembly fits). Taking these adaptations into account, a second prototype was made in metal. The cover was made in aluminum, while the pins, which require some strength to resist against the tensile force, were made out of steel. Two copies of this metal prototype, presented in figure 5.6, were made.

Figure 5.6: Left: Picture of the parts of the Self-Healing mechanical fuse. Right: The assembled Self-Healing Mechanical Fuse: top view, side view and bottom view.

5.2 Processing of SH-material

This section is devoted to the process used to shape the Diels-Alder polymer series, DPBM-FGE-J400, from the porous powder, which synthesis was discussed in subsection 4.2.2, to the cylindrical SH-part used in the SH-mechanical fuse, which design was explained in section 5.1.

To recapitulate the design of the SH-part, explained in the previous section 5.1: the polymer has to be shaped into a cylindrical part with a diameter of 5 mm and a length of 10 mm. This cylindrical part is fixed on a steel pin, which is provided with a T-shape end, over which the SH-material will be pressure molded (figure 5.7). To induce the brittle fracture on a desired precise location, a V-shaped groove has to be made into the cylindrical self-healing part. Therefor the end edges of the cylindrical SH-part will have to contain a chamfer with an angle of 45 ° (figure 5.7) and a depth of 0.25 mm. In what follows the shaping process is discussed and explained step by step.
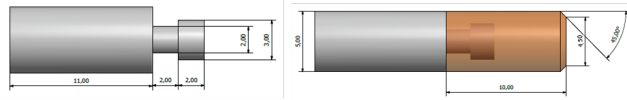
Figure 5.7: Left: Sketch illustrations of the steel pin, with a T-shape end. Right: Sketch Illustrations of the part created by connecting the SH-part on the steel, which is provided with a T-shape end.

Step 1: Cold pressing in the manually hydraulic press
The first stage of the shaping process consists of pressing the porous polymer powder in a Teflon tube, using a manually hydraulic press. More information about the type of hydraulic press used, can be found in Appendix A.9.1. Teflon is used because of its chemical inertness, which is required for the heating process, taking place further in the shaping process. The empty tube is placed in a steel holder (figure 5.8) and this holder is placed on top of a bottom part. Thereafter the porous powder can be poured into the Teflon tube and is pressed into a cylindrical part using a steel press pin and the hydraulic press. The steel press pin used is the one visible in the figure MF-SH-part: left, which is provided with a T-shape end. After this cold pressing process the steel pin remains inserted in the compressed powder in the Teflon tube.

Step 2: Heating process
The whole assembly is placed in a pre-heated oven at 70 °C. Next, the oven was heated up to 120 °C with a heating temperature ramp of 2.5 °C/min. When the oven reached 120 °C,the hot assembly was taken out of the oven and quickly brought to the hydraulic press setup. The oven remained at 120 °C.

Step 3: Hot pressing in the manually hydraulic press
The hot assembly was placed in the hydraulic press. At the higher temperature of 120 °C

Figure 5.8: Left: Different parts used for pressing the porous polymer powder into a cylindrical Teflon tube, from left to right: Bottom part, Teflon tube and steel holder. Right: The parts assembled. The powder can be poured into the Teflon tube and using a steel press pin this powder will be pressed into a cylindrical part in the hydraulic press.

($T_{gel} = 119.5$ °C) a lot of Diels-Alder bonds are broken, therefor the porous polymer powder has a gel-like structure and can be easily pressed together. By pressing the polymer powder together at this elevated temperature air bubbles will be removed. The steel pin is pressed further down into the Teflon tube, using a bolt, which was screwed in the steel pin. The result after this hot pressing process is a nearly impermeable cylindrical polymer, containing no air bubbles. This cylindrical part, with a gel-like structure remains in the hot assembly.

Step 4: Cooling process
The hot assembly is placed again in the oven at 120 °C, after which the oven immediately starts to naturally cool down to 55.5 °C with a cooling temperature ramp of 0.5 °C/min. Like for the Self-Healing process this cooling process is important and has to be done with a low cooling gradient (especially at lower temperature: between 70 °C and 55.5 °C), such that the Diels-Alder bonds can be formed as much as possible (see section 4.3.2 and section 5.3). The result after this temperature/press process is visible in figure 5.9.

Figure 5.9: Self-Healing part after the temperature/press process described in steps: 1 to 4. a) Top View and b) Side View.

Step 5: grinding a chamfer in the edges of the cylindrical SH-part
Like mentioned in the previous section 5.1.2, a V-groove in the SH-part is required to obtain a brittle fracture on a desired location when the fuse reaches its maximum tensile force. Therefor a chamfer has to be made on the edges of the cylindrical SH-part. The chamfer has an angle of 45 ° and a depth of 0.25 mm, like indicated on the figure 5.7. The chamfer was made using a manual grinder (tool information in Appendix A.9.2) and the result can be seen in figure 5.10.

Figure 5.10: SH-part with chamfer on the edge.

Step 6: Polishing of the contact surface

Finally the circle-shaped contact surface of the SH-part will be polished. In the SH-Mechanical Fuse assembly the contact surfaces of the two SH-parts will be placed against each other. The two parts will be joined together by a Self-Healing process in which the gap between the two contact surfaces will be filled and healed (section 5.3). The initial gap between the two SH-parts should be as small as possible, as maximum contact is required between the two contact surfaces. The contact surfaces are therefor polished using a polishing machine and fine silicon carbine grinding paper (P4000).

5.3 SH-Mechanical Fuse: Self-Healing process
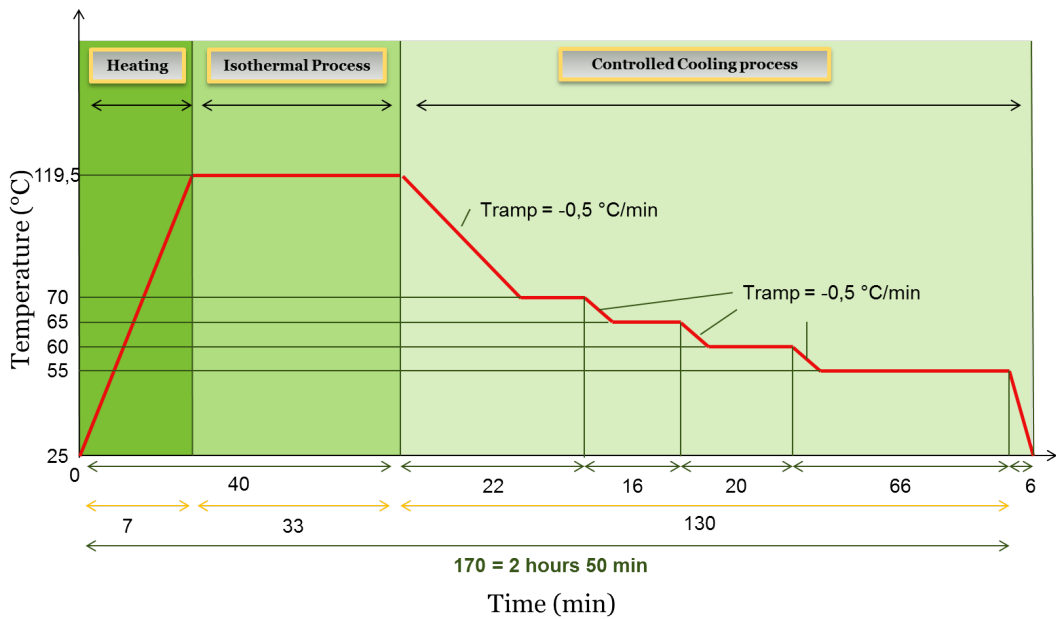
Figure 5.11: Practical Temperature profile of the Self-Healing profile of DPBM-FGE-J400 polymer in SH-mechanical fuse application. the SH-process is split in three stages: the heating stage, the isothermal stage and the controlled cooling phase.

In section 4.3.2 the SH-mechanism of the DA-polymer series was explained in general. In this section the temperature profile, which will be used for the healing process of the SH-mechanical fuse, will be explained using the kinetics/equilibrium simulation which was pro-

vided by G. Scheltjens [6]. To recapitulate, the SH-process consists of three stages: a heating process, an isothermal flow process and a controlled cooling process (figure 5.11). These three stages must meet a set of theoretical requirements, explained in section 4.3.2. However, the temperature profile presented in this section is a trade off between these theoretical requirements and what is practicable with the used heating devices. The designs for these temperature profiles of stages, visible in figure 5.11, will be discussed one by one in the following parts.

Heating stage

As mentioned in section 4.3.2 the heating up to T_{Ngel} can be done as fast as possible. This can be shown using the kinetics/equilibrium simulation provided by G. Scheltjens [6] and explained in Appendix A.1. We consider that when placed in a preheated oven at T_{gel}, the self-healing polymer will be heated up with a temperature ramp of about 15 °C/min. In figure 5.12 (in blue) the conversion response to a temperature increase from 25 °C to 119.5 °C, with a ramp of 15 °C/min is given. The reaction rate of the retro-Diels-Alder reaction (Appendix A.1 equation 1: $\frac{d[F]}{dt}$) increases with temperature, and therefor the kinetics of this reaction become faster with an increase of temperature. This can be seen on figure 5.12: at temperatures above 70 °C the kinetics become faster and the actual conversion (blue) will tend to go towards the equilibrium conversion (in black). On the blue graph it can be seen that when the temperature reaches T_{Ngel}, the conversion is almost equal to the equilibrium conversion. The red graph in figure 5.12 represents a hypothetical, instantaneous heating from 25 °C to 119.5 °C with an infinitely fast heating temperature ramp. To receive a conversion equal to the equilibrium at T_{Ngel} conversion the DPBM-FGE-J400 SH-part has to remain only for 60 seconds at this temperature. Because of this, the heating process until T_{Ngel} can be done as fast as possible. Therefor the fuse will be put in a pre-heated oven at T_{gel}. The time required for the SH-part to heat up to T_{Ngel} is 6.8 min, if it is considered that the heating temperature ramp, when placed in a pre-heated oven is 15 °C/min.

To determine up to which temperature the polymer could be heated up without any large deformations or flows, a theoretical calculation was done as well as a practical test. For both the theoretical calculation and the practical test, a cylindrical sample was placed in a position as shown in figure 5.3.a at a temperature of $T_{Ngel} = 119$ °C. The theoretical calculation, which can be found in Appendix A.7, were done for cylindrical parts with a diameter (D) of 5 mm and for two different lengths (L) of 10 mm and 20 mm. For the 10 mm part the theoretical maximum deflection (δ_{max}) was only 0.0093 mm and for the 20 mm part $\delta_{max} = 0.1481$ mm. Since the SH-parts in the MF are only 10 mm long, it can be concluded from this theoretical calculations that these small deflections will not be a problem in the design. To be sure a practical test was done with a cylindrical sample with a length of 20 mm and a diameter of 5 mm (figure 5.3.b). The sample was held at a temperature of $T_{Ngel} = 119$ °C for 3 hours. No visible deflection were observed after this test, from which we can conclude that the isothermal process can be done at 119 °C (figure 5.11) without problems of deformation.
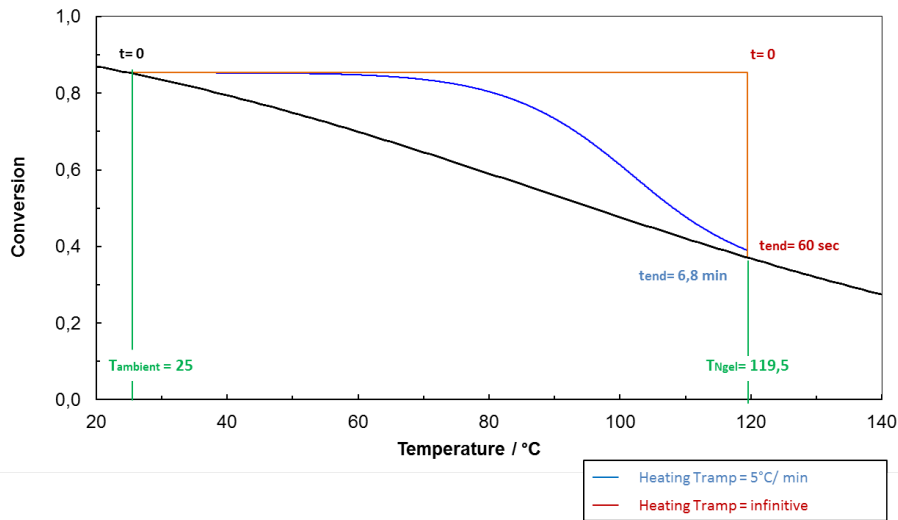
Figure 5.12: Kinetic/Equilibrium simulation (Appendix A.1) of the DPBM-FGE-J400 series used in the SH-MF. Simulation for a heating stage between $T_{ambient} = 25$ °C and $T_{Ngel} = 119.5$ °C with a temperature ramp of 15 °C/min and an infinitive temperature ramp.
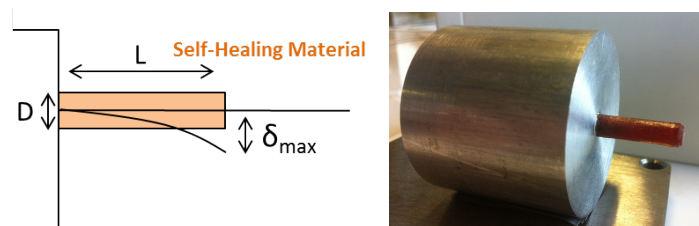
Figure 5.13: a) Sketch of the positioning of the cylindrical SH-part used in both the theoretical calculation (Appendix A.7) and the practical test. b) Practical test setup for measuring the deflection at a temperature of $T_{Ngel} = 119.5$ °C.

Isothermal flow stage

When the SH-polymer is brought up to 119.5 °C, enough DA-bonds will be broken to give the polymer chains the required mobility to slowly diffuse into macroscopic fracture gap and close it, a process which takes some time. It was experimentally seen that the time needed for fully filling the gap between the two SH-parts in the SH-MF is between 20 min and 30 min. This already contains the time needed to heat up the SH-MF in a pre-heated oven. Therefor in the healing process the SH-MF will remain at 119.5 °C in the oven over 40 minutes (figure 5.11), providing more than enough time for the polymer to seal the gap between the two SH-polymer parts.

Controlled cooling stage

Like mentioned in section 4.3.2 the cooling process is extremely important and will influence the conversion, stiffness and strength of the healed polymer. To find the right temperature

profile for this cooling process the kinetics/equilibrium simulation provided by G. Scheltjens [6] (Appendix A.1) was used.

For SH-polymer series that exhibit a glassy thermoset behavior at ambient temperature, like the DPBM-FGE-J400 series used in the SH-MF, the controlled cooling process will take place until the glass transition temperature (T_g) is reached. When the temperature reaches the T_g, the thermoset forms a highly cross-linked network in which the polymer chains have very little mobility. For temperatures below this temperature point the conversion will increase very slow towards the equilibrium conversion, roughly a factor 1000 slower then above T_g. In the SH-process of the SH-MF, the controlled cooling stage will be carried out between the T_{Ngel}: 119.5 °C and the T_g: 55.5 °C.

The oven used to perform the SH-process has a non-programmable temperature controller. Hence, a preferred temperature profile could not be inserted, instead the cooling profile had to be done stepwise by decreasing manually the oven temperature. To keep this process practical and reproducible, the stepwise cooling was carried out in four steps. To determine a proper practical cooling profile, e.g. the four step intervals and the related step durations, an analysis was done of numerous of Kinetics/Equilibrium simulations of different four step cooling profiles. The stepwise cooling profile and the four temperature intervals resulting from this analysis are visible in, respectively, figure 5.14 and table 5.1 and are discussed in the following paragraph.

The stepwise cooling described below was simulated for two different cases: for "closed oven method" and an"open oven method". The difference between these two methods is the cooling temperature ramps used for the steps in the cooling process:

- Closed oven method: During the stepwise cooling the oven remains closed. The oven cools with a temperature ramp of -0.5 °C/min during the steps.

- Open oven method: During the stepwise cooling the oven is opened during a step. Cooling takes place much faster with a cooling temperature rate of -5 °C/min.

Table 5.1: The step intervals and the step durations of the two simulation shown in figure 5.14. %x is the percentage of the equilibrium conversion that has to be reached before a step is completed and there may be continued to the next.

Interval	begin T	end T	% x	t until %x	
	°C	°C	%	TRamp = 0,5 °C/min in min	TRamp = 5 °C/min in min
1	119,5	70	99	103,1	21,6
2	70	65	99	15,5	10,8
3	65	60	99	19,6	15,2
4	60	55,5	99,9	65,4	61

The cooling process starts with a step from $T_{Ngel} = 119.5$ °C to 70 °C, which is a relatively large step compared to the ones who follow. This is because at high temperature the kinetics of the Diels-Alder equation are fast and therefor the Diels-Alder bonds are formed rapidly. It
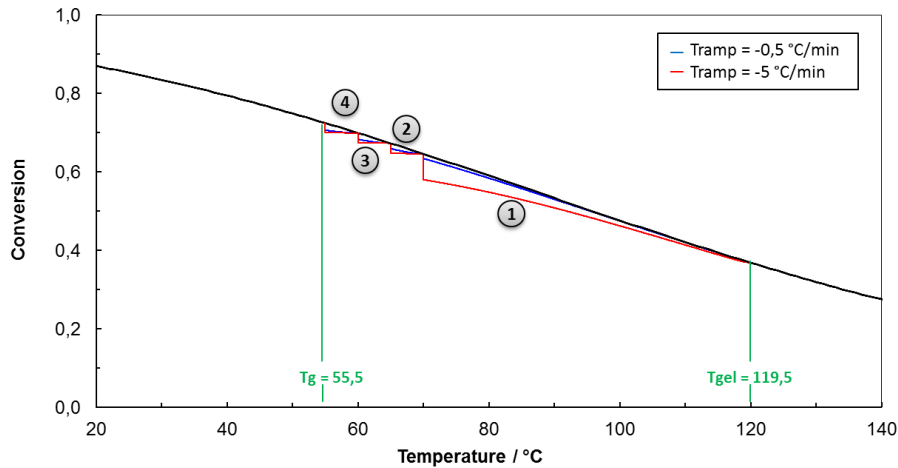
Figure 5.14: Kinematics/Equilibrium Simulation (Appendix A.1) of the DPBM-FGE-J400 series used in the SH-MF. Two simulation of the four steps controlled cooling process between $T_{Ngel} = 119.5\ °C$ and $T_g = 55.5\ °C$: one with a cooling temperature ramp of -0.5 $°C/min$ and the second with a ramp of -5 $°C/min$.

is not needed to stay for a long period at elevated temperatures above 70 $°C$ since the conversion, at high temperature, converges relatively fast towards the equilibrium conversion. This can be seen in the figure 5.14: above 70 $°C$, the conversion path of the "open oven method" and certainly that of the "closed oven method" do not deviate a lot from the equilibrium graph. At lower temperatures, below 70 $°C$, the kinetics of the reaction become significantly slower and as a result smaller steps of only 5 $°C$ are taken.

In the table 5.1 the step durations for both the closed and open oven method are listed. In this table the %x is the percentage of the equilibrium conversion that has to be reached before a step is completed and there may be continued to the next. If we compare the step durations of both methods it can be conclude that there is only a substantial difference between the durations of the first cooling step from 119.5 $°C$ to 70 $°C$. This is because at temperatures above 70 $°C$, the duration of the first step will be defined by the cooling temperature ramp of the step, while for the three remaining steps, at temperatures lower than 70 $°C$, the kinetics of the Diels-Alder reaction define the step duration. On basis of this, it was chosen to use the controlled cooling profile represented in figure 5.11, in which the oven will be opened during the first step and will remain closed during the further process.

Total temperature profile of the SH-process
In figure 5.11 the temperature profile of the full Self-Healing process is presented. This process will take 170 minutes or 2 hours and 50 minutes in total, after which the self-healing mechanical fuse will be fully cured. During the SH-process the mechanical fuses were placed in a holder, visible in figure 5.15. Using soft springs the SH-parts are gently pressed together such that there is maximum contact between the two contact surfaces of the parts during the self-healing process and only a small gap between the two surfaces. In figure 5.16 two pictures

are given of the SH-parts, which are joined after the self-healing process in the mechanical fuse. From now on these two SH-parts, which are joined, will be called the SH-specimen. Four of such SH-specimens were produced.

Figure 5.15: Holder with soft springs, in which the SH-MFs can be inserted. Due to the soft springs the SH-parts are gently pressed together in order to gain maximal contact between the two contact surfaces during the SH-process.

Figure 5.16: Pictures of the SH-parts which are joined together after the self-healing process in the mechanical fuse.

5.4 Experiments

In this section the experiments done on the self-healing mechanical fuse will be described and as well as the equipment used. the experimental results will be presented in this section, while the discussion of the data and the conclusion are written in the following section. First the experiment is explained in general, followed by a description of the equipment used and finally the actual measured data.

5.4.1 Experiment: Measuring of the fracture parameters of the SH-MF

To determine the fracture tensile force, stress and strain of the SH-MF, a "stress/strain tensile test until fracture" was used. Four self-healing polymer samples were made (processing was explained in section 5.2) and joined by the self-healing process described in section 5.3. The stress/strain tensile test was carried out one or two days after the self-healing process and at room temperature. To measure the influence of the self-healing cycles, the four samples were repeatedly self-healed and fractured in the tensile tests for three times, which makes a total of twelve tensile tests.

5.4.2 Equipment and testing parameters

The stress/strain tensile test was carried out in an universal testing machine (UTM), which is described in Appendix **??**. In order to place the SH-MFs between the clamps of the UTM, adapter pieces, with a required diameter of 10 mm, were screwed on both ends of the SH-MFs (figure 5.17). In figure 5.18 the SH-MF, placed in between the clamps of the UTM, can be seen. The stress/strain tensile tests were done with a controlled constant extension of 0.01 mm/min and the tensile force is measured with a sample frequency of 10 Hz.

Figure 5.17: Adapter pieces were screwed on both ends of the SH-MF such that the fuse could be placed between the clamps of the Universal Testing Machine (UTM).

Figure 5.18: The SH-MF which is placed between the clamps of the Universal Testing Machine (UTM).

5.4.3 Results

The results of the stress/strain tensile test are summarized in the table in figure 2, in Appendix A.8, and in the block diagrams in figure 5.19. The fracture strain and fracture stress were calculated using the measured fracture force and fracture displacement (for this calculation the actual diameter of the contact surface of the SH-part was used.
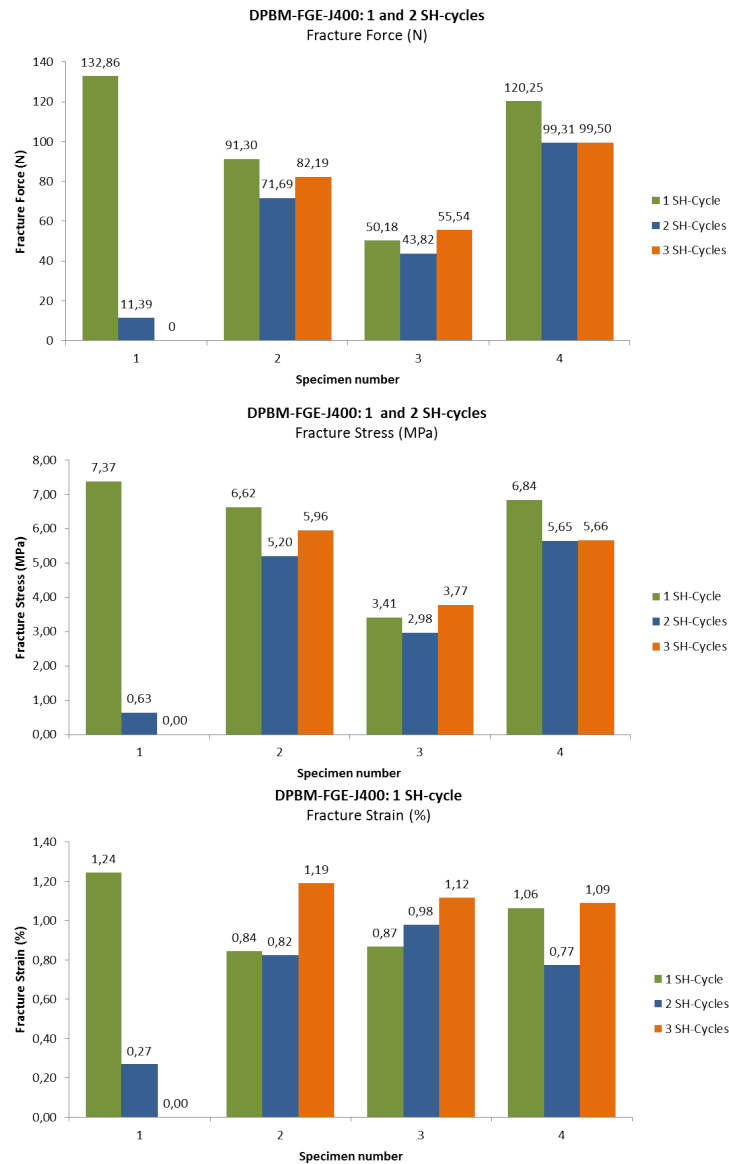
Figure 5.19: The results of the stress/strain tensile test until fracture of the 4 specimens which were inserted in the mechanical fuses. The fracture parameters are: fracture stress, strain and tensile force. These parameters were measured for the 4 specimens after 1, 2 and 3 self-healing cycles.

5.5 Discussion

First it has to be mentioned that the first SH-specimen that was made (specimen 1 in figure 5.19 and 2), could not be cured for the second time. During the first SH-process the two SH-parts were pressed too hard together which resulted in a deformation of the contact surfaces of the polymer parts. Although no macroscopic deformations occur at high temperatures under the natural weight of the SH-part, the piece will deform if a force is applied on it. Because of this it is extremely important that the pieces are pressed just a little bit together and that the springs are compressed only a little. Care has to be taken in the future applications: there has to be contact between the two pieces, which will be joined by the SH-process, but deformations will occur whenever a too large force is applied on the pieces.

If the fracture parameters: fracture force, stress and strain, after one SH-cycle, of the four different specimens are compared, it can be noticed that the values vary over a broad range, e.g. the fracture force varies between 133 N and 50 N. These large variations are mostly due to the shaping process of the SH-parts which is done manually. There might be small defects, impurities or chloroform CH_3Cl bubbles on the contact surface, which interfere with the SH-process. The chamfer at the edge of the SH-part, was made using the manual grinder (Appendix A.9.2) and it was impossible to create specimens with exactly the same chamfer using this basic tool.

What is more important is the reproducibility of the mechanical properties of the specimens after a SH-cycle. Lets compare the fracture parameters after each SH-cycle for the specimens individually. The fracture force and stress vary, but the results are in the same range. The variations are due to some parameters which influence the result of the SH-process: the pressure/force used to join the pieces together (something which is not measured), small defects on the contact surface which initiate the brittle fracture, and small deformations of the SH-parts that took place in the previous SH-process. What is interesting is that for increasing SH-cycles, there is no decreasing trend in the fracture force and stress. A decreasing trend in these parameters would mean that the mechanical properties would change after each SH-cycle. The strain is relatively small and is measured by measuring the extension of the whole fuse. Therefor these values are not very reliable since they can be influenced by for example small extensions in the parts of the assembled fuse other then the SH-parts.

All the tensile tests were carried out one or two days after the SH-process had took place. In section 4.3.2 and section 5.3 it is mentioned that the controlled cooling stage of the SH-process of the glassy thermoset series, DPBM-FGE-J400, is done in the temperature interval between $T_{gel} = 119.5$ °C and $T_g = 55.5$ °C. This because below the T_g the polymer chains lose a lot of mobility and therefor the conversion rate only increases very slow in time. Due to this can be considered that specimens that have been healed one or two days ago have approximately a conversion equal to the equilibrium conversion at $T_g = 55.5$ °C. As a result, the four specimens tested had approximately the same conversion during the tests. However if specimens remain at room temperature for a long period, weeks or months, before being tested (or used) in the UTM (or actuator), the conversion will have increased and the mechanical properties will have changed. This increase of conversion over a longer period has

to be taken in account in the future, if tests will be done over longer periods.

After being self-healed the specimen were stored in the lab at room temperature and the tensile tests were also carried out at room temperature. However a parameter which might have influenced the test result is the temperature history of the lab. Due to the slow increase in conversion at low temperature, the conversion of the polymer will depend less on the instantaneous temperature but more on the temperature history of the sample. The temperatures in the lab fluctuated between 20 °C and 28 °C in the period when the specimens were healed and tested in the UTM. Again due to the very slow conversion at low temperatures, it is assumed that this effect will not have had a great impact on the four specimens which were tested in the UTM after one or two days already. In the future it is recommended that the specimens will be stored in an air-conditioned cabin at a fixed temperature during the period between being healed and tested. Due to this temperature influence the SH-material will not be very suitable for applications where specific mechanical properties are required in an environments with fluctuating temperatures.

5.6 Conclusion

At first a choice was made between different ideas for the implementation of the Self-Healing mechanism in a compliant actuator and more specific in the Series Elastic Actuator (SEA). After an analysis, the principle of creating a Self-Healing Mechanical Fuse (SH-MF), which uses the glassy thermoset, DPBM-FGE-J400 polymer series, was considered to be the most feasible. Next a conceptual design of the SH-MF was created. Based on this design a first prototype was constructed in ABS plastic using a 3D printer. The prototype was inspected and some small adaptations were made in the design of the fuse. After this two copies of a second prototype were build in aluminum and steel, which would eventually be used for in the self-healing process and in the stress/strain tensile tests.

Using the material properties analyzed in the previous chapter 4 and practical trial and error, a shaping process was designed to shape the porous DPBM-FGE-J400 polymer powder into the desired cylindrical part, that would be used in the fuse. Two of these processed SH-parts were joined together by a self-healing process. The temperature profile of this process was determined by an analysis of the conversion in function of temperature and time, using the Equilibrium/Kinetics simulation provided by Scheltjens [6] (Appendix A.1). The two SH-parts, joined by the SH-process, will be called a SH-specimen.

Four of such SH-specimens were produced and were repeatedly healed and fractured, in a tensile test, for three times, which makes a total of twelve tensile tests. These tests provided data of the fracture force, strain and stress of the four fuses after one, two and three SH-cycles.

It can be concluded that the Self-Healing Mechanical Fuse could be healed at a relatively low temperature. The mechanical properties after three SH-cycles remain near the initial properties and depend on the quality of the SH-process. There was no decreasing trend of the fracture force and stress recorded, which indicates that the mechanical properties of the

fuse remain stable for at least three SH-cycles.

Both the shaping process of the SH-parts and the SH-process should be done in a more controlled way, such that influences such as: the chamfer at the edge of the SH-part and the pressure/force used to join the pieces together during the SH-process, are limited. In this way the variations of the fracture parameters between the different SH-MF will decrease. In the future, based on the influence of temperature and time on the conversion of the DA-bonds in the polymer, it should be considered to store the specimens in an air-conditioned cabin at a fixed temperature in between the SH-processes and the tensile tests.

5.7 Future Work on the SH-MF

In this thesis, the fuse was repeatedly subjected to a SH-process and fractured in a stress/strain tensile test for three times. From the results of the tensile tests it can be concluded that after the SH-process, the SH-MF retains its initial mechanical properties. However, in the near future it should be analyzed if this is also the case after a large number of SH-cycles (10, 30, 50 or 100).

The dimensions of the first SH-MF prototype (length: 94 mm, width: 12 mm) are to large to implement it in a series elastic actuator (SEA). A second, smaller and more elegant prototype, with a length of only a few centimeters (2 to 3 cm), has to be considered. The width and the length of the SH-part can easily be reduced, using a shaping process, similar to the one used in this thesis. The SH-MF design can be fine-tuned, to reduce its dimensions. As mentioned in the conclusion, in this second prototype, both the shaping process of the SH-parts and the SH-process should be done in a more controlled way, such that influences as: the chamfer at the edge of the SH-part and the pressure/force used to join the pieces together during the SH-process, are limited.

Up untill now the SH-process of the SH-MF is non-autonomous: the fuse has to be placed manually in an oven. In a third prototype, a controlled heating device (e.g., ohmic heater mats), using a temperature sensor (e.g., a thermocouple), has to be implemented in the design. This heating device will contain a programmable controller, which allows the heating device to produce a pre-programmed, specific temperature profile, required for the SH-process. To make the actuator system completely autonomous, a sensor has to be placed, which measures the length of the SH-MF continuously, to check whether the fuse is fractured or not. Whenever the fuse is fractured the actuator will be put in an offline mode, in which the SH-process can be started. If the SH-process is terminated, the actuator will be re-activated. This series of events will be done completely autonomously by the SH actuator system.

Chapter 6

Self-Healing Soft Pneumatic Actuator (SH-SPA)

In section 2 an introduction was given on Soft Pneumatic Actuators (SPA). In this chapter a feasibility study is performed on the construction of a Self-Healing Soft Pneumatic Actuator (SH-SPA) with the Diels-Alder polymer series described in chapter 4. The chapter starts with a section in which the conceptual design of a first prototype is discussed. This is followed by a part, explaining how the SH-material will be processed in the required shape. In the third section the design of the temperature profile for the self-healing process is clarified. Hereafter the experimental results are presented and discussed.

6.1 Conceptual design

6.1.1 Main idea: Self-Healing Soft Pneumatic Cell (SH-SPC)

To evaluate the potential of creating a SH-SPA from the DPBM-FGE-Jx series, the idea was to build a single Soft Pneumatic Cell (SPC) from the self-healing polymers. Most SPA, like for example the BSPA (figure 2.2) consist out of more cells, containing air chambers, which can be inflated by putting them under an over-pressure. From the start of the design it was assumed that if we were able to built a prototype containing a single cell out of SH-material, it would be straightforward to build a multi-cell prototype, a SPA.

Based on dimensions used in the literature [3, 4, 19, 20, 21, 22], it was decided to build a cubic cell with a side length of 15 mm. The dimensions of the cells used in the literature are a little smaller but such small dimensions would not be practical in the construction of a first prototype.

6.1.2 Choice of material

Soft pneumatic actuators are, like the name indicates, made out of soft polymer material. In the literature [3, 4, 19, 20, 21] most SPAs are constructed out of Ecoflex 00-30 (Smooth-On

Inc.), which is a very soft, elastic polymer with a tensile modulus of 69 kPa. The SH-material that will be used to construct the SH-SPC will be the most elastic series: the DPBM-FGE-J4000 series, which exhibits a tensile modulus (Storage modulus) of 7.8 MPa. The J4000 series is quite stiffer than the extremely soft Ecoflex, but this was the most elastic DA-series synthesized at the VUB.

In section 2.2.2 it was explained how in the design of most SPAs, the soft material (f.e. Ecoflexthe) was combined with a less elastic material to introduce a controlled anisotropy in the response of the elastomers to stress, caused by pressurizing the air chambers. Based on the BSPA (figure 2.2), one side, the bottom sheet, of the SH-cubic cell will be produced out of a less elastic material. When only one (cubic) cell is used, an anisotropic movement response cannot be created by pressurizing the air chamber. However, like mentioned in the introduction of the subsection 6.1.1, the author believes that if a one-cell prototype could be build, it would be straight forward to build a multi-cell prototype, which displays the anisotropic movement response.

The DPBM-FGE-J2000 (Storage modulus: 28 MPa) series is stiffer than the J4000 series (Storage modulus: 7.8 MPa) and is therefor suitable to be used as the less elastic material in the SPC design. Both the J2000 and the J4000 were synthesized (section 4.2.2) into sheets with a thickness of respectively 0.55 ± 0.04 mm and 0.76 ± 0.05 mm. In figure 6.1 the conceptual design of the first prototype of the SPC is presented.
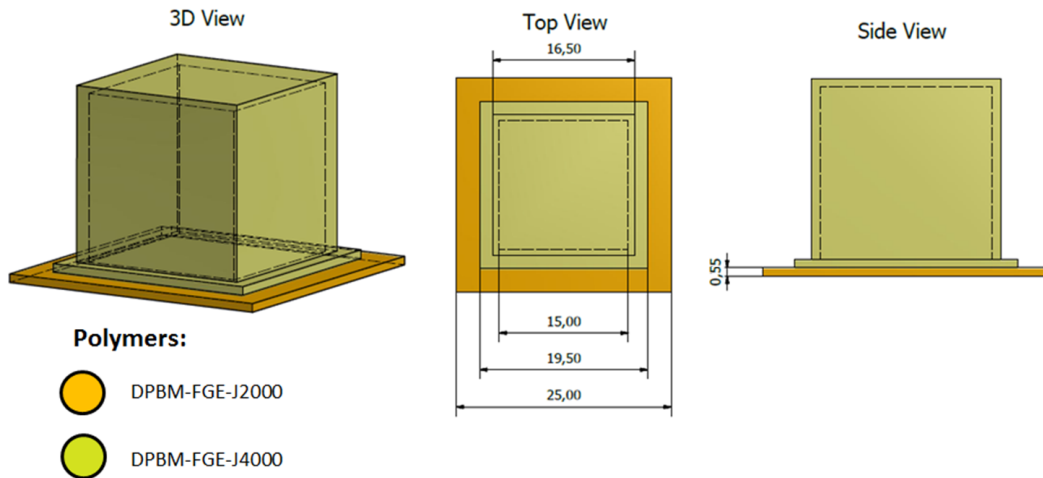
Figure 6.1: Conceptual design of the first SPC prototype, built using DPBM-FGE-J2000 and J4000.

The cubic part will consist out of an air chamber constructed out of the most elastic series: DPBM-FGE-J4000 (figure 6.1). The bottom plane of the cube will be constructed out of DPBM-FGE-J2000 which is stiffer. The two series only differ from each other in degree of polymerization (section 4.4.1) and therefor polymer chain length, Diels-Alder bonds can be formed in a self-healing process between the two polymers and they can be joined. Using

both the J2000 and J4000 series and their different mechanical properties, a fully self-healing part can be created in which the air chamber as well as the less-stretchable sheet have the self-healing property. In the bottom of the SPC, a small hole will be made in which a narrow metal tube (inner diameter: 2 mm) will be inserted through which the over-pressured air could injected in the cell.

6.2   Processing of SH-material

This section is devoted to the processing techniques used to shape the polymer sheets, of the DPBM-FGE-J4000 and J2000 series, into the cubic prototype discussed in the previous section 6.1.2. In this shaping process the self-healing property, of the polymer series, is used to create the 3 dimensional cubic part. The self-healing process is already explained in general in section 4.3.2, but will be explained specific for the SPC in a following section 6.3. In what follows in this section only the temperature profiles of the SH-processes used in the shaping process will be given and we will not go in detail in how the polymer series react on these SH-processes.

A Teflon mold (figure 6.2) was constructed in which the DPBM-FGE-J4000 sheets could be joined to form the top 3D cubic structure (figure 6.1: part in yellow). Teflon is used due to its chemical inertness and prevents the polymer from sticking to the mold, which would happen when glass or metal molds are used. First a plus shape was cut out of the synthesized DPBM-FGE-J4000 sheet (section 4.2.2) (figure 6.3 a and b). This plus sign is folded and placed into the Teflon Mold (figure 6.3 c and d).
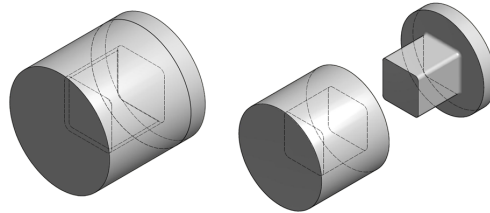
Figure 6.2: 3D autocad drawing of Cubic Mold used to construct the first 3D cubic structure using DPBM-FGE-J4000 and J2000.

To seal the sides of the cube, the self-healing property of the material will be used. The mold will be placed in an oven, at a temperature of 3 °C below the gel transition temperature (T_{gel}) (section 4.4.2). At this elevated temperature the polymer chains will have enough mobility to close the gaps between the vertical planes of the cube in a few hours. The temperature cannot exceed the T_{gel}, because the sheets inserted in the mold would start deforming. The self-healing process used to form the DPBM-FGE-J4000 (open) cube, is done in an oven at 78 °C (T_{gel}(J4000) = 81.0 °C) (section 4.4.2) for 4 hours. After this the part is cooled down naturally in the oven (gradient: ± 10°C/h) and gently removed from of the cubic mold (figure 6.4).

In the resulting open cubic part, there are a lot bubbles and cavities formed in the walls
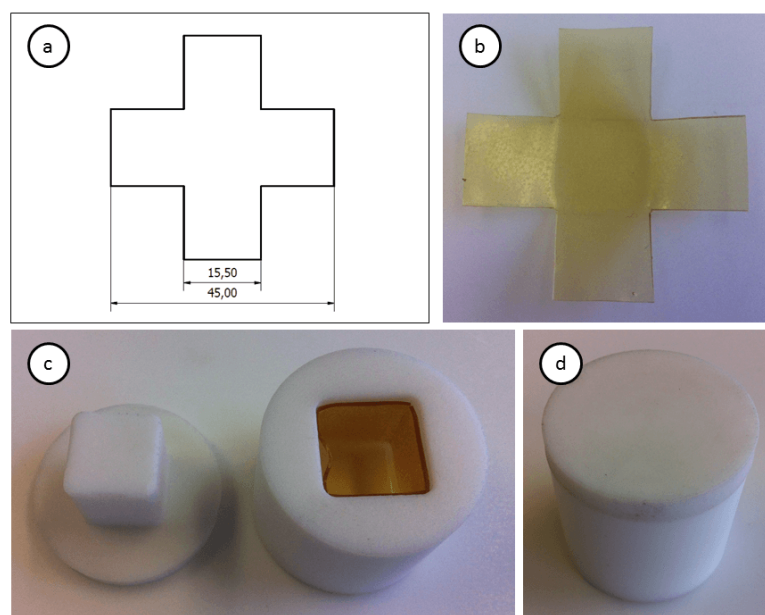
Figure 6.3: a) Technical drawing of the plus shape. b) plus sign cut out of the DPBM-FGE-J4000 synthesized polymer sheet. c)Cubic mold with folded and inserted DPBM-FGE-J4000 plus shape d) Closed cubic mold.

of the cube (figure 6.4). It is assumed that these are formed during the healing process due to remaining chloroform in the polymer. When the temperature as well as the polymer chain mobility increases, the diffusion rate of this chloroform increases. The chloroform molecules present between the polymer chains diffuse towards each other to form macroscopic bubbles and cavities in the polymer. This problem should be easily solved by extending the duration of the chloroform evaporation process (section 4.2.2) in the vacuum oven at 60 °C in the synthesis of the polymer DPBM-FGE-J4000. In the following subsection the percentage chloroform in the synthesized DPBM-FGE-J4000 polymer is measured.

Figure 6.4: Cubic part after being naturally cooled down in the oven and removed out of the cubic mold: Side-Top View and Side-Bottom View.

Thermogravimetric analysis (TGA)

In order to measure the percentage remaining chloroform in the DPBM-FGE-J4000 polymer a Thermogravimetric analysis (TGA) was done. This is a method where changes in mass are measured as a function of increasing temperature (with constant heating rate). The TGA instrument continuously weighs a sample as it is heated to temperatures. As the temperature increases, various components of the sample are decomposed and the weight percentage of each resulting mass change can be measured. The results are plotted with temperature on the X-axis and mass loss on the Y-axis.
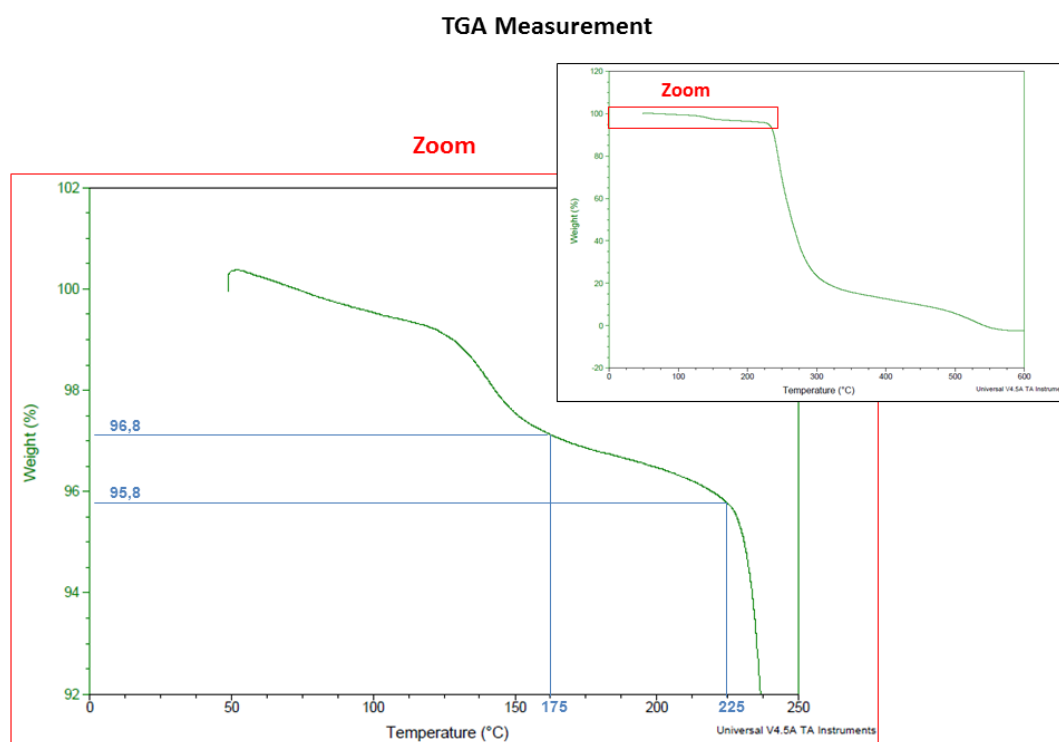
Figure 6.5: Thermogravimetric analysis (TGA) of DPBM-FGE-J4000 sample (sample size: 1.008 mg), using the Temperature ramp method: 0 °C to 600 °C with temperature ramp of 10.00 °C/min.

In figure 6.5, the TGA measurement for the DPBM-FGE-J4000 polymer sample is shown. In the zoomed graph it can be noticed that around 225 °C there is an onset point, after which the mass decreases tremendously, caused by the polymer which is decomposing. As a rule of thumb we consider that the actual start of the polymer decomposing is 50 °C before this point, at 175 °C. All mass losses before 175 °C are caused by the evaporation of the volatile chloroform. At 175 °C the mass percentage in function of the initial mass is 96.8 w%. The DPBM-FGE-J4000 polymer, used to create the 3D cubic part, contains still minimum 3.2

w% chloroform, which is the reason why bells and cavities are formed at higher temperature, during the self-healing process.

Afterward the bottom part of the cubic part was joined to the constructed DPBM-FGE-J4000 open cubic part. This bottom part is built-up out of a DPBM-FGE-J4000 sheet (figure 6.1: 19.5 x 19.5 x 0.75 mm) which was placed directly on the cubic part and a bottom DPBM-FGE-J2000 sheet (figure 6.1: 25.0 x 25.0 x 0.55 mm). The extra DPBM-FGE-J4000 sheet placed between the cubic part and the DPBM-GHE-J2000 sheet was used to create a better connection. The T_{gel} (section 4.4.2) of the J2000 series (98.5 °C) is higher than the one of J4000 (81.0 °C). The J4000 sheet was placed on top of the J2000 sheet, and this was placed in an oven at 90 °C. After 15 minutes at this high temperature, the top J4000 sheet turned into a gel-like structure, while the J2000 sheet remained solid. At that time, the sheets were taken out of the oven and the J4000 cubic part was quickly pushed on top of the gel-like J4000 sheet, which sealed the cubic part. The oven was brought to 60 °C before the whole part was reinserted. The oven was held at this temperature for 6 hours after which the oven was gradually cooled down at 10 °C/min to room temperature. The result is visualized in figure 6.6b and the actual dimensions of the part in figure 6.7.
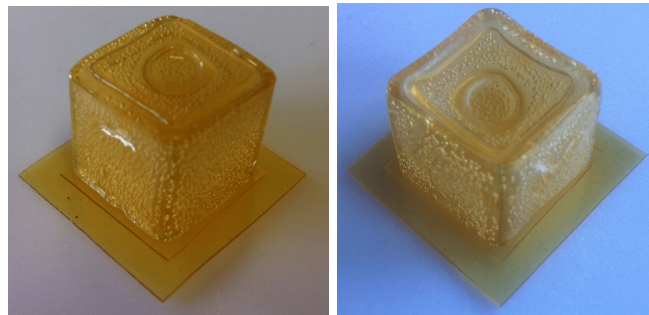
Figure 6.6: a) Cubic part, before self-healing to join the DPBM-FGE-J4000 cubic air chamber on the DPBM-FGE-J4000 bottom sheet which is placed on top of DBPM-FGE-J2000 sheet. b) Cubic part after self-healing.

Finally a small metal tube had to be inserted in the bottom plate of the SPC, presented in figure 6.6, through which the compressed air will be injected in the cell. The metal tube, which is screwed on a connector is shown in figure 6.8 a. A tiny hole was made in the bottom sheet of the cubic part with a needle. Two small pieces (5x5 mm) were cut out of the J4000 sheet and placed over the metal tube (figure 6.8 a). Next this metal piece was placed in an oven of 90 °C. Similar to the process used for sealing the cubic part, after the J4000 polymer pieces had received a gel-like structure, the metal piece was taken out of the oven. The hot metal tube was pressed through the tiny hole in the cubic part and the gel-like J4000 pieces sealed the connection. The oven was cooled down to 60 °C after which the assembly was reinserted and held at this temperature for 4 hours and cooled down naturally in the oven to room temperature. The result of the whole shaping process is visible in figure 6.8 b.

Dimensions 3D Cubic Part						
Material	DPBM-FGE-J4000				DPBM-FGE-J2000	
	a	b	c	f	d	e
dimension (mm)	0,76 ± 0,05	16,50 ± 0,50	18,5 ± 0,40	0,76 ± 0,05	24,75 ±0,30	55 ± 0,04
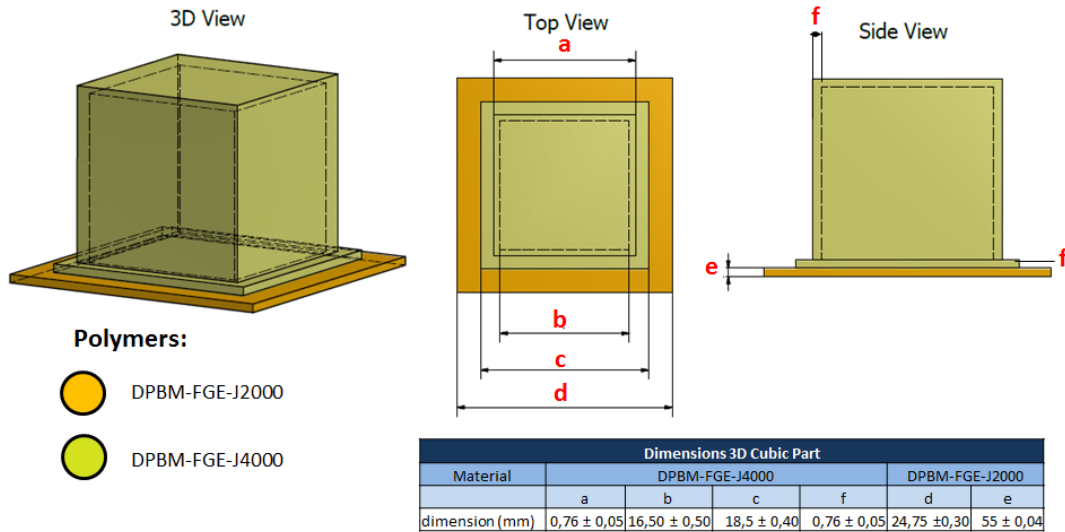
Figure 6.7: 3D cubic part: actual dimensions.

Figure 6.8: A tiny hole was made in the bottom plane of the 3D cubic part, through which a small metal tube, with a diameter of 2 mm, inserted. The metal tube is screwed on a connector part.

6.3   Self-Healing Soft Pneumatic Actuator: Self-Healing process

Like for the SH-process of the SH-MF, discussed in section 5.3, the self-healing process is divided in three stages (figure 6.9): The heating stage, the isothermal flow stage and the controlled cooling phase. The purpose of each stage is explained in section 5.3. In this part of the report design the temperature profile of the three stages and therefor the total SH-process will be presented and discussed. The temperature profile is a trade off between these theoretical requirements for the SH-process, discussed in section 4.3.2 and what is practicable with the used heating devices.
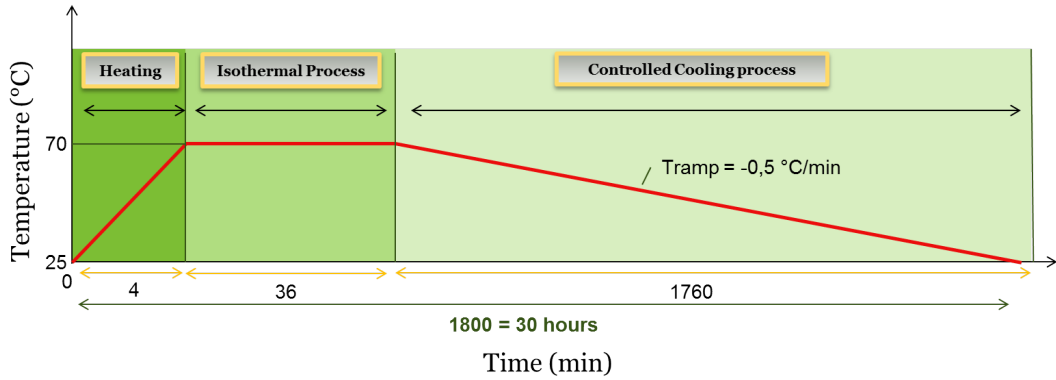
Figure 6.9: Practical Temperature profile of the Self-Healing profile of DPBM-FGE-J4000 polymer in SH-Soft Pneumatic Cell application. the SH-process is split in three stages: the heating stage, the isothermal flow stage and the controlled cooling phase.

Heating stage

Like mentioned before in temperature profile design of the SH-process of the SH-MF, the heating stage can be done as fast as possible (an explanation based on the Kinetics/Equilibrium simulations, explained in Appendix A.1, is given in section 5.3). Therefor when the SPC will be healed, it will be inserted in a pre-heated oven at near the gel transition temperature (T_{gel}), defined as the "Near gel temperature (T_{Ngel})". At high temperatures, upto 5 °C below the T_{gel}, the DPBM-FGE-J4000 series becomes soft and therefor the SH-SPA starts to deform and collapse. Therefor a safety factor is introduced and the isothermal stage is performed at a T_{Ngel} of 70 °C, 11 °C below the T_{gel}.

Isothermal flow stage

The isothermal stage is carried out at a T_{Ngel} of 70 °C, a temperature at which enough DA-bonds will be broken to give the polymer chains the required mobility to slowly flow into macroscopic fracture gap and close it. The SH-SPC is held at this temperature for 40 minutes (this value contains also the time required for the heating stage), giving the polymer enough time to flow into the gap.

Controlled cooling stage

The cooling stage, determines the conversion and therefor the mechanical properties of the DA-polymer after the SH-process and because of this it is very important that it is carried out in a controlled way. Like for the SH-MF, the temperature profile for this stage will constructed using the Kinetics/equilibrium simulation provided by Scheltjens [6] (Appendix A.1).

The oven, which was used, has a non-programmable temperature controller and therefor the cooling profile had to be done stepwise by decreasing manually the oven temperature. For the analysis of the temperature profile of this cooling stage, the number of cooling steps was limited to three, since a profile containing more steps is not really practical. This because

for each step the oven has to be manually regulated, which means that for a profile with a lot of steps, someone has to remain near the oven almost the entire SH-process. After an analysis of a number of Kinetics/Equilibrium simulations of different three step cooling profiles, the intervals between, $T_{Ngel} = 70$ °C and 50 °C, 50 °C and 40 °C and 40 °C and $T_{ambient} = 25$ °C were chosen (figure 6.10).

In figure 6.10 the results are given for Kinetics/Equilibrium simulations on four different temperature profiles. For both a three step cooling profile and a single step cooling profile, a simulation was done using "open oven method" and the other one using the "closed oven method". The two methods were defined in section 5.3 as:

- Closed oven method: During the stepwise cooling the oven remains closed. The oven cools with a temperature ramp of -0.5 °C/min during the steps.

- Open oven method: During the stepwise cooling the oven is opened during a step. Cooling takes place much faster with a cooling temperature rate of -5 °C/min.
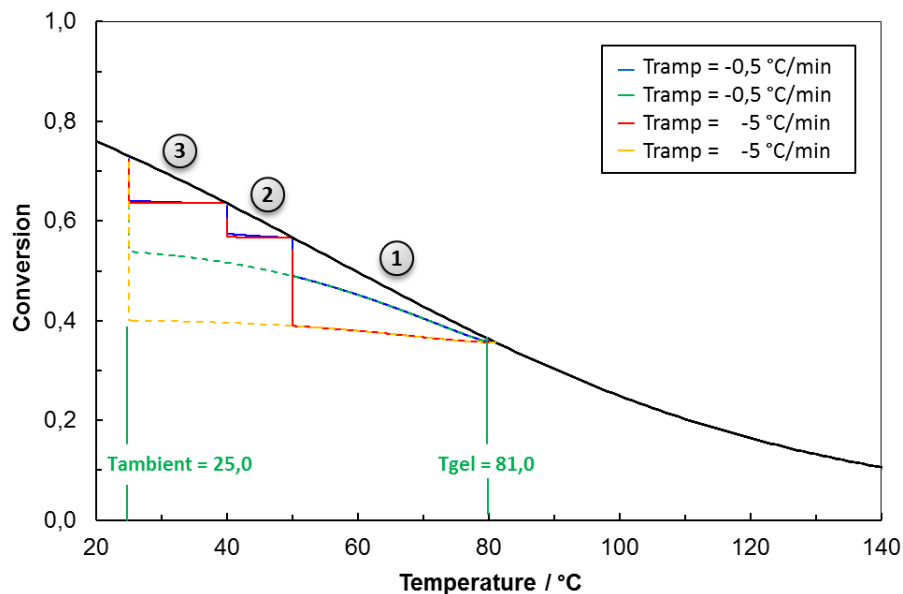
Figure 6.10: Kinematics/Equilibrium Simulation(Appendix A.1) of the DPBM-FGE-J4000 series used in the SH-SPC. Four simulation: Two simulations for a three steps controlled cooling process between $T_{Ngel} = 81.0$ °C and $T_{ambient} = 25.0$ °C: one with a cooling temperature ramp of -0.5 °C/min and the second with a ramp of -5 °C/min, and two simulations for a single step controlled cooling process with a temperature ramp of -0.5 °C/min and -5 °C/min.

In the table 6.1 the step durations for both the closed and open oven method are listed. In this table the %x is the percentage of the equilibrium conversion that has to be reached before a step is completed and there may be continued to the next. Let us first take a look at the

Table 6.1: The step intervals and the step durations of the three simulation shown in figure 6.10. %x is the percentage of the equilibrium conversion that has to be reached before a step is completed and there may be continued to the next.

Interval	begin T	end T	t until %x = 0,99			
			3step: TRamp = 0,5 °C/min	3step: TRamp = 5 °C/min	1step: TRamp = 0,5 °C/min	1step: TRamp = 5 °C/min
	°C	°C	min	min	min	min
1	81	50	111,2	93,9	/	/
2	50	40	98,8	92,7	/	/
3	40	25	1331,3	1326,7	/	/
4	81	25	/	/	1752,7	1862,3
Total	81	25	1430,2	1419,5	1752,7	1862,3
Total (hours)	81	25	23,8	23,7	29,2	31,0

difference between the open and closed oven method for the three step cooling profile. Opening the oven during the cooling process would make the process less then 10 minutes faster, therefor, if the three step method is used, it is advised to leave the oven closed, such that the SH-SPA remains in a controlled environment. However due to the combination of manual control of the temperature and the long duration of the stages, a single-step cooling profile was used in practice. For the single-step cooling, the open oven method takes about 2 hours longer then the closed oven method, which is why the cooling was carried out in a closed oven.

Total temperature profile of the SH-process
In figure 6.9 the temperature profile of the entire self-healing process is presented. The total duration of the SH-process is 30 hours.

6.4 Experiments

In this section the experiments done on the Self-Healing Soft Pneumatic Cell (SH-SPC), which design, construction and self-healing process were described in the previous sections 6.1, 6.2 and 6.3, will be discussed, as well as the equipment which is used. First a brief introduction is given which explains the tests in general and why the tests are done. Secondly a short overview is given on the equipment which was used for these tests, and after this the measured data is presented. This section is followed by a discussion on the measurements and a conclusion.

6.4.1 Experiments on the SH-SPC

In all the experiments done the air chamber of the SH-SPC was put under an overpressure. Like for the SPA seen in literature and discussed in section 2.2.2, the response of the SH-SPC on this overpressure is an elastic deformation, which eventually, if more cells are joined, can be used to create an anisotropic movement and therefor actuation. In a first experiment the air chamber of the SH-SPC will be put under different over-pressures and the deformation of the SPC will be analyzed by taking pictures and creating short movies with a digital camera. In a next experiment, a force sensor will be implemented in the testing setup and the force, that is applied by the top plane of the SH-SPC is measured in function of the overpressure in the air chamber. After this a small cut is made in the SH-SPC with a blade and the cell

is subjected to the SH-process described in section 6.3. The previous experiment is repeated for the healed cell and the data of the tests before and after a self-healing cycle are compared.

6.4.2 Equipment

First the test setup which was used for the first experiment, in which the air chamber of the SH-SPC was put under pressure and pictures were taken will be briefly explained. The setup is explained more in detail using schemes and pictures in Appendix A.9.3. A compressed air supply is available in the lab, which provides the overpressure required for the experiments. The pressure can be controlled manually using a pressure controller and the overpressure is measured using an analog manometer (unit: $kgf/cm_2 = 0.980681$ bar, readings: 0.01 kgf/cm_2 $= 9.80681$ mbar). To control the actuation of the soft pneumatic cell a button is placed in the1 setup: if the button is pressed the cell is connected to the compressed air supply, otherwise there is no connection between the cell and the compressed air supply. Like mentioned before, the pictures and movies are made with a fixed digital camera. For the experiments where the force applied by the upper plane of the cell were measured, a force sensor (capacity of 1 lb = 4.448 N) was added, which was fixed above the cell. The analog signal of the sensor was read using a DAQ board and the Labview software.

6.4.3 Results

Experiment 1

In figure 6.11 a sequence of pictures are presented, showing the elastic deformation of the SH-SPC for increasing overpressure. On the pictures, the elastic deformation is clearly visible.
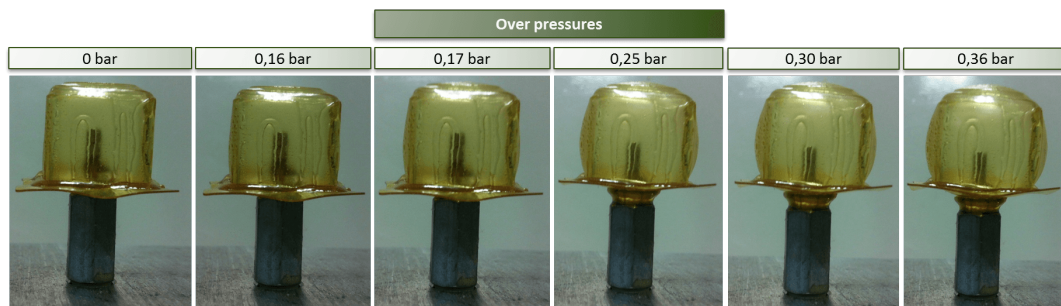
Figure 6.11: Experiment 1: Sequence of pictures showing the elastic deformation of the SH-SPC for increasing overpressure. The video can be seen at: https://www.youtube.com/watch?v=WTaz4dyS7-A&feature=youtu.be.

Experiment 2

For the next experiment the force applied by the top plane of the SH-SPC is measured using the force sensor. The force response to an actuation step is shown in figure 6.12 as well as a table presenting following parameters:

- **Overpressure**: (mbar).

- **Steady state force**: The constant force applied by the SH-SPC on the force sensor over a long time, when stabilized (Newton).

- **Overshoot**: the maximum peak value of the force response, measured from the steady state force (Newton).

- **Settling time**: the time elapsed starting at the beginning of the actuation of the cell until 2 % of the Steady State Force is reached.

Over-pressure response: parameters			
Measurement	1	2	3
Overpressure (bar)	0,23	0,28	0,31
Steady state force (N)	0,45	0,75	1,15
Overshoot (N)	0,7	0,05	0
Settling time to within 2% (sec)	4	3	0
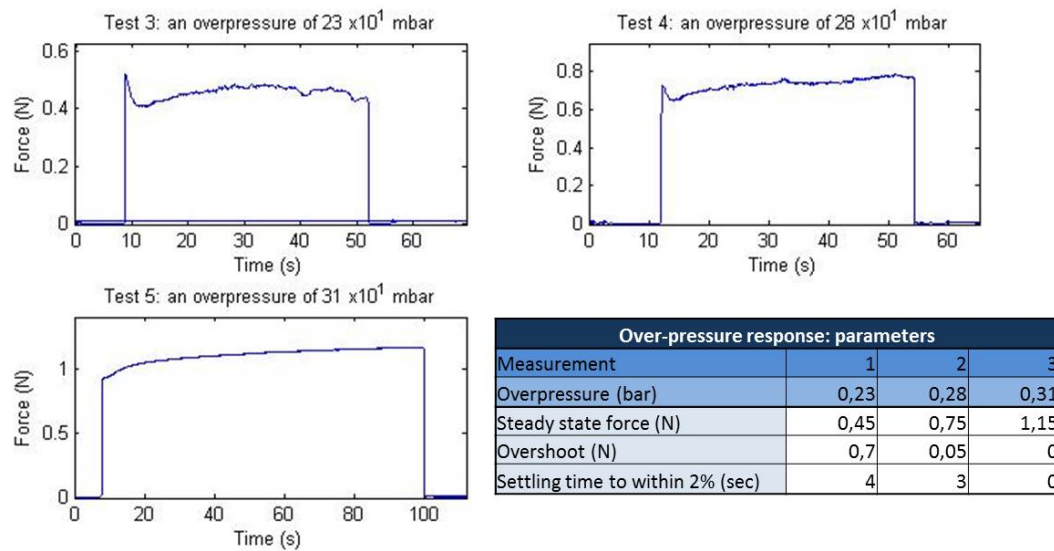
Figure 6.12: Experiment 2: The force response of the SH-SPC for three different over-pressures: 226, 284 and 314 mbar. In the table parameters characterizing this force response are presented: overpressure, steady state force, overshoot and settling time.

Unfortunately, no pictures were taken during this experiments. After these tests an incision was made with a blade in one of the side planes of the SH-SPC (figure 6.13). The dimensions of this incision: a length of 4.43 mm, a thickness of 0.30 mm and all the way through the wall of the cell. This incision was completely cured with the SH-process described in the previous section 6.3.
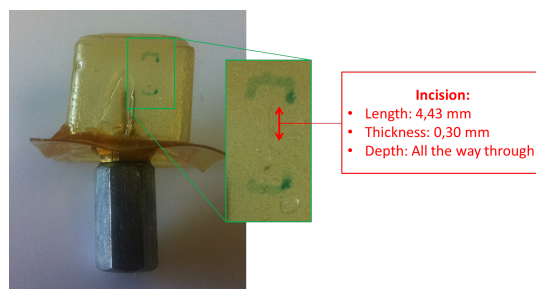
Figure 6.13: Picture showing the incision made in the side plane of the SH-SPC, which was afterward fully cured using the SH-process, described in section 6.3.

Experiment 3

After being healed in the SH-process, the SH-SPC was subjected to the same tests, the force response to actuations with different over-pressures of the air chamber. During this experiments pictures were made and the SH-SPC was tested for a broader range of over-pressures from 147 mbar to 422 mbar. In figure 6.15 the force responses are presented and in figure 6.14 the corresponding pictures are shown, together with the parameters defined in the description of previous experiment: the overpressure, the steady state force and the overshoot and the settling time, which characterize the force response.
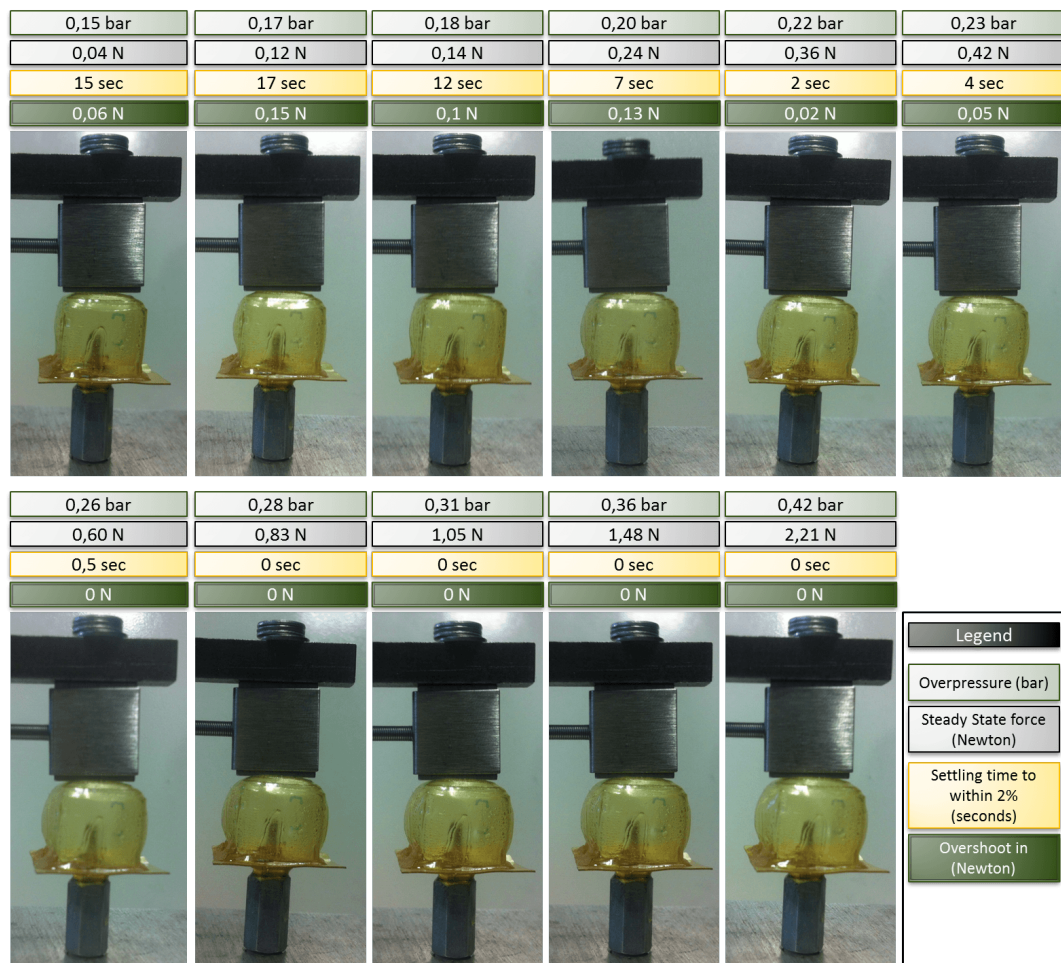
Figure 6.14: Experiment 3: Sequence of pictures of the SH-SPC in which an incision was made with a blade, which was afterward cured using the SH-process described in section 6.3. The pictures show the elastic deformation of the SH-SPC for increasing overpressure. On top of the SH-SPC the force sensor is visible. The parameters characterizing the force response are given above the pictures.
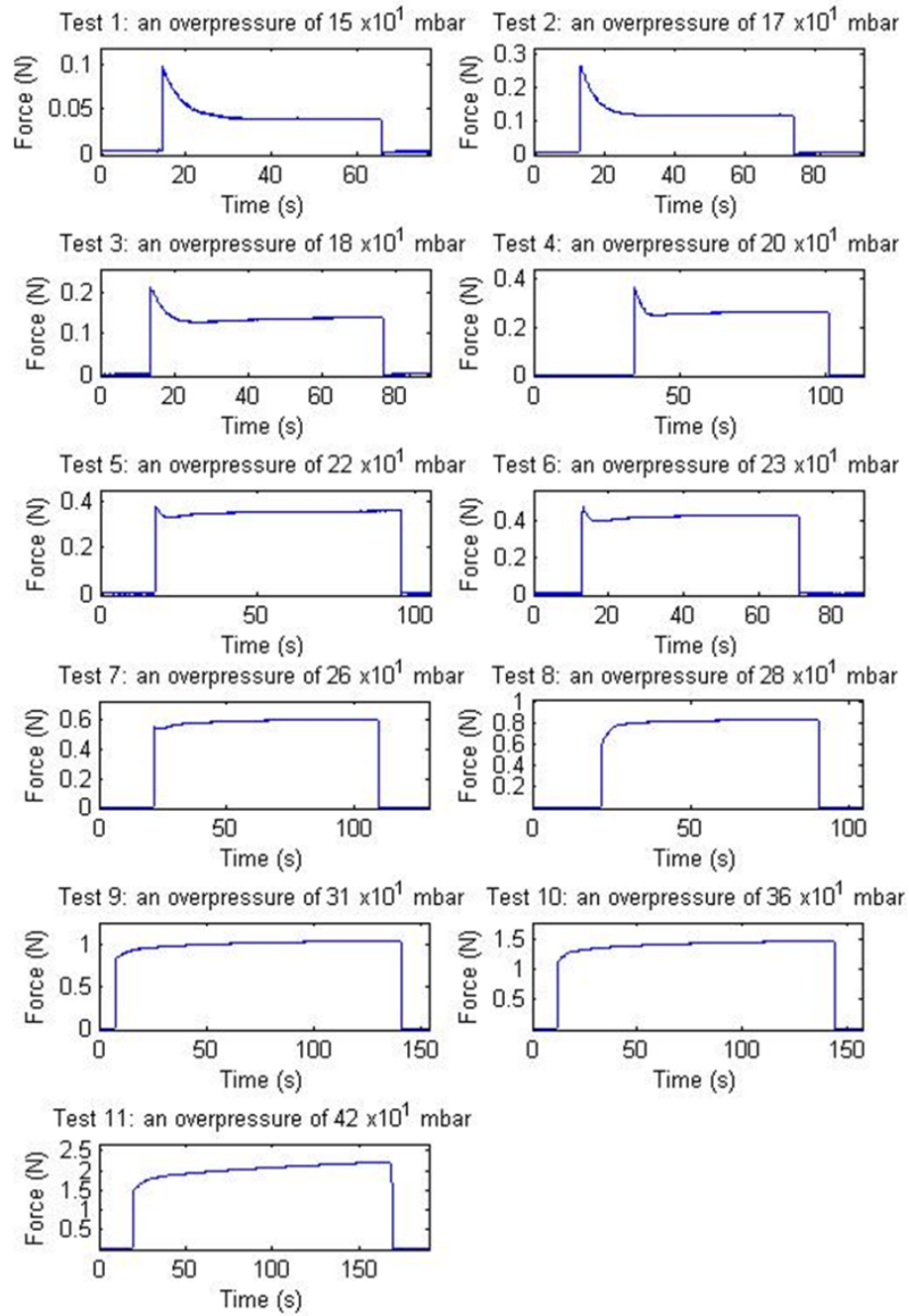
Figure 6.15: Experiment 3: The force response for different over-pressures for the SH-SPC, in which an incision was made with a blade, which was afterward cured using the SH-process described in section 6.3.

In figure 6.16 the force responses of experiment 2 (before the SH-cycle) were compared with the force responses of experiment 3 (after the SH-cycle).
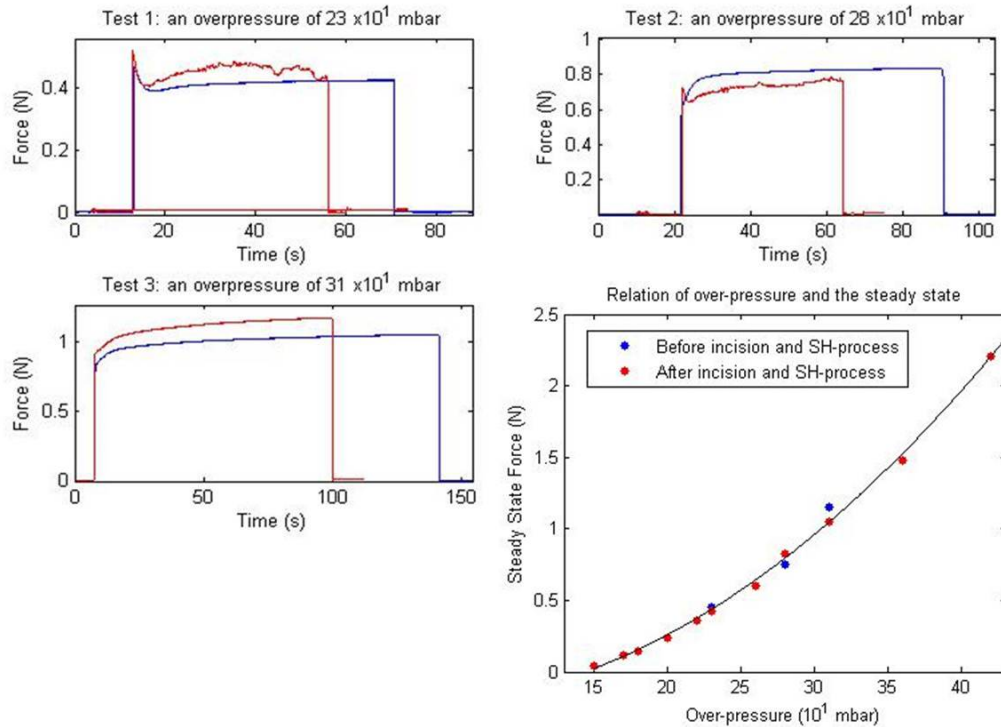
Figure 6.16: 3 line plots: The force responses of experiment 2, which measurements were done before the SH-process and the corresponding force responses of experiment 3, which was done after the SH-process. The responses are compared for 3 different over-pressures: 226, 284 and 314 mbar. Dot plot: The steady state force in function of the overpressure for both experiments 2, before the SH-proces, and experiment 3, after the SH-process took place.

6.5 Discussion

Experiment 1

Experiment 1 was a qualitative experiment, with the intention to examine whether the produced SH-SPC was cable to be subjected to certain over-pressures of the air chamber and to look at the elastic deformation of the cell. In this experiments the SH-SPA was pushed to its limits, the over-pressure was increased until a small perforation occurred in the cell at a maximum pressure of 0.46 mbar. This is a relatively high overpressure. In figure 6.17 a zoom of one of the pictures from experiment one (figure 6.11) is given, showing the SH-SPC under an overpressure of 0.36 bar. Based on the picture a rough measurement is made on the deformation of the cube and is shown on the figure. The combination of relative high

overpressure and high deformation shows that the two self-healing Diels-Alder series have potential for being used in soft robotics. By increasing the number of cells in the design, anisotropic elastic deformations can be introduced.
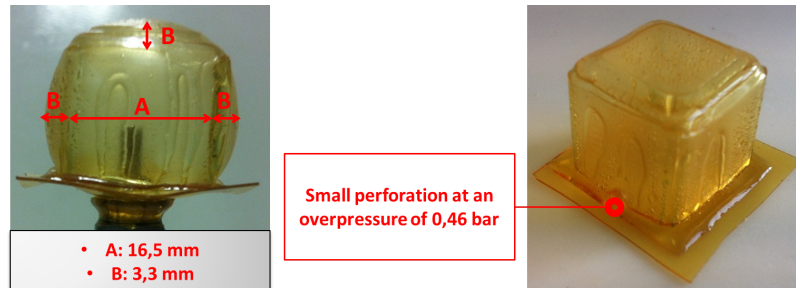
Figure 6.17: a) Pictures showing the elastic deformation of the SH-SPC for an increasing overpressure of 0.36 bar. b) The location where the perforation took place at an overpressure of 0.46 bar.

The location where the perforation took place is indicated in figure 6.17 b. At this location the cube, with 5 planes and created entirely out of the DPBM-FGE-J4000 series (figure 6.3 in section 6.2) is connected to the DPBM-FGE-J2000 sheet. The J4000 is more elastic and when the air chamber is put under overpressure, this series starts to deform. the J2000 series on the other hand, is less elastic and will only deform a little. This causes stress concentrations near the connection between the two polymer series. We can therefor conclude that the perforation of the SH-SPC took place on the location where failure was theoretically expected.

Experiment 2

In experiment 2 quantitative data, the force response to an actuation step, was measured. For an overpressure of 314 mbar a steady state force of 1.15 N was measured. In a paper of Yi Sun et al. [3], presented on the International Conference on Intelligent Robots and Systems (IROS) in 2013, quantitative force measurements are presented. The measurements were done on a multi-cell bending SPA (figure 2.2 in section 2), constructed out of Ecoflex 00-30 (Smooth-On Inc.) with a tensile modulus of 69 kPa, containing 10 cells with following dimensions: 8 mm - 4 mm - 2 mm with a wall thickness of 4 mm. Forces where measured in the range of 0.5 to 4.5 Newton, for over-pressures between 0.40 and 0.50 bar. However these measurements were done for the full actuator, which consists of 10 cells in series.

If we compare the force measured in experiment 2 and these values found in literature, it can be concluded that the SH-SHC can apply relative high forces. The DPBM-FGE-J4000 polymer series, which has a tensile modulus (storage modulus) of 7.8 MPa, used to build the SPC, is less soft in comparision with the Ecoflex 00-30 used by Yi Sun et al.. However, due to the high fracture strain (measurements were presented in section 4.4.3) of 446 %, the SPC can be used to create relative large deformation before a failure occurs. If multiple SH-SPCs would be put in series, a BSPA could be constructed, similar to the one produced by Yi

Sun et al., but stiffer. It can be concluded that based on the measurements presented in experiment 2, there is potential to construct soft pneumatic actuators, like for example the BSPA, from the self-healing DA-polymer series. These actuators will likely be able to create substantial, usable, elastic deformations and apply forces in the order of Newtons.

The shape of the force responses will be explained and discussed in the following experiment 3.

Experiment 3

As mentioned before, after experiment 2, an incision was made with a blade in the side plane of the cubic cell and was healed using the SH-process. The results of experiment 3 show in the first place that the incision was fully cured after the SH-process. Like in experiment 1, the cell was again pushed to its limits, the overpressure was increased until the cell failed. At an overpressure of 0.48 bar, a perforation took place at the location where the cell had failed in the previous experiment 1 (figure 6.17 b). From this it can be concluded that the incision was fully healed and that after the SH-process, no weak points are created where the incision was made. The overpressure, 0.48 bar, at which the perforation took place is very close to the value obtained in experiment 1: 0.46 bar.

If we analyze the shape of the force responses of both experiment 2 and 3 in, respectively, figure 6.12 and 6.14, for different over-pressures, a certain trend is visible. At low over-pressures, there is a relative high overshoot, which lasts several seconds, while at high over-pressures no overshoot occurs. All the responses, but especially the ones at high over-pressures, show a slow increase in force in the plateau after the force step. The author believes that these two trends, the force overshoot and the slow increase in force, are the result of one single principle: the elastic response of the DA-polymers, and in particular the DPBM-FGE-J4000 series, on an applied stress is not entirely instantaneous (This can be seen in the video: ref in subscribt of figure 6.11). The non-instantaneous part of the response is related to the viscous contribution, which was present in the DMA results of the DPBM-FGE-J4000 polymer series (section 4 in the figure 4.16 and the table 4.2). When compressed air is suddenly injected in the air chamber of the SPC, a part of the response of the polymer chains in the DPBM-FGE-J4000 cubic top part will be instantaneous, while another part of the response will take several seconds to unravel the chains. The DPBM-FGE-J2000 sheet on the bottom part, on the other hand will not show a large elastic strain response, however it is bendable and when the air chamber is put under an over-pressure it will bend (almost) instantaneously in a convex movement. This movement pushes the cell upwards.

These force responses shown in the figures 6.12 and 6.14 show very well one of the main drawbacks of soft pneumatic actuators: the very slow response on an actuation command. This is why pneumatic actuators based on soft elastic actuators will not be suitable for applications where fast actuation is required.

At low over-pressures the J2000 sheet bends and the J4000 cubic cell inflates partially instantaneously and the cell pushes on the force sensor. The delayed response of the chains of the

J4000 series, inflates the cubic part more. This additional inflation pushes the bended J2000 sheet a bit downwards at the sides, unbending the J2000 sheet a little. Due to this the force decreases in the first several second of the force response. At higher over-pressures the unraveling of the chains takes place faster and the pressure will be too high for the J2000 sheet to be unbended. This is the reason why only a little or no overshoot is registered. However at this high over-pressure there are some J4000 polymer chains which are still unraveling slowly, slowly inflating the cell more and more. Due to this small increase in volume of the air chamber, the force applied on the force sensor increases slowely.

In line plots and the dot plot in figure 6.16, the force responses measured for the over-pressures, 0.22, 0.28 and 0.31 bar, of both experiments 2 and 3 were compared. It was not easy to create exactly the same testing conditions for the two experiments before and after the SH-process: firstly, both sensor and cell were put in approximately the same position, however this was all done manually and therefor the positioning of these two parts were not exactly the same for the two tests. Secondly the manometer had a low resolution of only 0.01 bar, which means there might be an over-pressure difference of 0.005 bar between the two experiments. If the two experiments are compared, it can be concluded that when taking into account the fact that there was a little difference in testing conditions, the force responses in figure 6.16, have similar values for both experiments. From this experiment it can be concluded that the SH-SPC shows the same performance before and after the self-healing process.

In figure 6.16 a quadratic polynomial curve is drawn, fitting the data points of experiment 2 and 3. The relation found between the steady state force and the over-pressure was given by: $F_{SS} = 1.539e - 005P^2 - 0.000672P - 0.2242$, in which F_{SS} is the steady static force in Newton and P the overpressure in mbar. If in the future a controlled SH-pneumatic actuator will be build, it will be controlled with the over-pressure. In the graph in figure 6.16 the measured points do not vary a lot from this fitting curve, which benefits the control of the actuation in the future.

6.6   Conclusion

Based on the Soft Pneumatic Actuators (SPA) found in literature, which are made out of very soft elastic material, a first prototype, a Self-Healing Soft Pneumatic Cell (SH-SPC), was designed and developed using Diels-Alder (DA) polymers. Most SPA consist out of more cells, containing air chambers, which can be inflated by putting them under an over-pressure. However, this first prototype, the SPC, contains, as the name indicates, only one cell. The 15 by 15 by 15 mm cell was made out of the DPBM-FGE-J4000 series, the most elastic DA-series.

SPAs are designed to have an anisotropic response to a stress, generated by the over-pressure in the air chamber. In most SPAs this anisotropic response is generated by importing a less stretchable material in the design. When only one (small cubic) cell is used, only a relatively small anisotropic movement response can be created by pressurizing the air chamber. However, with the scope on a future multi-cell SPA prototype, a less stretchable SH-material, the DPBM-FGE-J2000 series, was implemented in the design.

In the shaping process of the cubic cell, the DA-polymer sheets were cut and folded to form the cubic part. Using the self-healing property of the DA-polymers, the walls of the cubic cell where joined. In this thesis it was shown that the self-healing property of the DA-polymer introduces an advantage in the shaping process: it can be used to join polymer sheets to form 3D structures. In the future different 3D polygon designs could be easily built from the DA-elastomer polymer sheets, using relative low temperature processes (around 70 °C). In the shaping process it was shown that a connection can be made between two different DA-polymer series, using the self-healing process.

The SPC was tested for different over-pressures in the air-chamber. In these test the elastic deformations were analyzed and the force applied by the top plane of the SPC was measured. The SPC could handle over-pressures up to 0.45 bar and at over-pressures above 0.2 bar the cell showed substantial deformations. Forces where measured up to above 2 Newton, which is adequate for soft pneumatic actuation (based force measurements on SPAs in literature [3]). The combination of relatively high forces that can be applied and high deformation shows that the two self-healing Diels-Alder series have high potential for being used in soft robotics.

A macroscopic incision was made in the SPC with a blade. Hereafter the cell was cured in a self-healing process, with a temperature profile which was carefully designed using a Kinetics/Equilibrium simultation of the DA-reaction. The healed SPC was subjected to the same test, which were already carried out before the incision was made. From these tests it could be concluded that the incision was completely healed after the SH-process and that the initial properties of the SPC were retrieved. If a "clean" fracture/ crack occurs in the SPC, or in the future in the SPAs, it can be healed using a self-healing process which takes about 30 hours (the SH-process can be upgraded to a duration of about 24 hours). With a clean fracture or crack is meant that the fracture surfaces can be easily brought in contact again, such that they could be healed together. The SPA are more likely to fail or to be damaged when inflated. When a crack or fracture occurs when the SPA is inflated, the over-pressure will be taken away and the actuator will return to its initial (non-inflated) form. This automatically presses the fracture surfaces together, providing excellent contact for the SH-process.

The force responses on an actuation step, force applied by the top surface of the SPC in function of time, was measured for different over-pressures. From this measurements it can be concluded that there exist a well defined relation between the force applied by the SPC surface and the over-pressure in the air chamber. This benefits the actuation control of SPAs, since this is done by an over-pressure controller. The force applied will be controlled by the over-pressure in the air chambers. The force responses show also a big disadvantage of the SPA: the very slow force and deformation response to an applied over-pressure. SPAs are not suitable for applications where fast, accurate actuations are required. However this is for SPAs in general and is independent on the fact whether dealing with a self-healing SPA or not.

From all the things mentioned in the paragraphs above, it can be said that the prototype of the SPC indicates that the self-healing DA-polymers can be used in the soft robotics.

The author believes that starting from this single-cell SPC, it is straightforward to build a multi-cell prototype, a Bending SPA, which will exhibit the anisotropic movement response. This would be the first SPA ever built completely out of self-healing polymer.

6.7 Future work on the SH-SPA

In the conclusion 6.6, it was already mentioned that it would be straightforward to create a soft pneumatic actuator, made completely out of self-healing polymers: a multi-cell prototype, a Bending SPA, containing an anisotropic movement response. This is something which can be build, tested and analyzed in the near future. But more complex 3D structures could be build by cutting, folding and healing the SH-polymer sheets. In literature [19] different soft elastic origami structures are described. Each of these contain a particular anisotropic response to a stress, which is most of the time caused by an over-pressure in an air chamber. A lot of these designs are worth being investigated. It should be analyzed whether it would be possible to build these structures out of SH-polymers using the shaping technique, which relays on the SH-property.

Complex smooth 3D polymer objects have to be cast or molded. The DA-polymers which were used in this thesis could not be used for polymer solution casting. Casting could not be introduced in the synthesis process, because the polymer is diluted to 30 $\%w$ in chloroform (CH_3Cl). Because if this polymer solution would be poured in a mold, the solvent would vaporize, but due to the low polymer concentration, this will lead to large cavities in the cast polymer piece. The polymer could also not be molded directly. Different molding techniques exist for polymers, like injection molding, extrusion molding and transfer molding. However, all of these techniques require the polymer to be heated up, such that it starts to flow. The DPBM-FGE-Jx series cannot be heated to the required temperatures because at these elevated temperature side reactions take place, creating an irreversible network and therefor the polymer will lose its SH-property. Compression molding might be a technique which could be used for shaping the DA-polymers in complex shapes, since the required temperatures are lower. The molds have to be chemical inert, such that the DA-polymers will not stick to it. Therefor Teflon molds were used in this thesis. Compression molding was not used in this thesis, since Teflon is to soft to be used for this molding technique. A metal mold, provided with a chemical inert coating would be a solution for this problem. It would be interesting to analyze if this shaping process could be used to create complex shapes, like presented in the paper of Martinez et al. [19].

Chapter 7

General conclusion

This thesis introduced a new material technology in the robotics: the self-healing (SH) polymer technology. SH-polymer were incorporated in two different compliant actuator designs. These are defined as the first self-healing compliant actuators. From a literature study it was concluded that SH-materials have never been used in any robotic application.

Currently there is an increase in interest in compliant actuators, which are used in unstructured, dynamic environment and in places where interaction with people is required. Usually these actuators are over-dimensioned to withstand unexpected extreme circumstances and avoid any damage. However, in many robotic applications compactness and weight are of great importance. The "self-healing compliant actuator", studied in this thesis, will bring a solution to this over-dimensioning. Using the SH ability, the actuators can be dimensioned based on their performance tasks, instead of on extreme unexpected loads. If an overload takes place the SH-part fails, protecting the other components of the actuator. Next the SH-part can be healed back to its initial state, after which the compliant actuator is ready to be used again. With this principle, "self-healing robotics" will lead to lighter systems and eventually to more efficient designs. The feasibility of developing such a self-healing compliant actuator was investigated.

A brief introduction was given on compliant actuators. From the different available compliant actuators, two were analyzed in particular, with the focus on implementing a SH-property: the series elastic actuator (SEA) and the soft pneumatic actuator (SPA). Before a conceptual design was developed for both of these actuator types, an analysis was carried out on the different self-healing polymer mechanisms present nowadays.

A large overview was given on the different self-healing mechanisms in polymers, which exist in literature. These mechanisms were analyzed one by one, in order to see whether they were capable to be used in a compliant actuator design. After this analysis, the Diels-Alder (DA) self-healing polymers were chosen to be the most suitable. The non-autonomous, SH mechanism of these Diels-Alder (DA) polymers is based on a reversible covalent network. In order to built the conceptual designs of the SH-SEA and the SH-SPA, the (thermo-) mechanical properties were characterized.

At the Materials and Chemistry department (Research group Physical Chemistry and Polymer Science, FYSC) of the Vrije Universiteit Brussel (VUB), they developed 4 series of the DA-polymer: DPBM-FGE-J230, J400, J2000 and J4000. These series differ in furan spacer length, the polymer chain length of the furan functional compound. By varying these polymer chain length, 4 polymer series were synthesized, with different mechanical properties but with the same self-healing mechanism incorporated, the reversible DA-bonds. The mechanical properties of the series vary from glassy brittle thermoset behavior, for the J230 and the J400 series, to elastomer behavior, for the J2000 and the J4000 series.

A conceptual design for a SH-SEA was developed. This design is based on a SH-mechanical fuse (SH-MF), which is placed in series with the compliant element of the actuator. The fuse acts as a sacrificial part and will break if the actuator is subjected to an over-load. If fractured the fuse can be cured using a SH-process. The center of the SH-MF contained a cylindrical SH-part, build out of the glassy thermoset DPBM-FGE-J400 series. A first prototype of this SH-MF was developed. Both the mechanical properties and the SH-ability of the fuse were analyzed. The SH-MF was repeatedly self-healed (non-autonomously in an oven) and fractured in a tensile test for three times. Using the tensile test the fracture force, strain and stress where measured after each SH-cycle. From the results of these tests, it can be conclude that the SH-MF could be healed at a relatively low temperature. There was no decreasing trend of the fracture force and stress recorded, which indicates that the mechanical properties of the fuse do not change after at least three SH-cycles.

Next the potential of developing a bending SPA, made entirely out of an elastic self-healing DA-polymer, was investigated. To do so, a soft pneumatic cell (SPC) was produced out of the most elastic, DPBM-FGE-J4000 series. Most SPAs consist out of more cells, containing air chambers, which can be inflated by putting them under an over-pressure. However, the first prototype, the cubic SPC, contains only one cell. In most SPAs an anisotropic response is generated by importing a less stretchable material in the design. Therefor such a less stretchable, yet bendable SH-material, the DPBM-FGE-J2000 series, was implemented in the design. The SH-property was used in the shaping process to make airtight connections between the 6 planes of the cubic cell. In this shaping process it was shown that a self-healing connection can be made between two different DA-polymer series. The SPC was tested for different over-pressures in the air-chamber. In these tests the elastic deformations were analyzed and the forces applied by the top plane of the SPC were measured. For over-pressures around 0.3 bar, the SPC showed substantial deformations and forces were measured in the order of Newtons. The combination of relative high forces and high deformations indicate that the two self-healing Diels-Alder series have a high potential to be used in soft robotics. A macroscopic incision was made in the SPC, which was healed using the SH-property of the DA-polymers. Hereafter the same tests, done before the incision was made, where carried out on the healed SPC. From these tests it could be concluded that the incision was completely healed after the SH-process and that the initial properties of the SPC were retrieved. Starting from this single-cell SPC, it is straightforward to build a multi-cell prototype, a Bending SPA, which will contain the anisotropic movement response. This would be the first SPA ever built completely out of self-healing polymer.

Finally it can be concluded that the DA-polymers can be processed in macroscopic shapes, which can be implemented and used in compliant actuators. This first study, which lasted only one year and a half, lead to a working prototype for both of the actuator types: the SH-SPA and the SH-SEA, thus accomplishing the project goals. This indicates that it is worthwhile to continue this study and to investigate if the Diels-Alder or other available self-healing polymers can be used for multiple robotic applications.

Bibliography

[1] K. A. Williams, D. R. Dreyer, and C. W. Bielawski, "The underlying chemistry of self-healing materials," *MRS Bulletin*, vol. 33, pp. 759–765, 8 2008.

[2] J. E. Pratt and B. T. Krupp, "Series elastic actuators for legged robots," *Proceedings of SPIE 5422, Unmanned Ground Vehicle Technology VI*, vol. 5422, pp. 135–144, September 2004.

[3] Y. Sun, Y. S. Song, and J. Paik, "Characterization of silicone rubber based soft pneumatic actuators," in *Proceedings IEEE/RSJ International Conference on Intelligent Robots and Systems (IROS)*, pp. 4446 – 4453, November 2013.

[4] P. Polygerinos, S. Lyne, Z. Wang, L. F. Nicolini, B. Mosadegh, G. M. Whitesides, and C. J. Walsh, "Towards a soft pneumatic glove for hand rehabilitation," in *Proceedings of IEEE/RSJ International Conference on Intelligent Robots and Systems (IROS)*, November 2013.

[5] D. Y. Wu, S. Meure, and D. Solomon, "Self-healing polymeric materials: A review of recent developments," *Progress in Polymer Science*, vol. 33, no. 5, pp. 479 – 522, 2008.

[6] G. Scheltjens, M. Diaz, J. Brancart, G. Van Assche, and B. Van Mele, "A self-healing polymer network based on reversible covalent bonding," *Reactive and Functional Polymers*, vol. 73, no. 2, pp. 413 – 420, 2013. Network Polymers towards High Performance Materials.

[7] J. Menczel and R. Prime, *Thermal Analysis of Polymers, Fundamentals and Applications*. Wiley, 2009.

[8] F. J. Apple and D. R. Koerner, *Stress Concentration Factors for U Shaped, Hyperbolic and Rounded V Shaped Notches*. ASME Paper 69DE2, 1969.

[9] http://www.specac.com/, "Specac: Ir sampling accessories & press solutions," 2014.

[10] http://www.proxxon.com/, "Proxxon: The fine tool company," 2014.

[11] P. Cain, P. Kazanzides, J. Zuhars, B. Mittelstadt, and H. Paul, "Safety considerations in a surgical robot," *Biomedical science instrumentation*, vol. 29, pp. 291–294, 1993.

[12] A. Bicchi, S. Rizzini, and G. Tonietti, "Compliant design for intrinsic safety: general issues and preliminary design," in *Proceedings of IEEE/RSJ International Conference on Intelligent Robots and Systems (IROS)*, vol. 4, pp. 1864–1869, 2001.

[13] M. Van Damme, B. Vanderborght, R. Van Ham, B. Verrelst, F. Daerden, and D. Lefeber, "Proxy-based sliding mode control of a manipulator actuated by pleated pneumatic artificial muscles," in *Proceedings of IEEE International Conference on Robotics and Automation (ICRA)*, pp. 4355–4360, April 2007.

[14] R. Ham, T. Sugar, B. Vanderborght, K. Hollander, and D. Lefeber, "Compliant actuator designs," *IEEE Robotics Automation Magazine*, vol. 16, pp. 81–94, September 2009.

[15] G. Pratt and M. Williamson, "Series elastic actuators," in *Proceedings of IEEE/RSJ International Conference on Intelligent Robots and Systems 95. 'Human Robot Interaction and Cooperative Robots',*, vol. 1, pp. 399–406, August 1995.

[16] R. V. Ham, B. Vanderborght, M. V. Damme, B. Verrelst, and D. Lefeber, "Maccepa, the mechanically adjustable compliance and controllable equilibrium position actuator: Design and implementation in a biped robot," *Robotics and Autonomous Systems*, vol. 55, no. 10, pp. 761 – 768, 2007.

[17] http://www.poly soft.com/WireRopeFuse, "Polytechnic software associates," 2014.

[18] A. Flocchini, "Mechanical fuse," Jan. 5 1988. US Patent 4,716,635.

[19] R. V. Martinez, C. R. Fish, X. Chen, and G. M. Whitesides, "Elastomeric origami: Programmable paper-elastomer composites as pneumatic actuators," *Advanced Functional Materials*, vol. 22, no. 7, pp. 1376–1384, 2012.

[20] Y. S. Song, Y. Sun, R. van den Brand, J. von Zitzewitz, S. Micera, G. Courtine, and J. Paik, "Soft robot for gait rehabilitation of spinalized rodents," in *Proceedings of IEEE/RSJ International Conference on Intelligent Robots and Systems (IROS)*, pp. 971 – 976, November November 3-7, 2013.

[21] R. F. Shepherd, F. Ilievski, W. Choi, S. A. Morin, A. A. Stokes, A. D. Mazzeo, X. Chen, M. Wang, and G. M. Whitesides, "Multigait soft robot," *Proceedings of the National Academy of Sciences (NAS)*, vol. 108, no. 51, pp. 20400–20403, 2011.

[22] S. Kim, C. Laschi, and B. Trimmer, "Soft robotics: a bioinspired evolution in robotics," *Trends in Biotechnology*, vol. 31, no. 5, pp. 287 – 294, 2013.

[23] R. V. Martinez, C. R. Fish, X. Chen, and G. M. Whitesides, "Elastomeric origami: Programmable paper-elastomer composites as pneumatic actuators," *Advanced Functional Materials*, vol. 22, no. 7, pp. 1376–1384, 2012.

[24] P. L. Bertrand Tondu, "The mckibben muscle and its use in actuating robot-arms showing similarities with human arm behaviour," *Industrial Robot: An International Journal*, vol. Vol. 24, no. 6, pp. 432 – 439, 1997.

[25] B. Verrelst, R. Ham, B. Vanderborght, F. Daerden, D. Lefeber, and J. Vermeulen, "The pneumatic biped "lucy" actuated with pleated pneumatic artificial muscles," *Autonomous Robots*, vol. 18, no. 2, pp. 201–213, 2005.

[26] B. Vanderborght, B. Verrelst, R. Van Ham, and D. Lefeber, "Controlling a bipedal walking robot actuated by pleated pneumatic artificial muscles," *Robotica*, vol. 24, pp. 401–410, 7 2006.

Appendix

A.1 Kinetics/Equilibrium simulation

A Kinetics/Equilibrium simulation is provided by G. Scheltjens [6] which models the temperature dependence of the equilibrium conversion for the Diels-Alder reaction between DPBM, the maleimide carrying group and FGE-Jeffamine, the furan carrying group. The equations used in this simulation are summarized below.

The reaction rates for furan (F), Maleimide (M) and the Diels-Alder Adduct (A) are given in equation 1:

$$-\frac{d[M]}{dt} = -\frac{d[F]}{dt} = \frac{d[A]}{dt} = k_{DA}[F][M] - k_{rDA}[A] \tag{1}$$

In this equation the rate constants k_{DA} and k_{rDA}, which are a function of temperature, are given by equation 2. In this equation A_{DA} and A_{rDA} are the pre-exponential factors, or frequency factors. E_{DA} and E_{rDA} are the activation energies, R is the gas constant and T is temperature:

$$k_{DA} = A_{DA}e^{\frac{-E_{DA}}{RT}} \quad and \quad k_{rDA} = A_{rDA}e^{\frac{-E_{rDA}}{RT}} \tag{2}$$

It is considered that the initial concentrations of Maleimide and Furan are equal. Therefor the equation 3, in which x(t) is the conversion to Diels-Alder Adduct (A) at time t, can be written.

$$[M]_0 = [F]_0 \quad \Leftrightarrow \quad \frac{dx}{dt} = k_{DA}[F]_0(1 - x(t))^2 - k_{DA}x(t) \quad with \quad x(t) = \frac{[A]}{[F]_0} \tag{3}$$

The equilibrium constant (K) of the Diels-Alder equilibrium reaction is given by the formula 4:

$$ln(K) = ln\left(\frac{x}{[M]_0(1-x)^2}\right) = ln\left(\frac{k_{DA}}{k_{rDA}}\right) = \frac{\Delta_r S^0}{R} - \frac{\Delta_r H^0}{RT} \tag{4}$$

A.1.1 Equilibrium simulation: Conversion/temperature graphs

The theoretical conversion (x(t)) in equilibrium state varies with temperature. The equilibrium conversion (x) for a given temperature (T) can be found by solving equation 3 for

$\frac{dx}{dt} = 0$. If this is done for all temperatures in a given temperature interval, the equilibrium conversion can be plotted in function of temperature. In figures 1, 2 and 3 the equilibrium conversion (x) is plotted in function of temperature for the DPBM-FGE-J400, J2000 and J4000 series.

Using the Glass Transition Temperature (T_g) and the Gel Transition Temperature (T_{gel}) (gel conversion point, x_{gel}) the graph can be divided in different zones, with specific polymer network structure:

- Yellow zone: Viscous Gel ($x_{gel} > x$)
    - Relatively high Temperature$\rightarrow$ low cross link density$\rightarrow$ no network
- Green zone: Elastic Solid ($x_g > x > x_{gel}$)
    - Relatively mean to high temperature $\rightarrow$ medium to high cross link density$\rightarrow$ network structure $\rightarrow$ Elastic solid behavior
- Blue zone: Glassy Thermoset ($x > x_g$)
    - Relatively low temperature $\rightarrow$ high cross link density$\rightarrow$ network structure $\rightarrow$ very limited chain mobility $\rightarrow$ glassy, brittle behavior
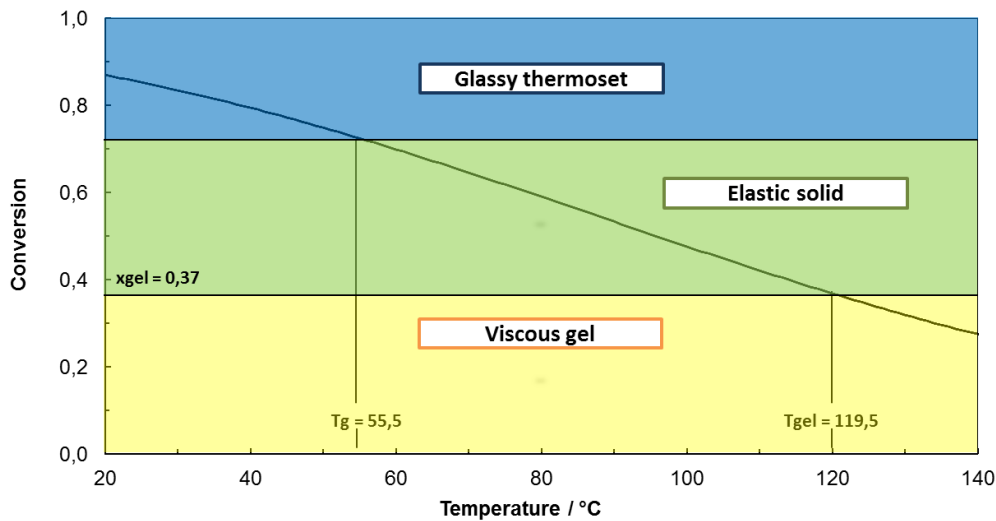
Figure 1: Equilibrium simulation of the Diels-Alder reaction equilibrium for DPBM-FGE-J400 starting at equilibrium.

A.1.2 Kinetics/Equilibrium simulation: Conversion/temperature graphs

Besides plotting the equilibrium conversion/temperature plot, the simulation can take in account the kinetics and the conversion variation resulting from a cooling or heating temperature profile can be modeled. To do this the equation 3 has to be solved for the given temperature profile. Consider for example a simulation of the DPBM-FGE-J400 series with
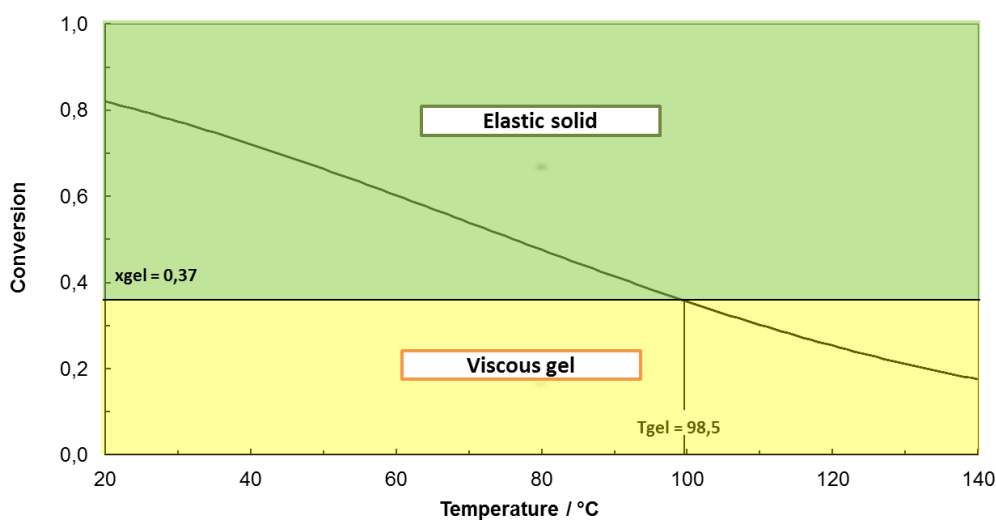
Figure 2: Equilibrium simulation of the Diels-Alder reaction equilibrium for DPBM-FGE-J2000 starting at equilibrium.
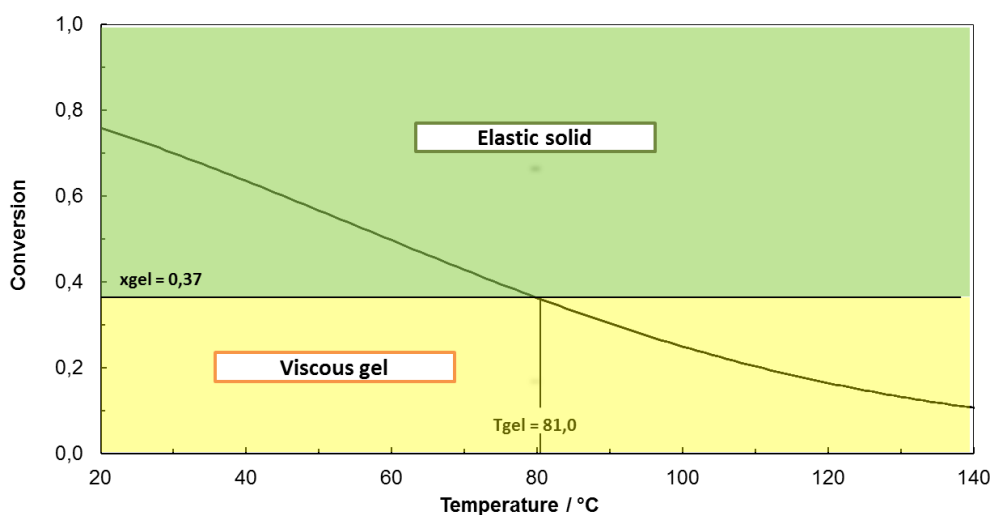
Figure 3: Equilibrium simulation of the Diels-Alder reaction equilibrium for DPBM-FGE-J4000 starting at equilibrium.

a temperature profile: cooling down from 119.5 °C (T_{gel}) to 55.5 °C (T_g) with a temperature ramp of -5 °C/min followed by an isothermal process at 55.5 °C until 99,9 % of the equilibrium conversion (x) is reached. The result of this simulation is plotted in figure 4. The deviation of the conversion "path" (in blue) in function of temperature from the equilibrium conversion/temperature graph (in black) is clearly visible. At high temperature the conversion path is near the equilibrium graph due to fast kinetics of the Diels-Alder reaction but at lower temperatures the kinetics of the reaction decrease, resulting in a deviation of the

conversion path from the equilibrium graph. The time required to reach the conversion of 99.9 % of the equilibrium conversion is 179.5 min which consist of the cooling process from 119.5 °C to 55 °C of 12.8 min and an isothermal process at 55.5 °C of 166,7 min. This was an illustration of how the kinetic aspect of the simulation can be used. In the sections 6.3 and 6.3 this kinetic aspect of the simulation will be used to design the temperature profiles of the cooling step in the self-healing process of the Diels-Alder polymers implemented in the two different applications.
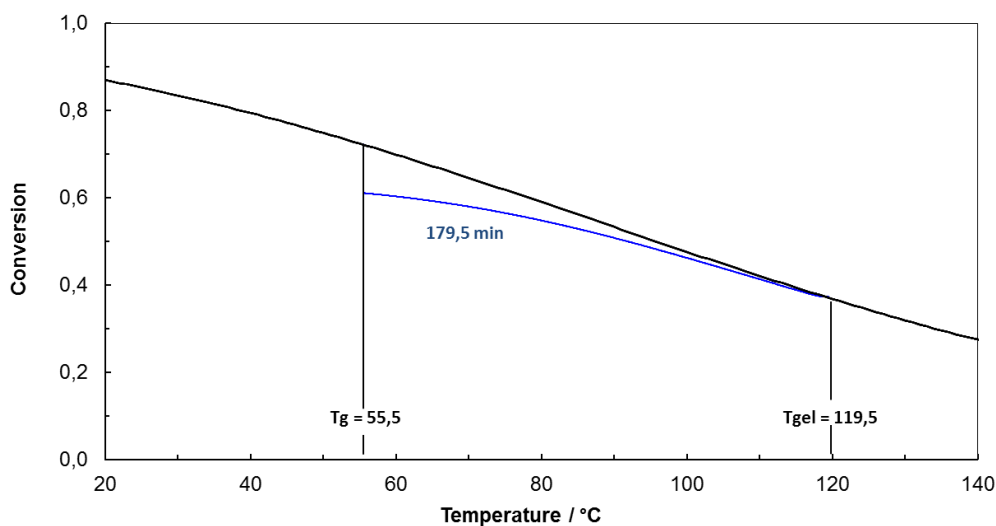
Figure 4: Kinetic/Equilibrium simulation of the Diels-Alder reaction equilibrium for DPBM-FGE-J400 starting at equilibrium for a cooling temperature profile: ooling down from 119.5 °C (T_{gel}) to 55.5 °C (T_g) with a temperature ramp of -5 °C/min followed by staying at 55.5 °C until 99,9 % of the equilibrium conversion (x) is reached.

A.2 Density Measurements of DA-polymer series

Density Measurements DPBM-FGE-J4000								
Sheet Number	Length (mm)	Width (mm)	Thickness (mm)	Volume (mm3)	Volume (ml)	Mass (g)	Density (g/ml)	Fault (g/ml)
1	16,32	14,61	0,64	152,60	0,15260	0,1561	1,02	
2	14,80	14,43	0,71	151,63	0,15163	0,1558	1,03	
3	14,06	14,72	0,76	157,29	0,15729	0,1651	1,05	
4	14,81	14,94	0,76	168,16	0,16816	0,1828	1,09	
Total Mean							1,05	0,02

Density Measurements DPBM-FGE-J2000								
Sheet Number	Length (mm)	Width (mm)	Thickness (mm)	Volume (mm3)	Volume (ml)	Mass (g)	Density (g/ml)	Fault (g/ml)
1	14,74	15,68	0,52	120,18	0,12018	0,1384	1,15	
2	15,16	15,66	0,57	135,32	0,13532	0,1503	1,11	
3	14,63	14,74	0,55	118,61	0,11861	0,1359	1,15	
4	16,21	15,18	0,51	125,49	0,12549	0,1394	1,11	
Total Mean							1,13	0,02

Density Measurements DPBM-FGE-J400								
Sheet Number	VolumeT(ml)	VolumeM (ml)	Volume Polymer (ml)	MassT (g)	MassM (g)	Mass Polymer (g)	Density (g/ml)	Fault (g/ml)
1	0,60	0,31	0,29	2,6052	2,25870	0,3465	1,19	
2	0,60	0,29	0,31	2,2045	1,83310	0,3714	1,20	
3	0,09	0,00	0,09	0,1069	0,00000	0,1069	1,19	
Total Mean							1,19	0,01

Figure 5: Measurements and calculations for the density of the DPBM-FGE-Jx series.

A.3   The viscoelastic behavior of polymers

In this Appendix section the viscoelastic behavior of polymers will be explained in detail. In contrast to metals, polymers have a viscoelastic behavior, that is intermediate between that of an ideal elastic solid and that of an ideal viscous liquid, showing characteristics of both [7]. The timescale and temperature of observation are critical to the relative degree of solid- and liquid like behavior exhibited by viscoelastic materials. Generally, they will behave more solid like at lower temperature or short timescale, but more liquid like at higher temperatures or longer timescales. Thermal analysts are frequently called on to measure the mechanical properties of polymers. Of the different methods for viscoelastic property characterization, dynamic techniques are most popular, since they are readily adapted for studies of both polymeric solids and liquids [7]. They are collectively referred to as Dynamic Mechanical Analysis or DMA. In the following subsection the characterization parameters used to describe the viscoelastic behavior with the DMA method will be introduced.

DMA: parameters [7]
A DMA test is used to characterize materials and more specifically study the viscoelastic behavior of polymers. This viscoelastic property of a polymer is studied by dynamic mechanical analysis where a sinusoidal force (stress σ) is applied to the material and the resulting displacement (strain ϵ) is measured or the other way around. Consider what happens if a sinusoidal strain (ϵ) is applied and the stress (σ) is measured, the equations [7] for stress (σ) and strain (ϵ) are respectively given by eq.6 and eq.5

$$\epsilon = \epsilon_0 sin(t\omega) \tag{5}$$

$$\sigma = \sigma_0 sin(t\omega + \delta) \tag{6}$$

In which ω: is frequency of strain oscillations, t: time and δ: the phase lag between stress and strain. First we consider that the sinusoidal strain (ϵ) (eq.5) is applied to an ideal elastic solid. Then at any point in time the stress will be proportional to the strain in accordance with the Hooke's law (eq.7).

$$\sigma(t) = E\epsilon(t) = E\epsilon_0 sin(\omega t) = \sigma_0 sin(\omega t) \tag{7}$$

For a perfectly elastic solid, the resulting strain and the stress will be perfectly in phase. If we now consider that the sinusoidal shear strain (γ) (eq.8) is applied to an ideal liquid.

$$\gamma = \gamma_0 sin(\omega t) \tag{8}$$

At any point in time the stress (τ) will be proportional to the strain rate in accordance with Newton's law of viscosity (eq.9).

$$\tau(t) = \eta\dot{\gamma} = \eta d\gamma(t)/dt = \eta\gamma_0\omega cos(\omega t) = \eta\gamma_0\omega sin(\omega t + \frac{\pi}{2}) \tag{9}$$

Thus for a purely viscous fluid, there will be a 90 °C phase lag of strain with respect to stress. This 90 ° phase difference between sinusoidal stress and strain in liquids is the key to the use of DMA as a tool for the characterization of viscoelastic materials. Since a viscoelastic material has properties intermediate between those of an ideal solid and an ideal liquid, it

exhibits a phase lag somewhere between 0 ° (ideal solid) and 90 ° (liquid). In other words, the phase lag (δ) is a measure of relative degree of viscous character to elastic character.

DMA: The Complex Modulus [7]

DMA data are most commonly reported using the complex modulus (E^*), defined as the ratio of the sinusoidal stress (σ) to strain (ϵ) (eq.10):

$$E^* = \frac{\sigma(t)}{\epsilon(t)} = \frac{\sigma_0.e^{i(\omega t+\delta)}}{\epsilon_0.e^{i\omega t}} = (\frac{\sigma_0}{\epsilon_0})e^{i\delta} = \frac{\sigma_0}{\epsilon_0}(cos(\delta) + isin(\delta)) \tag{10}$$

This complex modulus (E^*) can be divided into a real and imaginary component:

$$E^* = E' + iE'' \tag{11}$$

$$E' = \frac{\sigma_0}{\epsilon_0}cos(\delta) \tag{12}$$

$$E'' = \frac{\sigma_0}{\epsilon_0}sin(\delta) \tag{13}$$

E' (eq.12) is known as the storage modulus and is a measure of the elastic character or solidlike nature of the material. E" (eq.13) is known as the loss modulus and is a measure of the viscous character or liquidlike nature of the material. The larger E' is relative to E", the more of the energy required to deform sample is elastically recoverable. The larger E" is relative to E', the more of the deformation energy is viscously dissipated in heat. For an ideal elastic solid the phase lag is zero. Thus, E' is simply the Young's modulus of the material and E" is zero. For an ideal viscous liquid the phase lag is 90 ° or π radians. Thus, the storage modulus is zero and the loss modulus is related to the viscosity of the material. In a physical sense, the storage modulus is related to the stiffness of the material while the loss modulus is reflected in the damping capacity of the material. The ratio between the loss modulus and storage modulus is defined as the material loss factor or loss tangent, more commonly: $\tan(\delta)$ (eq.14).

$$\frac{E''}{E'} = \frac{sin(\delta)}{cos(\delta)} = tan(\delta) \tag{14}$$

Tan(δ) ranges from zero for an ideal elastic solid to infinity for an ideal liquid. It represents the ratio of energy dissipated to energy to energy stored per cycle of deformation.

A.4   DMA: Frequency Sweep Method

In this appendix session the measurements of the frequency sweep DMA test are presented. This DMA Frequency Sweep Method was performed for the three DPBM-FGE-Jx series, using discrete frequencies: 0.1, 0.3, 0.6, 1.0, 3.0, 6.0 and 10,0 Hz.
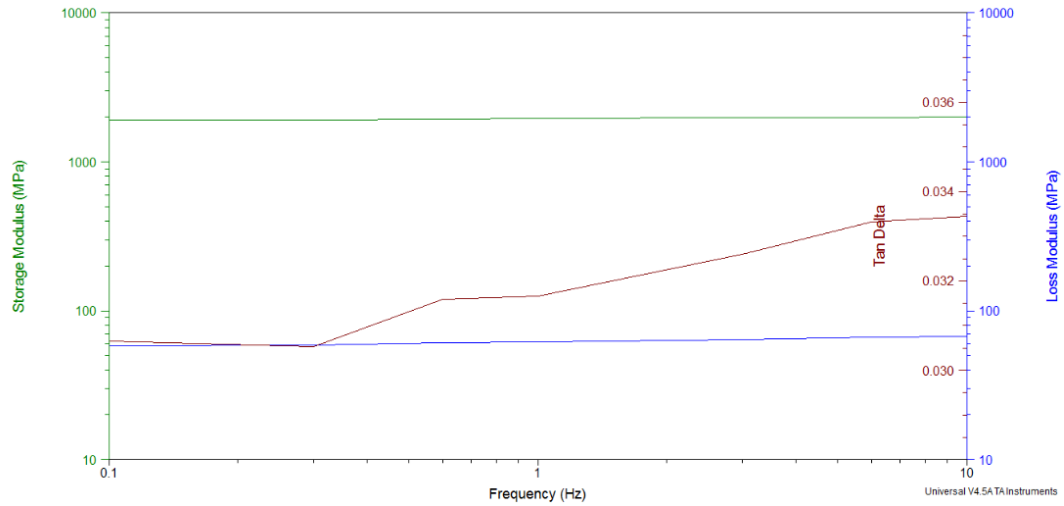
Figure 6: Result of the DMA test using the Frequency Sweep method. The sample (dimensions: 10.2 mm, 5.2 mm, 0.35 mm) was tested for the discrete frequencies:0.1, 0.3, 0.6, 1.0, 3.0, 6.0 and 10,0 Hz. The test was carried out at room temperature of 24.5 °C with the testing parameters: Poisson ratio = 0.44, oscillation strain = 0.30 % and a static force = 0.10 N.
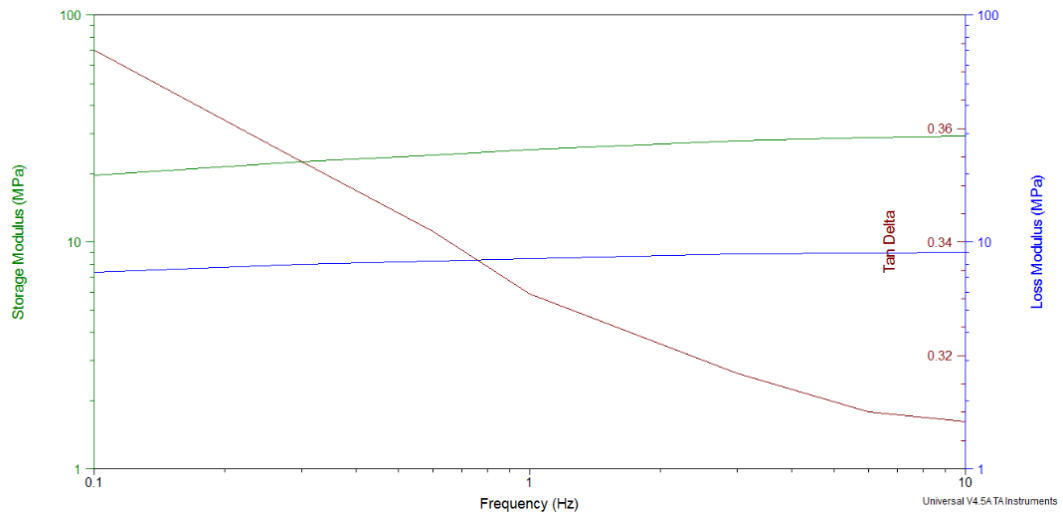
Figure 7: Result of the DMA test using the Frequency Sweep method. The sample (dimensions: 7.2 mm, 5.6 mm, 0.40 mm) was tested for the discrete frequencies: 0.1, 0.3, 0.6, 1.0, 3.0, 6.0 and 10,0 Hz. The test was carried out at room temperature of 24.5 °C with the testing parameters: Poisson ratio = 0.44, oscillation strain = 5.00 % and a static force = 0.10 N.
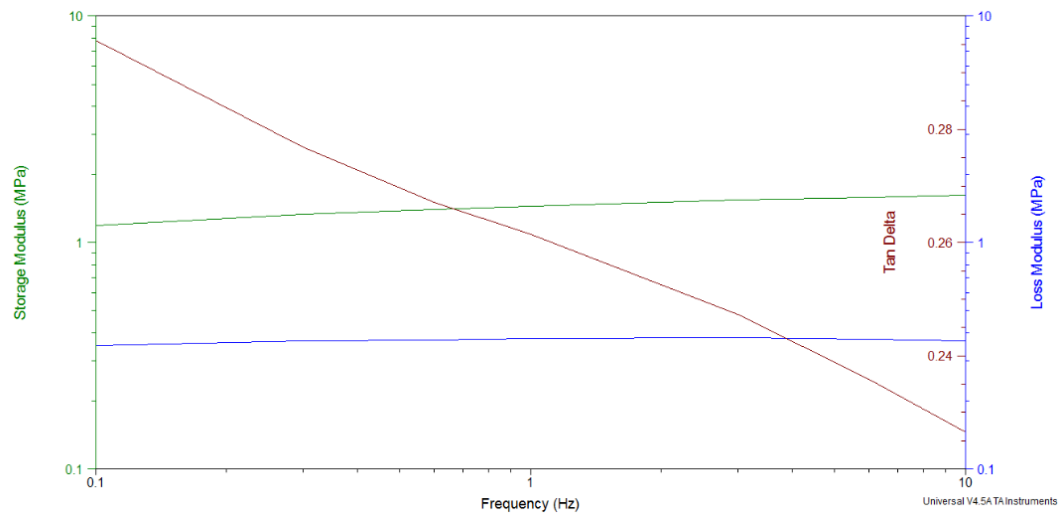
Figure 8: Result of the DMA test using the Frequency Sweep method. The sample (dimensions: 10.3 mm, 5.6 mm, 0.60 mm) was tested for the discrete frequencies: 0,1; 0,3; 0,6; 1,0; 3,0; 6,0 and 10,0 Hz. The test was carried out at room temperature of 24.5 °C with the testing parameters: Poisson ratio = 0.44, oscillation strain = 20.00 % and a static force = 0.10 N.

A.5 Stress-Strain curves of the Diels-Alder polymer series

The stress/strain graphs of the tensile tests carried out on the three DPBM-FGE-Jx series are presented in this appendix section. The test was done with minimum four samples for each series. For each series a mean value of the fracture strain and fracture tension was calculated and the maximum deviation. The graphs for the DPBM-FGE-J400, J2000 and J4000 are respectively shown in figure 9, 10 and 11

Test	Fracture Strain (%)	Fracture tension (Mpa)
1	0,7449	10,91
2	1,574	22,53
3	1,924	27,32
4	0,6987	9,924
Mean	1,24 ± 0,69	17,671 ± 9,649
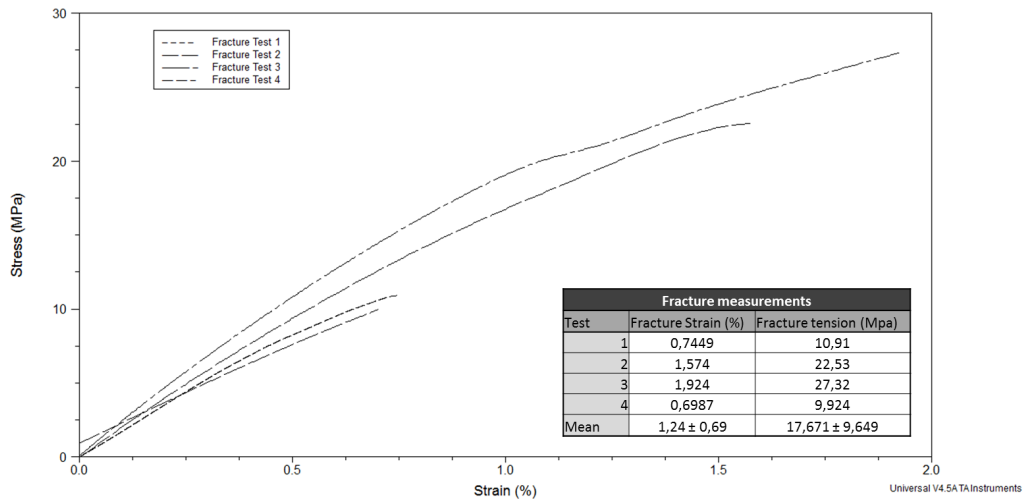
Figure 9: Static Stress-Strain Test until fraction for the DPBM-FGE-J400 series: Test conditions: Static Force = 0.001 N, Isothermal at 25 °C, Poisson ratio = 0.44 and Force Ramp = 1,00 N/min.
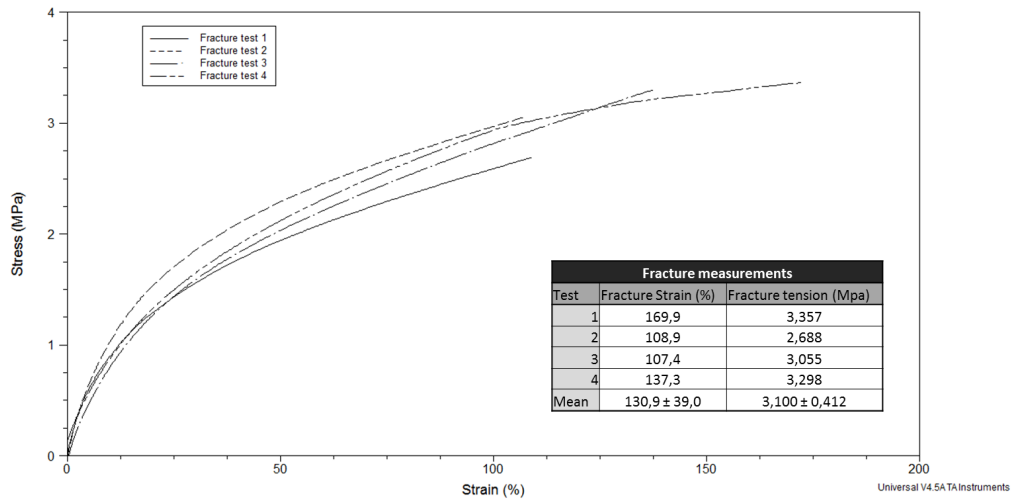
Figure 10: Static Stress-Strain Test until fraction for the DPBM-FGE-J2000 series: Test conditions: Static Force = 0.001 N, Isothermal at 25 °C, Poisson ratio = 0.44 and Force Ramp = 1,00 N/min.
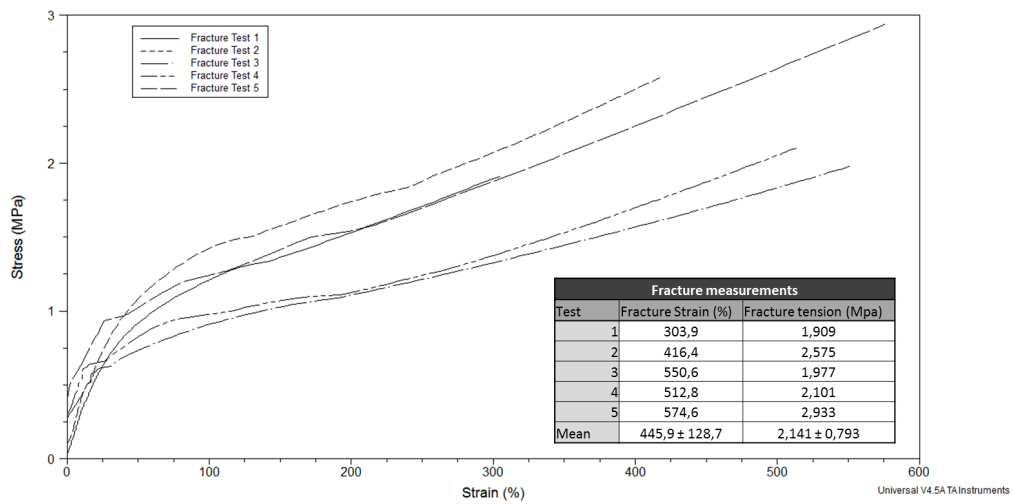
Figure 11: Static Stress-Strain Test until fraction for the DPBM-FGE-J4000 series: Test conditions: Static Force = 0.001 N, Isothermal at 25 °C, Poisson ratio = 0.44 and Force Ramp = 1,00 N/min.

A.6   Stress-Concentration Groove
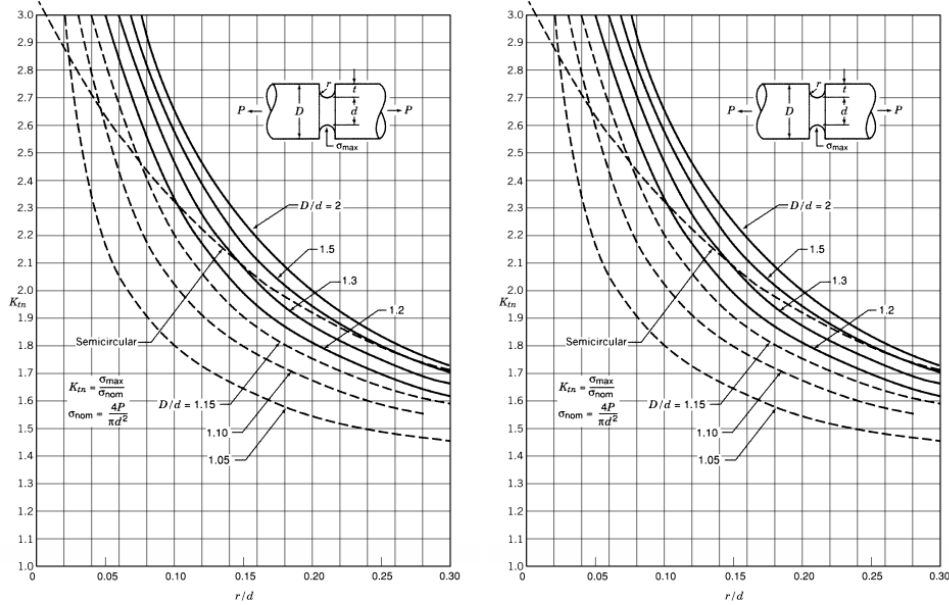
Figure 12: a)Stress concentration factor, Kt for a round tension bar with a U-groove [8]. b) Stress concentration factor, Kt for a flat tension bar with opposite V Notches[8].

To induce the brittle fracture on a desired precise location and not for example at the connection of the SH-material to the other system parts, a groove will have to be made into the cylindrical self-healing part. A lot of different groove shapes exist like for example circular-, U- or V-shape grooves and a choice has to be made to obtain the largest stress concentration $K_{tu} = \frac{\sigma_{max}}{\sigma_{mean}}$ on the desired fracture location. Theoretical curves (figure A.6) were used to obtain the theoretical ideal shape.

For a round tension bar with a U groove, the stress concentration factor K_{tu} in function of the r/d ratio for different D/d ratios is visible in figure A.6 a. The K_{tu} increases when r/d is decreasing, when the U-groove is getting narrower. In Figure 11 the influence of the angle of the V-shape groove on a flat tension bar is visualized. The $K_{t\alpha}$, the stress concentration factor for a V-shape groove with angle α is related to the K_{tu} of an equivalent U-shape groove with angle $\alpha = 0$. The approximation is made that the influence of the angle on a bar in tension with opposite V-grooves is the same as for a round tension bar with V-groove. On this graph we see that the angle has little effect up to 90° for not too deep grooves. For V-shapes with angle higher than 90° the concentration factor will decrease significantly. The most practical shape, in terms of construction and stress concentration factor, for the groove in the cylindrical self-healing material will be a V-shape with an angle below 90° with a small as possible round off radius r at the V-point.

Parameters chosen and calculations

Practical design parameters:

- D/d = 1.1

  - practical dimension(outer sample diameter D will be in the order of mm: ± 5mm)
    * Not too big to have still to have still a big enough inner diameter d
    * Not too small to be able to make it with macroscopic tools

- r/d = 0.10

  - as small as possible: depending on the tool precision

- $80° < \alpha < 90°$: neglecting the influence of the angle.

- This results in stress concentration factor: $K_t = 2,2$

  - The meaning of stress concentration factor:
    * When a certain force F is applied on the cylindrical SH part with section surface A. The maximum stress that will appear in that part is given by: $\sigma_{max} = K_t \sigma_{mean} = K_t \frac{F}{A}$

A.7   Maximum Deflection

The maximum deviation of a cylindrical DPBM-FGE-J400 sample, which was held horizontal at a temperature of 120 °C. The sample has a diameter of 5 mm. The calculations where done for two samples with a length of 10 mm and 20 mm. The formulas that were used in the calculations are presented in figure 13. The calculations are given in the table 1.

$$\theta = \frac{\omega l^3}{6EI} \qquad\qquad y = \frac{\omega x^2}{24EI}\left(x^2 + 6l^2 - 4lx\right) \qquad\qquad \delta_{max} = \frac{\omega l^4}{8EI}$$
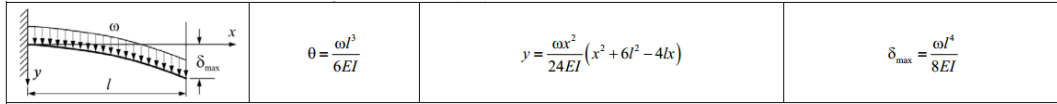
Figure 13: Formulas for calculation of the Maximum Deflection for a cantilever subjected to a uniform distributed load ω (N/m).

In these formulas:

- E = Young's Modulus of the polymer (considered her equal to the Storage modulus) (MPa)

- I = Area moments of inertia (m^4)

- ω = uniform distributed load (N/m)

- l = length

Table 1: Calculations of the Maximum Deflection for two DPBM-FGE-J400 samples with a length of 10 mm and 20 mm.

Calculations: Maximum Deflection of DPBM-FGE-J400 samples					
sample	length (mm)	cylinderdiameter (mm)	intersection surface (mm2)	volume cilinder (mm3)	volume cilinder (cm3)
1	10	5	19,63	196,35	0,19635
2	20	5	19,63	392,70	0,39270

sample	polymer density (g/ml)	polymer weight (g)	force applied by polymer (N)	Uniformly distributed load ω (N/mm)
1	1,19	0,234	0,0023	0,00023
2	1,19	0,469	0,0046	0,00023

	moment of inertia (mm4)		Storage Modulus DPBM-FGE-J400 at 119,5 °C	
	30,68		MPa (=M N/m2)	1,012
			N/mm2	1,012

sample	Maximum Deflection (mm)
1	0,0093
2	0,1481

A.8 SH-MF: Results of the stress/strain tensile test

The results of the stress/strain tensile test are summarized in the table 2. The fracture strain and fracture stress were calculated using the measured fracture force and fracture displacement (for this calculation the actual diameter of the contact surface of the SH-part was used.

Table 2: The results of the stress/strain tensile test until fracture of the 4 specimens which were inserted in the mechanical fuses. The fracture parameters are: fracture stress, strain and tensile force. These parameters were measured for the 4 specimens after 1, 2 and 3 self-healing cycles.

Fracture characteristics: DPBM-FGE-F400 SH-MF				
1 Self-Healing cycle				

	Fracture Force	Fracture Displacement	Fracture Stress	Fracture Strain
	(N)	(mm)	(MPa)	(%)
Specimen 1	132,86	0,15	7,37	1,24
Specimen 2	91,30	0,09	6,62	0,84
Specimen 3	50,18	0,06	3,41	0,87
Specimen 4	120,25	0,14	6,84	1,06

Fracture characteristics: DPBM-FGE-F400 SH-MF				
2 Self-Healing cycle				

	Fracture Force	Fracture Displacement	Fracture Stress	Fracture Strain
	(N)	(mm)	(MPa)	(%)
Specimen 1	11,39	0,03	0,63	0,27
Specimen 2	71,69	0,09	5,20	0,82
Specimen 3	43,82	0,07	2,98	0,98
Specimen 4	99,31	0,10	5,65	0,77

Fracture characteristics: DPBM-FGE-F400 SH-MF				
3 Self-Healing cycle				

	Fracture Force	Fracture Displacement	Fracture Stress	Fracture Strain
	(N)	(mm)	(MPa)	(%)
Specimen 1	0	0,00	0,00	0,00
Specimen 2	82,19	0,13	5,96	1,19
Specimen 3	55,54	0,08	3,77	1,12
Specimen 4	99,50	0,15	5,66	1,09

A.9   Equipment

A.9.1   Manual Hydraulic Press

In the shape process of the Self-Healing part used in the Self-Healing Mechanical Fuse (SH-MF), explained in section 5.3, a manual hydraulic press was used. The press used is presented in figure 14.

Figure 14: Picture of the manual hydraulic press used for the shaping proces of the DPBM-FGE-J400 SH-part, which is used in the SH-Mechanical Fuse: Specac: Atlas 15T Manual Hydraulic Press [9].

A.9.2   Manual Grinder

In the shape process of the Self-Healing part used in the Self-Healing Mechanical Fuse (SH-MF), explained in section 5.3 a manual grinder tool is required to make the chamfer on the edges of the cylindrical SH-part. The manual grinder of the supplier Proxxon is presenter in figure .

A.9.3   SPA pneumatic actuation test setup

In the subsection 6.4 the experiment done on the SH-Soft Pneumatic Cell (SH-SPC)are described. The SH-SPC is put under an overpressure, the elastic deformation is analyzed using a camera and the force applied by the different planes of the cubic cell is measured. A picture and a schematic of the setup used for this experiment are presented in respectively the figure 16 and the figure 18. A compressed air supply is provided in the lab. The pressure can be controlled using a pressure controller. the overpressure is measured using an analog manometer (unit: $kgf/cm_2 = 0.980681$ bar, readings: 0.01 $kgf/cm_2 = 9.80681$ mbar). To control the actuation of the soft pneumatic cell a button is placed in the1 setup: if the button is pressed the cell is connected to the compressed air supply, otherwise there is no

Figure 15: PROXXON FBS240/E used for the grinding of a chamfer on the edges of the cylindrical SH-part [10].

connection between the cell and the compressed air supply. The pictures and movies are made with a fixed digital camera.
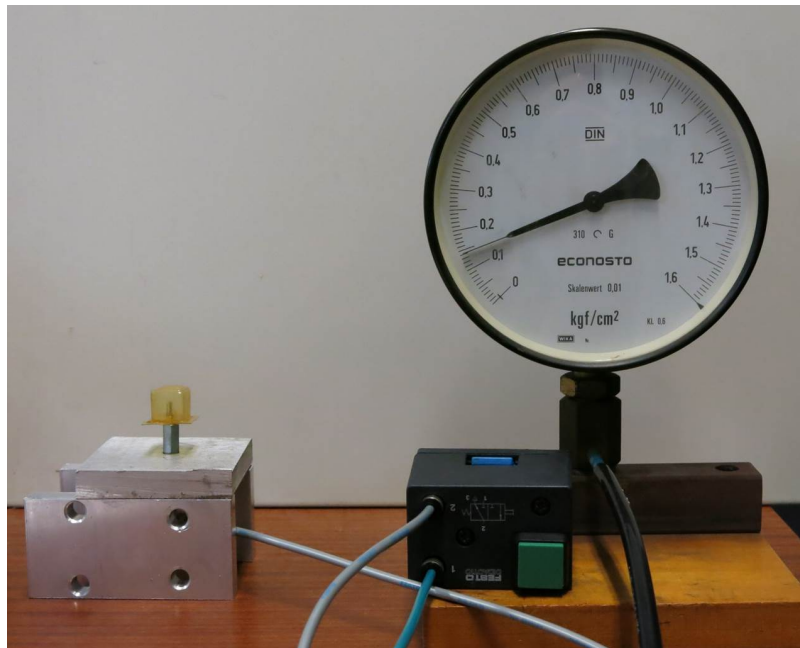
Figure 16: Picture of the setup used to test the soft pneumatic cell (SPC).

For the experiments where the force applied by the upper plane of the cell were measured, a force sensor (capacity of 1 lb = 4.448 N) was added, which was fixed above the cell. The analog signal of the sensor was read using a DAQ board and the Labview software. The setup for this tests is represented in the figure 18.
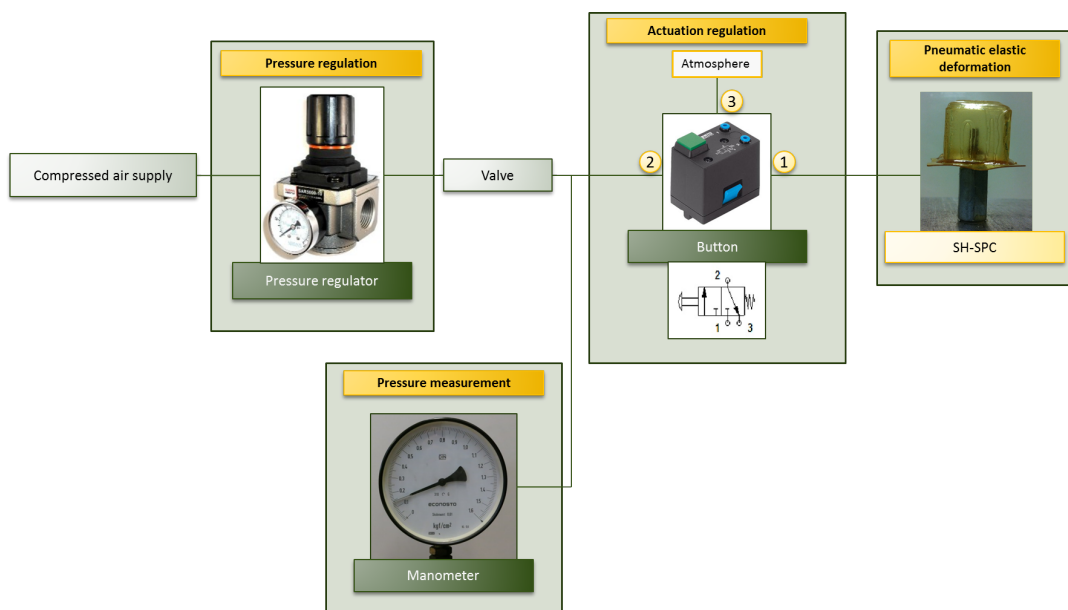
Figure 17: Scheme of the setup used to test the soft pneumatic cell (SPC).
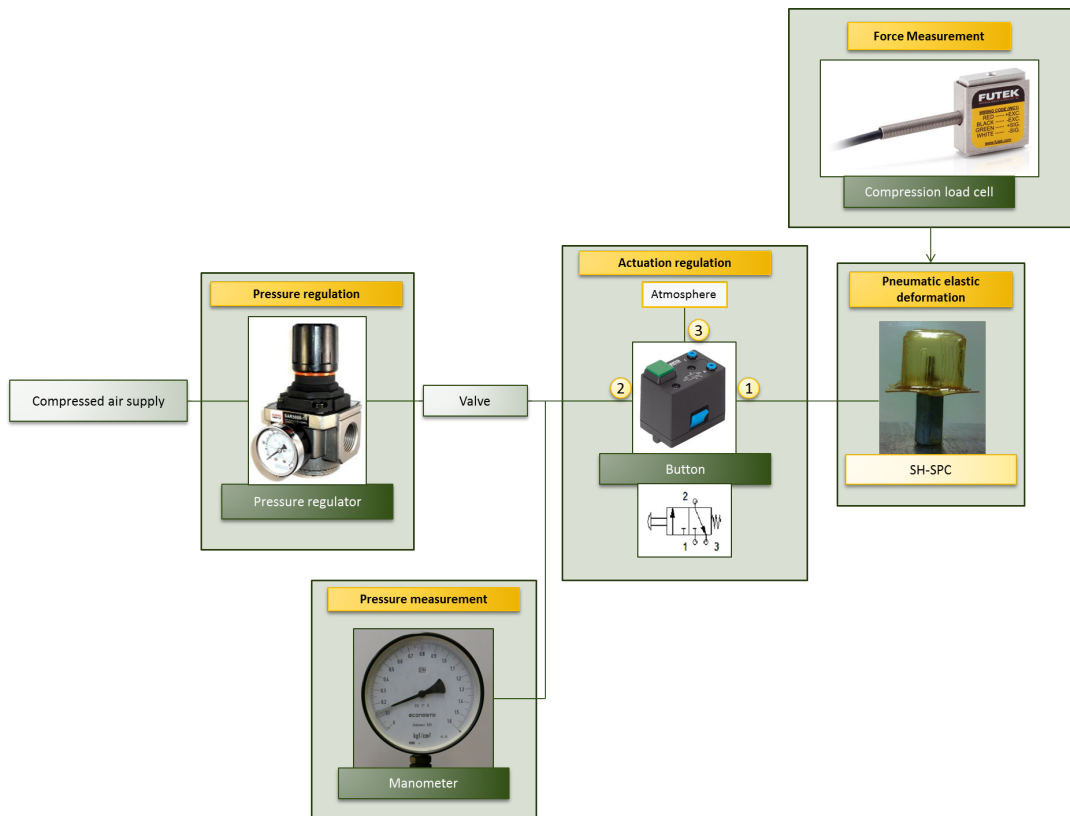
Figure 18: PROXXON FBS240/E used for the grinding of a chamfer on the edges of the cylindrical SH-part [10].

A.10   Self-Healing Mechanical Fuse (SH-MF): Prototype

In this section the prototype of the SH-MF is illustrated using images of the different components and the total assembly of the fuse.
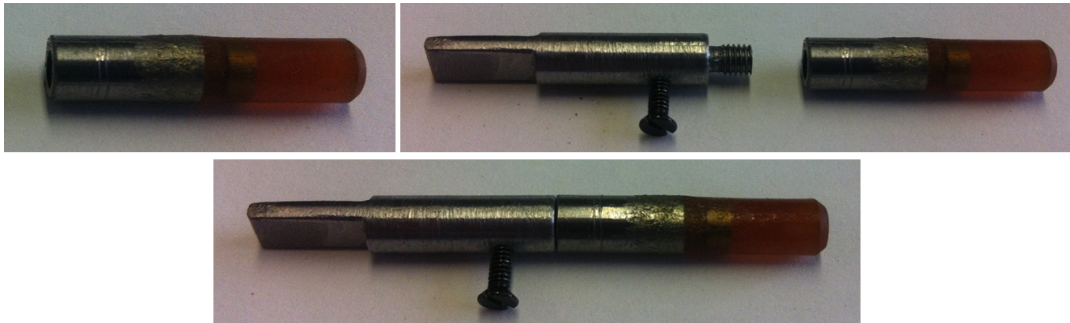
Figure 19: a) SH-cylindrical part, pressure molded over the steel pin with T-shape end. b) this SH-cylindrical part will be connected to a longer steel pin using thread. c) The assembly of the two parts is called "SH-Assembly".

3D printed Prototype of the Self-Healing Mechanical Fuse

The first prototype of the SH-MF was made in ABS plastic using a 3D printer.

Figure 20: The components of a 3D printed Prototype of the Self-Healing Mechanical Fuse (SH-MF): 2 pins with a T-end, a glass tube, ABS-cover (two parts).

Figure 21: 3D printed Prototype of the Self-Healing Mechanical Fuse (SH-MF)

Metal Prototype of Self-Healing Mechanical Fuse

Figure 22: Parts of the Self-Healing Mechanical Fuse: two SH-Assemblies, formed with the components of figure 23, Glass Tube, Aluminum Cover (two parts).

Figure 23: Self-Healing Mechanical Fuse (SH-MF). This fuse is not subjected to a first self-healing cycle yet. a) Upper View, b) Side View and c) Bottom View